A PETROLOGIC-SEISMIC MODEL OF YOUNG AND THICK OCEANIC CRUST BASED ON THE SAMAIL OPHIOLITE (IBRA AREA), OMAN, AND ITS VELOCITY-DEPTH PROFILE

A THESIS SUBMITTED TO THE GRADUATE DIVISION OF THE
UNIVERSITY OF HAWAII IN PARTIAL FULFULLMENT
OF THE REQUIREMENTS FOR THE DEGREE OF

MASTER OF SCIENCE

IN GEOLOGY AND GEOPHYSICS

DECEMBER 1981

By

James Arthur Hornbeck

Thesis Committee:

Murli H. Manghnani, Chairman
John M. Sinton
Joseph F. Gettrust

We certify that we have read this thesis and that in our opinion it is satisfactory in scope and quality as a thesis for the degree of Master of Science in Geology and Geophysics.

THESIS COMMITTEE

_____

Chairman

_____

_____

ACKNOWLEDGEMENTS

I thank Drs. John M. Sinton and Joseph F. Gettrust for their critical reviews of this thesis. I am especially thankful to Dr. Murli H. Manghnani for his continuous encouragement and financial support of this study. To Dr. Chandra Rai, Dr. Keith Katahara, John Balogh, Nirmal Devnani, and Teruyuki Matsui go my warmest thanks for their helpful discussions and invaluable assistance in the High Pressure Lab. Most of all I thank Kathryn Gibbs for her companionship and unending support during my graduate work at the University of Hawaii. The Samail ophiolite rock samples were provided by Drs. J. S. Pallister, R. G. Coleman, F. Boudier, and M. H. Manghnani.

ABSTRACT

The stratigraphically complete Samail ophiolite, a well-preserved fragment of Tethyan oceanic lithosphere in the Ibra area of Oman, provides an ideal opportunity to develop a petrologic-seismic model of young (4 to 8 m.y.) and thick (7.0 to 8.0 km) oceanic crust that formed at a moderate-to-fast spreading (3 to 5 cm yr^{-1}, half-rate) mid-ocean ridge. Compressional (V_p) and shear (V_s) wave velocities and bulk density (ρ) for 61 rock samples of metabasalt, metadiabase, plagiogranite, massive metagabbro, cumulate gabbro, and serpentenized harzburgite tectonite from the volcanic, the sheeted dike, the gabbro, and the peridotite members of the ophiolite were measured at *in situ* crustal lithostatic pressure and water saturation conditions. V_p and V_s were corrected for *in situ* temperatures (35° C km^{-1}) with the measured temperature derivatives of V_p and V_s (dV_p/dT and dV_s/dT) of -1.91 and $-1.18 * 10^{-4}$ km sec^{-1} $^oC^{-1}$, respectively, for a massive metagabbro, and -4.41 and $-4.24 * 10^{-4}$ km sec^{-1} $^oC^{-1}$, respectively, for a cumulate olivine-pyroxene gabbro. Poisson's ratio (σ) was calculated from the adjusted velocities. Because the mean atomic weight ($\overline{M}$) of the Samail rocks varies from only 20.6 to 22.1 (i.e. $\overline{M} \sim 21$), the velocity-density systematics for all of the rocks except serpentenized harzburgite tectonites are described by the linear equations, $V_p = -5.73 + 4.21\rho$ and $V_s = -2.03 + 1.97\rho$.

The velocity-depth profile of the Samail ophiolite shows that V_p and V_s increase rapidly with depth (~ 0.7 sec^{-1}) from 4.4 and 2.3 km sec^{-1} in the uppermost vesicular metabasalts to 6.85 and 3.0 km sec^{-1},

respectively, near the base of the sheeted dike complex at a depth of 2.5 km. Velocities increase downward due to: (1) decreasing effective porosity of the metabasalts, (2) decreasing pore pressure in the metabasalts, (3) increasing bulk density of the ophiolite lithology (2.3 to 2.9 g cm^{-3}), (4) increasing lithostatic confining pressure on the rocks, and (5) increasing metamorphic grade (zeolite to greenschist to lower amphibolite facies) with depth. In the same depth interval Poisson's ratio decreases from 0.32 to 0.27. In the gabbros, from a depth of 2.5 to 7.4 km, V_p and V_s increase slowly (0 to 0.04 sec^{-1}) from 6.7 and 3.75 km sec^{-1} to 7.35 and 3.9 km sec^{-1}, respectively. Velocities in the gabbros increase downward due to : (1) increasing olivine content (0 to 8%) in the rocks, and (2) increasing lithostatic confining pressure on the rocks with depth. Bulk density of the gabbros is constant (2.9 to 3.0 g cm^{-3}) while Poisson's ratio varies from 0.27 to 0.32. Below depths of 8.0 km, V_p, V_s, and bulk density are low and highly variable (V_p = 5.8 to 8.1 km sec^{-1}, V_s = 2.8 to 4.5 km sec^{-1}, ρ = 2.7 to 3.3 g cm^{-3}) in the harzburgite tectonites due to their post-detachment serpentenization (0 to 87%) and to their velocity anisotropy (ΔV_p and ΔV_s = 0.4 to 8.8%). Velocity anisotropy in the harzburgite tectonites is caused by the subsolidus alignment of olivine grains subparallel to the regional foliation and spinel lineation of the peridotite member.

The seismic velocity structure of the Samail ophiolite, inferred from its velocity-depth profile, is consistent with the classical explosion and airgun-sonobuoy seismic velocity structures of normal

oceanic crust and correlates closely with marine seismic reflection-refraction data for a section of oceanic crust that formed 4.5 m.y. ago at the East Pacific Rise. For these reasons a petrologic-seismic model of young and thick oceanic crust is presented that is based on the Samail ophiolite and its velocity-depth profile.

Seismic velocities in the model are shown to increase rapidly (~ 1.0 sec^{-1}) and smoothly through "layer 2" and slowly (< 0.1 sec^{-1}) through "layer 3" such that "layer 2C, 3A, and 3B" refractors are not seismically distinct in young oceanic crust. A distinct "layer 2-layer 3" seismic velocity boundary is caused by the petrologic contact between low density (< 2.9 g cm^{-3}) sheeted dikes and high density (> 2.9 g cm^{-3}) massive metagabbros, the presence of plagiogranites and associated quartz-rich metagabbros and metadiabases near the contact, and the appearance of amphibolite facies assemblages near the contact.

"Layer 2", extending as much as 2.5 km beneath a layer of oceanic sediments, consists of zeolite facies metabasalts and greenschist facies metadiabases. "Layer 3", extending 4.5 to 5.5 km beneath "layer 2", consists of: (1) an upper unit of massive metagabbros (~ 1.0 km thick) that are hydrothermally metamorphosed to the amphibolite facies, (2) a thick (3.5 to 4.0 km) middle unit of fresh cumulate olivine-pyroxene gabbros, and (3) a thin layer (0 to 0.6 km) of basal cumulate peridotites. The layer of basal cumulate peridotites appears to comprise a thin crust-mantle transition zone in which velocities that are characteristic in the lower oceanic crust increase to those that are

velocities ($V_p > 8.0$ km sec^{-1}, $V_s > 4.5$ km sec^{-1}) within the thin transition zone marks the seismic Moho at a depth of 7.0 to 8.0 km below the oceanic sediments. The petrologic Moho occurs at the petrologic contact between a very thin (< 0.1 km) layer of crustal cumulus dunite and harzburgite tectonites of the upper mantle.

The model indicates that the seismic velocity structure of "layer 2" in young oceanic crust is controlled by both the primary igneous petrology of the region and the subsequent metamorphic assemblages in the rocks that result from high temperature, hydrothermal metamorphism near a spreading ridge; the seismic velocity structure of "layer 3" is primarily controlled by the igneous petrology of the region. In contrast, the seismic velocity structure of "layer 3" in older oceanic crust may be controlled by low temperature hydrothermal metamorphism of the gabbros in the region.

TABLE OF CONTENTS

TABLE OF CONTENTS (Continued)

LIST OF TABLES

LIST OF ILLUSTRATIONS

LIST OF ILLUSTRATIONS (Continued)

1. INTRODUCTION

The inaccessible oceanic crust is defined by its seismic velocity structures that have been determined from marine seismic refraction data. Christensen and Salisbury (1975), averaging seismic refraction data from main ocean basins, have suggested that normal oceanic crust has an average thickness of 7.0 to 8.5 km, has 3 to 5 discrete and homogeneous layers of constant velocity, was generated at a mid-ocean ridge at least 40 m.y. ago, and is found in main ocean basins. Kennett and Orcutt (1976), using synthetic seismograms to model marine seismic reflection-refraction data, have suggested that seismic velocities continuously and smoothly vary with depth in the oceanic crust. Moreover, the seismic velocity structure of oceanic crust varies with the age of the crustal section (Moores and Jackson, 1974; Christensen and Salisbury, 1975; Houtz and Ewing, 1976; Spudich and Orcutt, 1980b; Kempner and Gettrust, 1981b), the rate at which the crust is spreading away from a ridge crest (Moores and Jackson, 1974; Sleep, 1975; Kusznir and Bott, 1976; Kusznir, 1980), and the tectonic provenance in which the crust is generated (Shor et al., 1971; Christensen and Salisbury, 1975). However, the marine seismic refraction techniques now used lack the seismic resolution necessary to distinquish fine seismic details or to consistently measure shear wave velocities in the oceanic crust (Christensen and Salisbury, 1975; Spudich and Orcutt, 1980b). To determine the detailed seismic velocity structures of oceanic crust and detailed petrologic interpretations of these structures, geophysicists and geologists are studying ophiolites.

Many assemblages of mafic to ultramafic rocks known as ophiolites are interpreted as allochthonous slices of ancient oceanic crust and upper mantle that have been tectonically transported from a site of generation and emplaced onto continental margins (Dewey and Bird, 1971; Davies, 1971; Coleman, 1971,1977). Abundant geologic (Miyashiro et al., 1970; Christensen and Salisbury, 1975; Coleman, 1977) and geophysical (Bailey et al., 1970; Milsom, 1973; Finlayson et al., 1976; Christensen, 1978) evidence support this interpretation. Structural and petrologic differences between the often stratigraphically incomplete and tectonically disrupted ophiolites, evidence that many ophiolites are thinner than the seismic thickness of normal oceanic crust (Christensen and Salisbury, 1975), and chemical and petrologic differences between the sedimentary and igneous rocks from mid-ocean ridges and some ophiolites (Dewey and Bird, 1971) suggest that ophiolites represent fragments of ancient oceanic crust that formed in different tectonic provenances (Coleman, 1977) and at different spreading rates (Moores and Jackson, 1974). If ancient and contemporary oceanic crust are comparable, then well-exposed and stratigraphically complete ophiolites can provide petrologic interpretations for all sections of the contemporary oceanic crust once the formation-to-emplacement age, the spreading rate, and the tectonic provenance in which the ophiolites were formed are determined.

The oceanic crust is defined by its seismic velocity structures while ophiolites are defined by their petrology and structural field relations. To make a valid comparison between oceanic crust and an

ophiolite the velocity structure of the ophiolite must be determined. According to Salisbury and Christensen (1978), in-place seismic refraction surveys of ophiolites result in lower velocities than those that are measured in oceanic crust because of: (1) subaerial weathering; (2) a decrease in lithostatic confining pressure due to erosion of overlying rocks; (3) the loss of free water from pores, joints, and fractures following emplacement; (4) the creation of joints and fractures due to emplacement tectonics and lithostatic unloading; and (5) partial to complete serpentenization of the ultramafics. Therefore elastic wave velocities in ophiolite rock samples are measured in the laboratory under simulated in situ ocean crustal conditions of water saturation (seawater and circulating hydrothermal fluids), confining pressure (lithostatic overburden), and temperature (geothermal gradients). Birch (1960), Nur and Simmons (1969), Christensen (1979), and Kern and Richter (1981) have shown the dependence of compressional and shear wave velocities in rocks on these variables.

Compressional (V_p) and shear (V_s) wave velocities have been measured in the laboratory as functions of confining pressure (depth) in rock samples from the Troodos ophiolite (Poster, 1973) and Newfoundland ophiolites (Peterson et al., 1974), as functions of confining pressure and water saturation in rocks from the Coast Range ophiolites (Christensen, 1978), and as functions of confining pressure and temperature in rocks from the Papua New Guinea ophiolite (Kroenke et al., 1976). Although the measured velocities of these ophiolites were within the range of the seismic velocities of oceanic crust, sufficient

stratigraphic control for the data was not established. Moreover, the velocity structures of these ophiolites were compared to the seismic velocity structures of normal oceanic crust; subsequent investigations have suggested that only the Newfoundland and the Coast Range ophiolites were generated at mid-ocean ridges (Coleman, 1977; Hopson, 1981; Kempner, 1981).

Employing oriented samples from known stratigraphic positions, Salisbury and Christensen (1978) developed a laboratory measured V_p and V_s velocity-depth profile of the Bay of Islands (BOI) ophiolite, Newfoundland. Their velocity-depth profile and the BOI ophiolite provide a detailed petrologic-seismic model of old ($\geq$ 45 m.y.) and thick ($\sim$6 km) oceanic crust that formed at a moderately fast spreading (3 to 5 cm yr^{-1}) mid-ocean ridge. Nichols et al. (1980), using laboratory techniques, developed a velocity-depth profile of the Pt. Sal ophiolite. The Pt. Sal ophiolite and its velocity-depth profile provide a detailed petrologic-seismic model of thin (< 5 km thick) and mature ($\sim$20 m.y. old) oceanic crust that formed at a slow-spreading mid-ocean ridge or in a back arc basin (Hopson, 1981).

The southeastern part (Ibra area) of the Samail ophiolite, Oman, provides an excellent opportunity to develop an oceanic crustal model because: (1) its complete crustal stratigraphy is well-exposed and, except for the pillow lavas, is comparable in thickness to normal oceanic crust; (2) the velocity-depth profile of the northern part of the ophiolite is consistent with the seismic velocity structures of normal oceanic crust (Christensen, 1978; Christensen and Smewing, 1981);

and (3) the Ibra area of the ophiolite has not been intensely affected by emplacement or post-emplacement tectonics or metamorphism.

Radiometric dating of zircons in plagiogranites from the Samail ophiolite indicates that the crustal section of the ophiolite crystallized 94 to 98 m.y. ago (Tilton et al., 1981), while initial detachment from the upper mantle occurred approximately 90 m.y. ago in an oceanic environment (Gealey, 1977; Coleman, 1981; Lanphere, 1981); the ophiolite therefore represents young (4 to 8 m.y. old) Tethyan oceanic crust. Geologic evidence of a large, long-lived magma chamber roofed by a relatively thin, but 100%, sheeted dike complex (Pallister and Hopson, 1981); the lack of alkalic volcanism or intrusions (McCulloch et al., 1980); and the mid-ocean ridge basalt (MORB) affinities of submarine extruded lavas, sheeted dikes, and plutonic gabbros (McCulloch et al., 1981; Pallister and Knight, 1981; Chen and Pallister, 1981) indicate crust formation at a moderate-to-fast spreading (3 to 5 cm yr^{-1}, half-rate) mid-ocean ridge (Pallister and Hopson, 1981)

The objectives of this study are to: (1) determine the velocity structure of the Samail ophiolite in the Ibra area of Oman and relate this velocity structure to the lithology of the ophiolite, (2) establish the relationship between the Samail ophiolite and the oceanic crust, and (3) present a petrologic-seismic model of thick (7 to 8 km) and young (4 to 8 m.y. old) oceanic crust that formed at a moderate-to-fast spreading (3 to 5 cm yr^{-1}, half-rate) mid-ocean ridge.

This thesis presents the V_p and V_s and bulk density (ρ) data for 61 representative rock samples from the Ibra area of the Samail ophiolite, Oman. V_p, V_s, and ρ are measured as functions of confining pressure and water saturation at 25° C and then corrected for temperature effects at depth in the crust. These data, correlated with petrographic analyses of the rock samples, are used to: (1) determine the variation of V_p, V_s, and ρ with lithology and stratigraphic position in the ophiolite; (2) determine the variation of V_p, V_s, and ρ with the effective porosity, mineralogy, and texture of the rocks; (3) determine the velocity-density systematics of the Samail rocks; (4) determine the variation of Poisson's ratio (σ) with lithology and stratigraphic position in the ophiolite; (5) determine the variation of velocity anisotropy (ΔV_p and ΔV_s) with lithology and stratigraphic position in the ophiolite; and (6) determine temperature derivatives of velocity (dV_p/dT, dV_s/dT) for a massive metagabbro and a fresh cumulate gabbro. A velocity-depth profile for the Ibra area of the Samail ophiolite is presented. This profile is correlated with the seismic velocity structures of normal oceanic crust and the velocity-depth function for a section of oceanic crust that formed 4.5 m.y. ago at the fast-spreading ($\sim$5 cm yr^{-1}, half-rate) East Pacific Rise. A petrologic-seismic model of young and thick oceanic crust, based on the petrology and velocity-depth profile of the Samail ophiolite, is presented. Implications of the model for young and thick oceanic crust are also discussed.

2. GEOLOGY OF THE SAMAIL OPHIOLITE

2.1 Regional Geology of the Oman Mountains

The Samail ophiolite is an arcuate chain of "large plates and fragments" (Glennie et al., 1974) of a once continuous nappe of Tethyan oceanic crust that is now exposed for over 30,000 km^2 throughout the Oman Mountains of northern Oman and the United Arab Emirates (Figure 1). As described by Glennie et al. (1974), the ophiolite is the uppermost unit of a stacked series of allochthonous nappes emplaced on the Arabian continental margin from the late Cenomanian (90 m.y.) to the latest Campanian (71 m.y.). The base of the ophiolite is in thrust contact with the imbricated, laterally time-equivalent nappes of Permian to Cenomanian pelagic sediments of the Hawasina Group. Deposited contemporaneously with the Hawasina Group and in thrust contact with its base are the thick, continental shelf carbonates of the autochthonous Hajar Super-Group. Uncomformably overlain by the Hajar Super-Group, Precambrian to pre-Permian schists and phyllites, exposed in the Saih Hatat window, form the crystalline basement rocks of the Arabian continent. Widely scattered shallow-marine carbonates of the latest Campanian to Maestrichtian (71 to 65 m.y.) unconformably overlie the Samail ophiolite and locally the Hawasina Group. Late Tertiary folding and extensive erosion of the emplaced nappes produced the Oman Mountains and exposed the complete ophiolite stratigraphy.

Figure 1. Regional geologic map of the Oman Mountains (after Glennie et al., 1974). The Ibra area of the Samail ophiolite and the locations of ophiolite samples from outside the Ibra area are also shown.

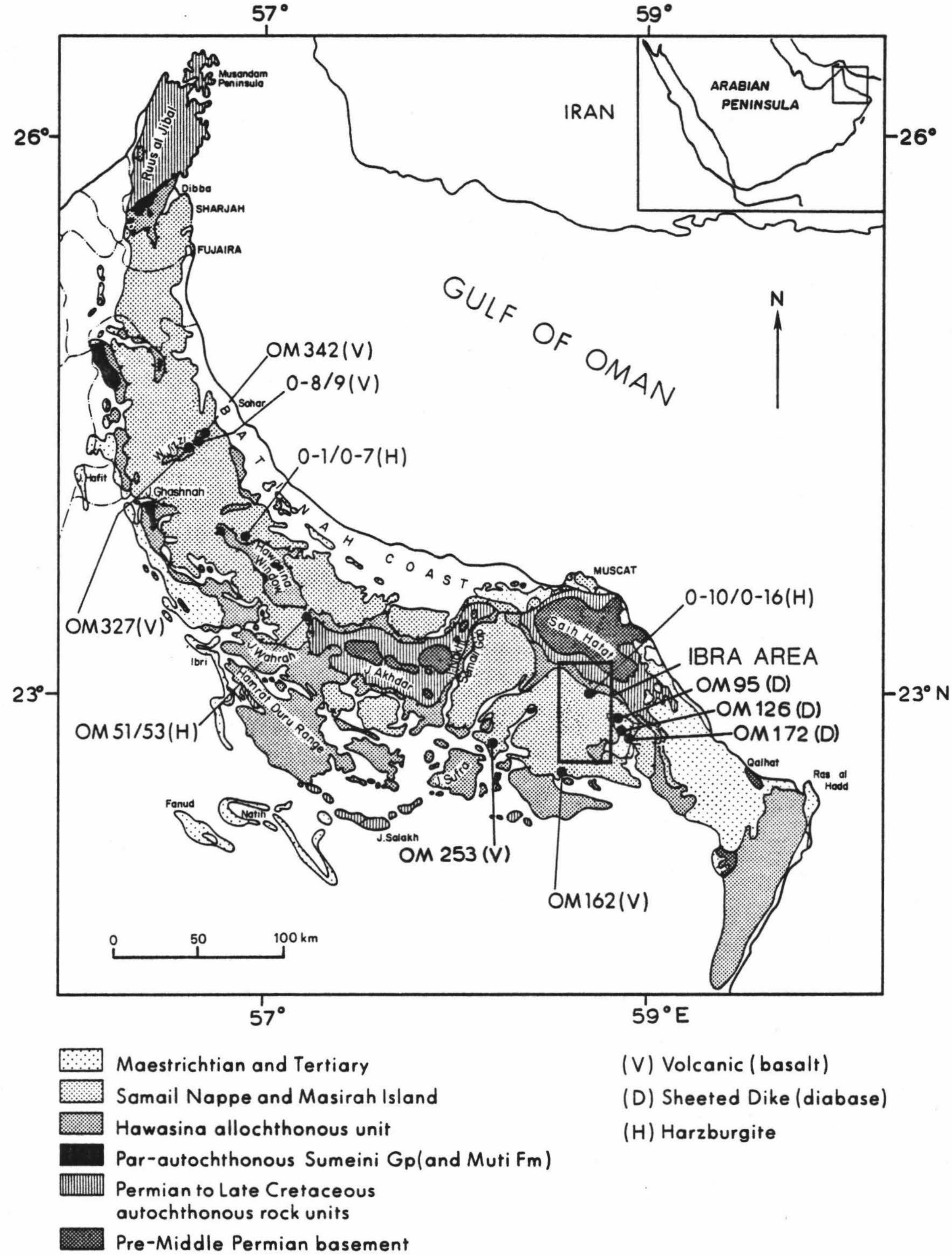
57°
59°
26°
23°
23° N
59° E
IRAN
ARABIAN
PENINSULA
GULF OF OMAN
N
Musandam
Peninsula
Ruus al Jibal
Dibba
SHARJAH
FUJAIRA
Sohar
BATINAH COAST
MUSCAT
Saih Hatat
IBRA AREA
Hafit
J.Ghashnah
J.Wahrah
Ibri
Hamrat Duru Range
J.Akhdar
Sufra
Fanud
Natih
J.Salakh
Qalhat
Ras al
Hadd
OM342(V)
0-8/9(V)
0-1/0-7(H)
OM327(V)
0-10/0-16(H)
OM95 (D)
OM126 (D)
OM172 (D)
OM51/53(H)
OM 253 (V)
OM162(V)
0
50
100 km
Maestrichtian and Tertiary
Samail Nappe and Masirah Island
Hawasina allochthonous unit
Par-autochthonous Sumeini Gp(and Muti Fm)
Permian to Late Cretaceous
autochthonous rock units
Pre-Middle Permian basement
(V) Volcanic (basalt)
(D) Sheeted Dike (diabase)
(H) Harzburgite

2.2 Lithology of the Samail Ophiolite

One of the thickest and best preserved sections of the Samail ophiolite is exposed in the Ibra area, southeast of the Samail Gap (Glennie et al., 1974; Figure 1). Bailey (1981) and Hopson et al. (1981) have regionally mapped a 30 km wide transect of the ophiolote from Muscat on the Gulf of Oman to Ibra, 130 km to the south (Figure 2). They and Glennie et al. (1974) recognized five mappable members of the ophiolite: (1) a volcanic member (V); (2) a sheeted dike complex (SD); (3) a gabbro member with two mappable units, layered gabbro (G) and high-level gabbro (HG); and (4) a peridotite member (H). Pallister and Hopson (1981) recognized an additional mappable unit in the gabbro member, the transitional gabbro (TG). The complete ophiolite stratigraphy that was mapped by Pallister and Hopson (1981) is used in this thesis and is generally described below from top to bottom:

Volcanic Member:

This uppermost unit, only 0.5 km thick and poorly exposed in the Ibra area, consists of bulbous pillow lavas that alternate locally with less abundant flows of massive lava. Vesicles, now amygdules filled with calcite, smectite, or chalcedony, are common within the lavas. The unit varies from 0.3 to 2.0 km in thickness throughout the ophiolite.

Only hydrothermally metamorphosed aphyric to microphyric metabasalts are exposed in the Ibra Valley. Microphenocryst assemblages of olivine, clinopyroxene,and plagioclase float in a matrix of chlorite, epidote, zeolites, and iron-titanium oxides (Christensen and Smewing, 1981). The basalts have been pervasively altered from the zeolite to

Figure 2. Geologic map of the Ibra area of the Samail ophiolite in the southeastern Oman Mountains (after Hopson et al., 1981). Sample locations along the Wadi Kadir and Wadi Gideah East sections are also shown.

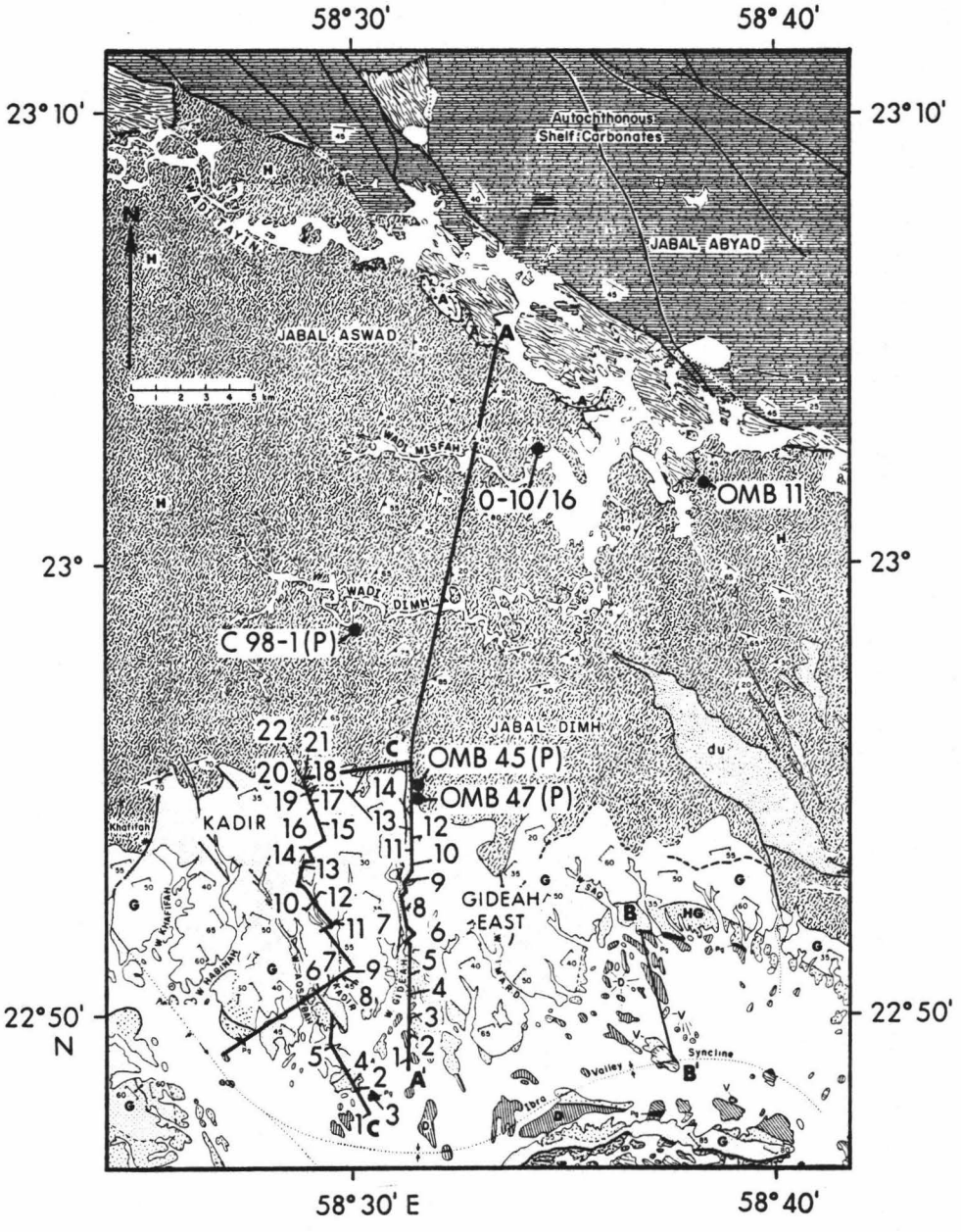

(V) Volcanic (basalt)

(D) Sheeted Dike (diabase)

(Pg) Plagiogranite

(HG) High-Level Gabbro

(G) Cumulate Gabbro

(H) Harzburgite

(du) Dunite

(A) Amphibolite

the greenschist facies with metamorphic grade increasing with depth. Olivine has been completely replaced by chlorite, talc, magnetite, and serpentine; plagioclase has been albitized; and clinopyroxene is the only primary mineral to survive.

Sheeted Dike complex:

The bedded lavas grade within a few tens of meters to the sheeted dike complex of parallel to subparallel diabase and basalt dikes. The complex, varying in thickness from 1.2 to 1.6 km in the Ibra area, consists of 100% vertical dikes that trend NNW ($345^{o} \pm 10$) and are approximately 15^{o} from perpendicular to the cumulate layering and planar lamination of the underlying cumulate gabbros. The pervasively altered dikes are predominantly fine- to medium-grained, olivine-clinopyroxene and clinopyroxene phyric metadiabases.

The metadiabases have undergone two styles of metamorphism. Within the upper 1.0 km of the dike complex,the metadiabases are altered to the greenschist facies due to hydrothermal metamorphism. Clinopyroxene is partially to completely replaced by epidote and chlorite; plagioclase is pervasively saussuritized; and minor olivine is completely replaced by chlorite, magnetite, serpentine, and talc within the metadiabases. Within 0.4 to 0.6 km of the base of the dike complex, the metadiabases are altered to the lower amphibolite facies. This higher grade of alteration is the result of contact metamorphism of the metadiabases by the underlying high-level gabbro that intruded the base of the dike complex (Christensen and Smewing, 1981). Within the basal metadiabases, clinopyroxene and early formed greenschist facies assemblages are

partially to completely replaced by fibrous green amphibole (uralite).

High-Level Gabbro:

The high-level gabbro, varying in thickness from 0.2 to 1.0 km in the Ibra area, represents an intrusive sandwich horizon between the overlying dike complex and the underlying gabbro member (Hopson et al., 1981). The non-cumulus, medium- to coarse-grained metagabbros of this unit locally grade into hornblende diorites, quartz diorites or plagiogranites near the sheeted dike contact. These late-stage differentiates, collectively termed plagiogranites by Coleman and Peterman (1975), form discontinuous thin sills ($\sim$1.0 km^2) of insignificant volume. The widespread occurrence of quartz in the upper metagabbros and basal dikes is related to the presence of the late-stage intrusives near the high-level gabbro-sheeted dike contact.

The massive metagabbros of this unit display an isotropic, hypidiomorphic granular texture, variable amounts of hornblende, and pervasive hydrothermal metamorphism. While the grade of metamorphism increases from lower to upper amphibolite facies the extent of metamorphism decreases with depth in the high-level gabbro. The metagabbros have non-cumulus phases of hornblende, clinopyroxene, plagioclase, and minor quartz (1 to 4% by modal percentage). Clinopyroxene is partially replaced by uralite; olivine is partially to completely replaced by smectite, chlorite, and magnetite; and plagioclase (An_{10-60}) within the plagiogranites is extensively saussuritized.

Transitional Gabbro:

The high-level gabbro grades downward to the transitional gabbro which is always less than 1.0 km thick in the Ibra area. The cumulus clinopyroxene and olivine-clinopyroxene gabbros of this unit display planar lamination due to the random distribution of the long axes of tabular plagioclase, clinopyroxene, and, rarely, olivine grains in a plane parallel to the cumulate layering of the underlying layered gabbros.

The transitional gabbros are fine- to medium-grained mesocumulates with a uniform grain size. They lack the primary hornblende of the high-level gabbros. Olivine in these rocks is partially to completely serpentenized. The incipient alteration of primary clinopyroxene to brown hornblende and uralite indicates only minor hydrothermal metamorphism of the gabbros in this unit to the upper amphibolite facies.

Layered Gabbro:

The layered gabbro, 2.6 to 5.5 km thick in the Ibra area, is characterized by fresh gabbros with cumulate layering, cumulus textures, and planar lamination in thin section. Variation in relative abundance and/or grain size (1 to 5 mm) of the primary cumulus phases (unzoned plagioclase, clinopyroxene, and olivine) defines the layers which vary from millimeters to tens of meters in thickness. Planar lamination and cumulate layering are parallel and form a vergence angle of 15^{o} with the gabbro-harzburgite tectonite contact. No metamorphic tectonite fabric is seen in this section.

Early cumulus olivine and Cr-spinel form basal cumulus dunites with interstitial plagioclase (Coleman, 1977). The cumulus dunites are overlain by distinctive and laterally continuous layer-sets of interlayered clinopyroxene gabbros, wehrlites, melagabbros, and dunites that vary in thickness from 0 to 0.6 km. These layer-sets also recur at higher stratigraphic levels. The basal layer-sets are referred to as basal cumulate peridotites in this thesis. Medium- to coarse-grained cumulate olivine-clinopyroxene gabbros with adcumulus textures and minor brown to green hornblende are the predominant rocks above the basal cumulate peridotites. Orthopyroxene does not appear as a cumulus phase.

Christensen and Smewing (1981) noted that fractures and joints in the transitional and layered gabbros are lined with upper amphibolite facies assemblages. Away from the fractures and joints, clinopyroxene and plagioclase are fresh to incipiently replaced by uralite and brown hornblende or saussurite, respectively, while olivine is extensively serpentenized. This alteration pattern suggests that hydrothermal seawater was confined to existing fractures in the cumulate gabbros. Gregory and Taylor (1981) noted that the seawater locally penetrated the harzburgite tectonites underlying the layered gabbros.

Peridotite member:

This unit, with a thickness of 9 to 12 km in the Ibra area, comprises 60% of the ophiolite and consists predominantly of harzburgite tectonites with concordant and discordant dunite bodies and minor websterite and gabbro dikes. The geology of this member, a piece of the uppermost mantle, is thoroughly discussed by Boudier and Coleman (1981).

Harzburgite tectonites with minor clinopyroxene and orthopyroxene bands (3 to 10 cm thick) exhibit a coarse porhyroclastic texture. Elongate olivine grains (2 to 5 mm) are aligned with their [100] crystallographic axes trending northeast and dipping slightly southwest. Near the base of this unit the harzburgites locally display mylonitic textures that are related to the basal thrust plane marking the contact of the Samail ophiolite with the Hawasina Group. A narrow discontinuous zone of high grade amphibolites is tectonically welded to the base of the peridotite member.

Lizardite and clinochrysotile with brucite and magnetite replace on the average 62% and 81% of the harzburgites and dunites, respectively. The preservation of delicate, serpentine mesh structures within the harzburgites suggests that serpentenization occurred at least after detachment of the nappe (Boudier and Coleman, 1981)

2.3 The Wadi Kadir and Wadi Gideah East Stratigraphic Sections

In Figure 3 are shown two stratigrapic columns, Wadi Kadir and Wadi Gideah East (named for two nearby wadis - seasonal streambeds), that are constructed for the closely spaced (3 to 5 km) stratigraphic sections C-C′-A and A′-C-A (Figure 2), respectively, through the Ibra area of the Samail ophiolite (Hopson et al., 1981; Pallister and Hopson, 1981) Also shown are the metamorphic assemblages of the rock members and the stratigraphic positions of the collected rock samples. The base of the cumulus dunite of the gabbro member is interpreted as the base of the crustal section and, as such, marks the crust-mantle contact.

Figure 3. Stratigraphic columns of the Samail ophiolite along the Wadi Kadir and Wadi Gideah East sections (after Hopson et al., 1981). The stratigraphic position of the metamorphic assemblages in the Samail ophiolite and the representative rock samples are also shown. The Aqsaybah Fault Zone is shown between depths of 4.0 to 5.0 km in the Wadi Kadir column.

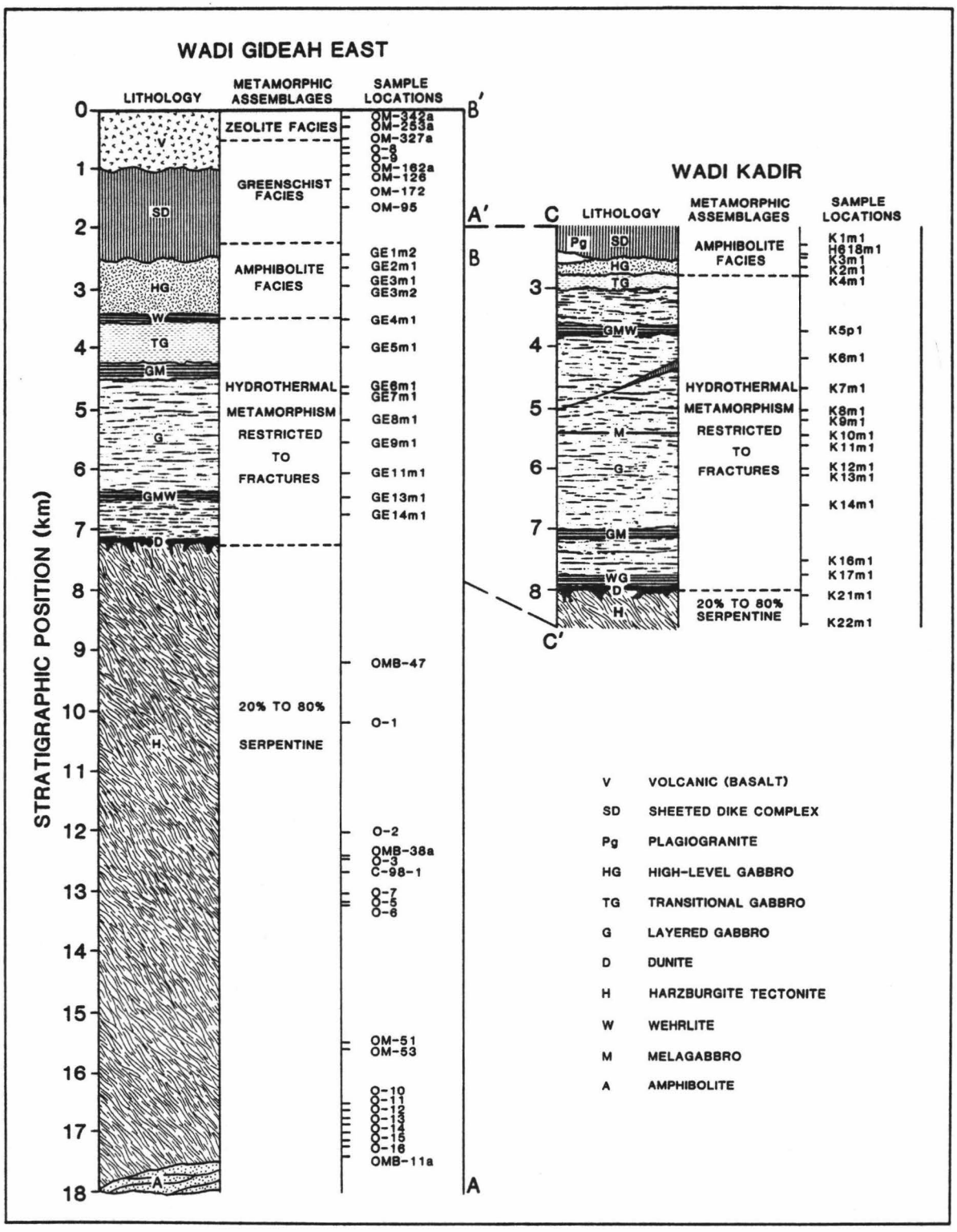
WADI GIDEAH EAST
LITHOLOGY
METAMORPHIC ASSEMBLAGES
SAMPLE LOCATIONS
STRATIGRAPHIC POSITION (km)
ZEOLITE FACIES
GREENSCHIST FACIES
AMPHIBOLITE FACIES
HYDROTHERMAL METAMORPHISM RESTRICTED TO FRACTURES
20% TO 80% SERPENTINE
OM-342a
OM-253a
OM-327a
O-8
O-9
OM-162a
OM-126
OM-172
OM-95
GE1m2
GE2m1
GE3m1
GE3m2
GE4m1
GE5m1
GE6m1
GE7m1
GE8m1
GE9m1
GE11m1
GE13m1
GE14m1
OMB-47
O-1
O-2
OMB-38a
O-3
C-98-1
O-7
O-5
O-6
OM-51
OM-53
O-10
O-11
O-12
O-13
O-14
O-15
O-16
OMB-11a
A
A'
B
B'
WADI KADIR
C
C'
AMPHIBOLITE FACIES
HYDROTHERMAL METAMORPHISM RESTRICTED TO FRACTURES
20% TO 80% SERPENTINE
K1m1
H618m1
K3m1
K2m1
K4m1
K5p1
K6m1
K7m1
K8m1
K9m1
K10m1
K11m1
K12m1
K13m1
K14m1
K16m1
K17m1
K21m1
K22m1
V VOLCANIC (BASALT)
SD SHEETED DIKE COMPLEX
Pg PLAGIOGRANITE
HG HIGH-LEVEL GABBRO
TG TRANSITIONAL GABBRO
G LAYERED GABBRO
D DUNITE
H HARZBURGITE TECTONITE
W WEHRLITE
M MELAGABBRO
A AMPHIBOLITE

The columns show a total ophiolite thickness of 18.0 km (Wadi Gideah East) to 19.0 km (Wadi Kadir); the crustal section of the ophiolite varies in thickness from 8.0 km (Wadi Kadir) to 7.1 km (Wadi Gideah East). Stratigraphic thicknesses of 1.0 km for the volcanic member and 1.5 km for the sheeted dike complex for both columns are measured along section B-B′ (Figure 2) (Hopson et al., 1981; Gregory and Taylor, 1981). A stratigraphic thickness of 9.0 to 12.0 km for the peridotite member for both columns is measured along section C-A′ (Hopson et al., 1981).

The gabbro member along sections C-C′ (Wadi Kadir) and A′-C′ (Wadi Gideah East) shows variations in thickness and structure. Wadi Kadir has a total gabbro member thickness of 5.5 km that consists of 0.25 km of high-level gabbros, 0.25 km of transitional gabbros, and 5.0 km of layered gabbros. Wadi Gideah East has a total gabbro member thickness of 4.5 km that consists of 1.0 km of high-level gabbros, 0.8 km of transitional gabbros, and 2.7 km of layered gabbros. The basal, cumulate peridotites are 0.1 km thick in the Wadi Kadir section while in the Wadi Gideah East section they are missing; cumulate gabbros are in contact with the basal, cumulus dunite. The Wadi Kadir section is cut by the pre-detachment Aqsaybah fault zone which shows a maximum lateral displacement of 120 m (Pallister and Hopson, 1981).

3. EXPERIMENTAL PROCEDURE

3.1 Sample Collection

Sixty-one representative rock samples from the Samail ophiolite were used in this study (Figure 3). Their field locations are shown in Figures 1 and 2. Due to the variety of lithologies through the layered gabbro, rock samples were collected at closely spaced intervals along the traverses A′-C′ and C-C′ (Figure 2). Samples from the volcanic member were collected throughout the Samail ophiolite since basalt exposures in the Ibra Valley are limited. Samples from the uppermost sheeted dike complex were likewise collected outside the Ibra area. Due to the rugged terrain and serpentenization of the peridotite member, harzburgite tectonites were collected along available roadcuts and wadis. No samples were collected from the basal cumulate peridotites or cumulus dunite.

3.2 Laboratory Techniques

3.2.1 Sample Preparation

To determine rock velocities as functions of confining pressure, 162 cores were cut from the rock samples with a drill press and a 1.27, 1.90, or 2.54 cm diameter diamond bit. Whenever possible three mutually perpendicular cores were taken from each rock to measure velocity anisotropy (ΔV_p, ΔV_s) of the rock samples. In the cumulate gabbros cores `a′ were cut perpendicular to planar textures, if any, while cores `b′ and `c′ were cut perpendicular to each other and cores `a′ and parallel to the textures. This core orientation assumes that the planar

textures were originally horizontal; an assumption in error by approximately 15° (Pallister and Hopson, 1981). In seven of the harzburgite tectonites (discussed later) the cores were cut parallel to the crystallographic directions of aligned olivine grains. After trimming the cores to right cylinders from 2.54 to 6.40 cm in length, their ends were polished flat and parallel to within 0.013 cm and subsequently coated with silver conducting paint (Silver Print, GC Electronics). Samples located stratigraphically below the high-level gabbro were air dried and then jacketed with copper foil (0.008 cm thick). Samples from higher stratigraphic members were vacuum dried for twelve hours, saturated for twenty-four hours in distilled water under a pressure of 160 psi of nitrogen gas, and then wrapped with fine mesh, screen-wire before jacketing. After aluminum electrodes and transducers were placed on the core ends, the assemblies were sealed with gum rubber tubing to exclude the liquid pressure-medium from the rock cores (Figure 4a). Compressional and shear mode barium titanate transducers with a resonant frequency of 500-KHz were accoustically bonded to the rock cores by silicon oil or poly- -methyl-styrene resin (Dow Chemical resin 276-V9), respectively.

To determine the effect of high temperature on V_p and V_s, single cores were cut parallel to the planar lamination and cumulate layering of rocks (K2m1) and (K9m1), respectively. The cores, 1.9 cm in diameter, were trimmed to right cylinders about 5.0 cm in length. The ends of the samples and stainless-steel (Type 303) end-plugs were polished optically flat and parallel to within 0.001 cm. The air-dried

4a

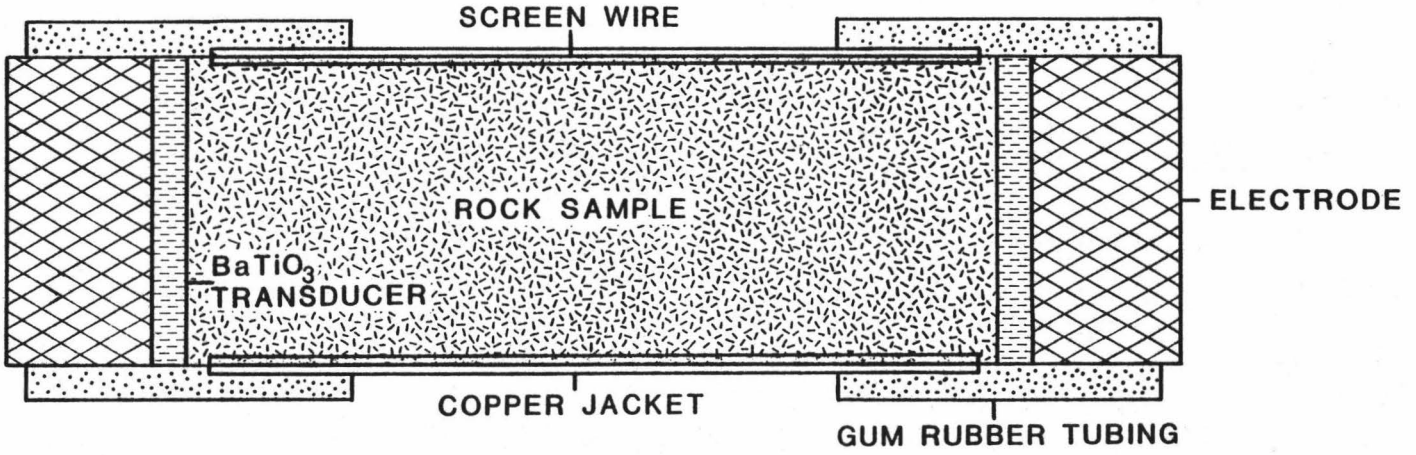

4b

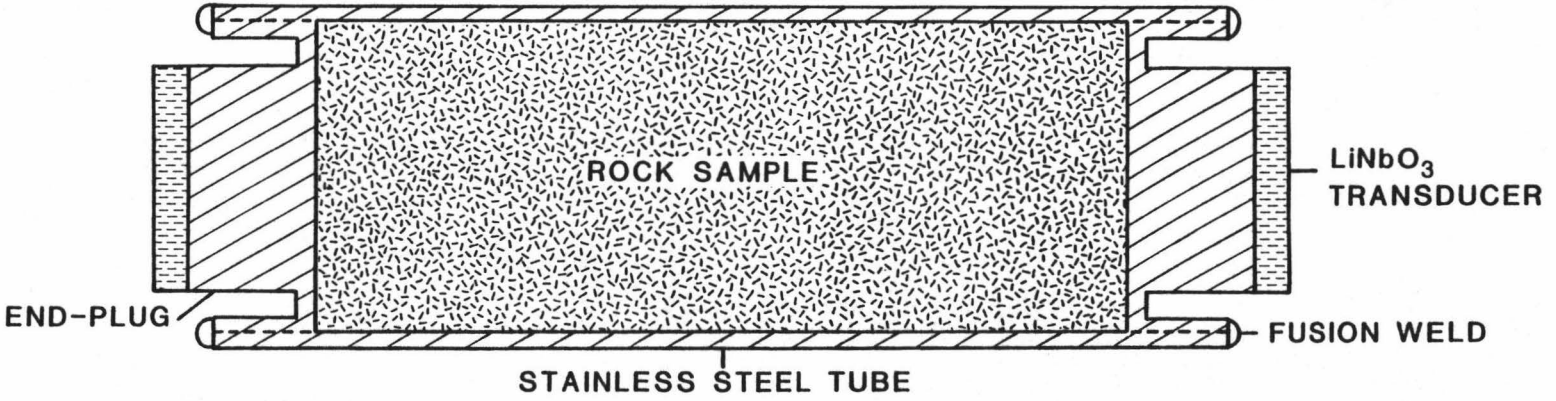

FIGURE 4. High pressure and high temperature sample assemblies

cores and end-plugs were inserted into close fitting, stainless-steel tubes (wall thickness 0.010 cm). To exclude the gas pressure-medium, the assemblies were sealed by low temperature, electron-beam welding (Electrofusion Corporation, Menlo Park, CA) and certified air tight to $1.0 * 10^{-10}$ cm^3 std atm sec^{-1}. Both compressional and shear mode lithium niobate transducers with a resonant frequency of 1-MHz were accoustically bonded to the end-plugs with VHT lacquer (Sperex Corporation) (Figure 4b).

3.2.2 Pressure and Temperature Apparatus

Two Harwood pressure vessels connected to a two-stage intensifier system were used to maintain hydrostatic confining pressure on the prepared samples. For the high pressure experiments a liquid pressure-medium (1 part oil to 10 parts petroleum ether) was used in a 1.0 GPa pressure vessel. For the high temperature experiments, a pressure-medium of high-purity nitrogen gas was used in a water-cooled, 1.5 GPa pressure vessel. Pressures were measured to within 0.2% by a manganin coil exposed directly to the pressure mediums.

Temperatures to 300^{o} C were achieved with a furnace that fit snugly inside the 1.5 GPa pressure vessel. A continuously wound coil of nichrome wire (20 gauge) was equally divided into a two-zone heating element with no gap between the zones. Each zone was independently and manually controlled by a DC-power supply to maintain a minimum temperature gradient across the length of the samples. Temperatures inside the furnace were monitored by three chromel-alumel thermocouples, one in the middle and at each end of the samples. They were in contact

with the sample assemblies. The thermocouples and the digital temperature display (Omega Trendicator) were calibrated to the freezing and boiling points of water. Measured temperatures were probably accurate to within 1.0%.

3.2.3 Velocity Measurements

Velocities were measured in all core samples at room temperature (25° C) for both increasing and decreasing pressure cycles at 0.02 GPa intervals for confining pressures between 0 and 0.1 GPa, at 0.15 GPa, and at 0.2 Gpa intervals between 0.2 and 1.0 GPa. The basalts were subjected to a maximum confining pressure of only 0.3 GPa to prevent collapse of vesicles. The diabase samples were subjected to a maximum confining pressure of 0.5 GPa while the gabbros and peridotites were subjected to a confining pressure of 1.0 GPa. Approximately ten minutes elapsed between readings to allow the temperature of the sample to stabilize at 25° C following a pressure change.

Velocities in samples K2mlb′ and K9mlb′ were measured for increasing and decreasing temperature cycles at intervals of 25° C from 25° C to 300° C. A constant confining pressure of 0.21 GPa, the calculated lithostatic confining pressure on rock sample K9ml, was maintained during all of the high temperature experiments. Each core was seasoned (Christensen, 1979) by slowly cycling the temperature to 300° C and back until the velocity readings were repeatable to at least 0.5%. On the final temperature run, temperatures were increased at the average rate of 2° C min^{-1}. At each temperature setting fifteen minutes was allowed for the rock core to heat evenly throughout.

The direction of particle motion must be considered for propagating shear waves; vertically polarized shear waves occur in the oceanic crust (Ewing et al., 1957). In the cumulate gabbros with apparent planar lamination or cumulate layering, shear velocities parallel to the cumulus textures (cores `b´ and `c´) were measured with particle displacement perpendicular to the textures. Because cores `a´ are perpendicular to the textures, this direction was essentially isotropic to both V_p and V_s and the direction of particle displacement was not a factor.

The pulse transmission technique (Birch, 1960) was used to measure the velocities in the samples. Figure 5 is a schematic diagram of the equipment. A square wave, produced by the pulse generator, is transmitted to the driving transducers of the sample assembly and the mercury column. An elastic wave travels through the sample and the mercury column and is converted back into electrical pulses by the receiving transducers. These electrical pulses are then amplified, filtered, and simultaneously displayed on the oscilloscope. The first arrivals from the mercury column and the sample are aligned on the oscilloscope by adjusting the separation distance of the transducers in the mercury column.

The mercury column was calibrated to: (1) eliminate systematic operator errors in matching the first arrivals, (2) establish absolute velocity values, and (3) eliminate time-delay errors caused by the electronic equipment. Calibration of the mercury column was achieved by adjusting the transducer separation in the mercury column to measure the

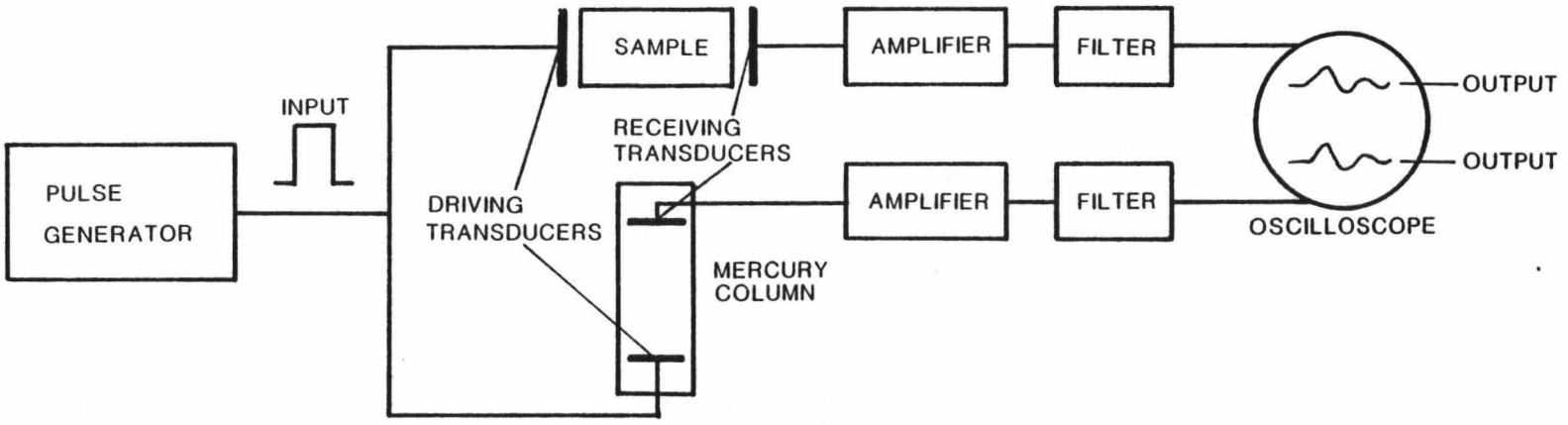

FIGURE 5. Schematic diagram of the pulse transmission equipment

known V_p and V_s (5.07 and 3.08 km sec^{-1}, respectively) in a stainless-steel bar. Because the velocities depend on the type of elastic wave being measured, the system was recalibrated whenever transducers were changed from shear to compressional or vice-versa.

Both V_p and V_s for the high pressure experiments were calculated by:

$$V = \frac{L\, V_m}{L_m * 2.54 \text{ cm in}^{-1}} \text{ , km sec}^{-1}.$$

L (cm) is the measured core length, V_m is the compressional velocity in mercury (1.450 km sec^{-1} at 25° C), L_m (inches) is the separation distance of the transducers in the mercury column, and V (km sec^{-1}) is V_p or V_s in the rock sample.

Both V_p and V_s for the high temperature experiments were calculated by:

$$V = \frac{L}{\frac{L_m * 2.54 \text{ cm in}^{-1}}{V_m} - \frac{L_e}{V_e}} \text{ , km sec}^{-1}.$$

V is V_p or V_s in the rock sample, L_e (cm) is the total measured length of two end-plugs, and V_e is V_p or V_s in the end-plugs at high temperature and pressure. L_e/V_e is the travel-time delay of the steel end-plugs.

To determine the travel-time delay of the steel end-plugs, V_p and V_s were determined as functions of pressure and temperature for a bar of the same material. The results, shown in Figure 6a-b, have been corrected for length changes of the steel bar that were caused by high pressure and temperature effects (discussed below). Initial V_p and V_s at 25° C and atmospheric pressure were determined for the steel bar using the calibrated mercury column and a bench-press velocity table.

V_p and V_s for the steel end-plugs at 0.21 GPa confining pressure and 25° C were read from the experimentally determined velocity-pressure curve of the steel bar (Figure 6a). Using the experimentally determined temperature derivatives of V_p and V_s for the steel bar at 0.21 GPa confining pressure (Figure 6b), V_p and V_s in the steel end-plugs and, subsequently, the travel-time delay of the end-plugs were calculated at each temperature setting.

The velocity data measured by the above procedure were fit by smooth curves. The smoothed data were then corrected for length changes of the rock sample and end-plugs that were caused by high temperature and pressure effects. The length corrected velocities were obtained from the relation:

$$V = V_o \left(\frac{L}{L_o} \right), \text{ km sec}^{-1}.$$

V is the length corrected V_p or V_s, V_o is the measured V_p or V_s at 25° C and atmospheric pressure, L (cm) is the true length of the sample or end-plugs at high pressure or temperature, and L_o is their initial

Figure 6. Length corrected compressional (V_p) and shear (V_s) wave velocities in a bar of stainless-steel (Type 303).

Figure 6a. V_p and V_s as functions of confining pressure at 25° C.

V_{po} (V_p at 25°C) = 5.7472 km sec^{-1}

V_{so} (V_s at 25°C) = 3.1451 km sec^{-1}

$dV_p/dP = 6.15 \pm 0.07 * 10^{-2}$ km sec^{-1} GPa^{-1}

$dV_s/dp = 4.78 \pm 0.08 * 10^{-2}$ km sec^{-1} GPa^{-1}

Figure 6b. V_p and V_s as functions of temperature at 0.21 GPa confining pressure.

$dV_p/dT = -6.62 \pm 0.19 * 10^{-4}$ km sec^{-1} $^oC^{-1}$

$dV_s/dT = -2.86 \pm 0.01 * 10^{-4}$ km sec^{-1} $^oC^{-1}$

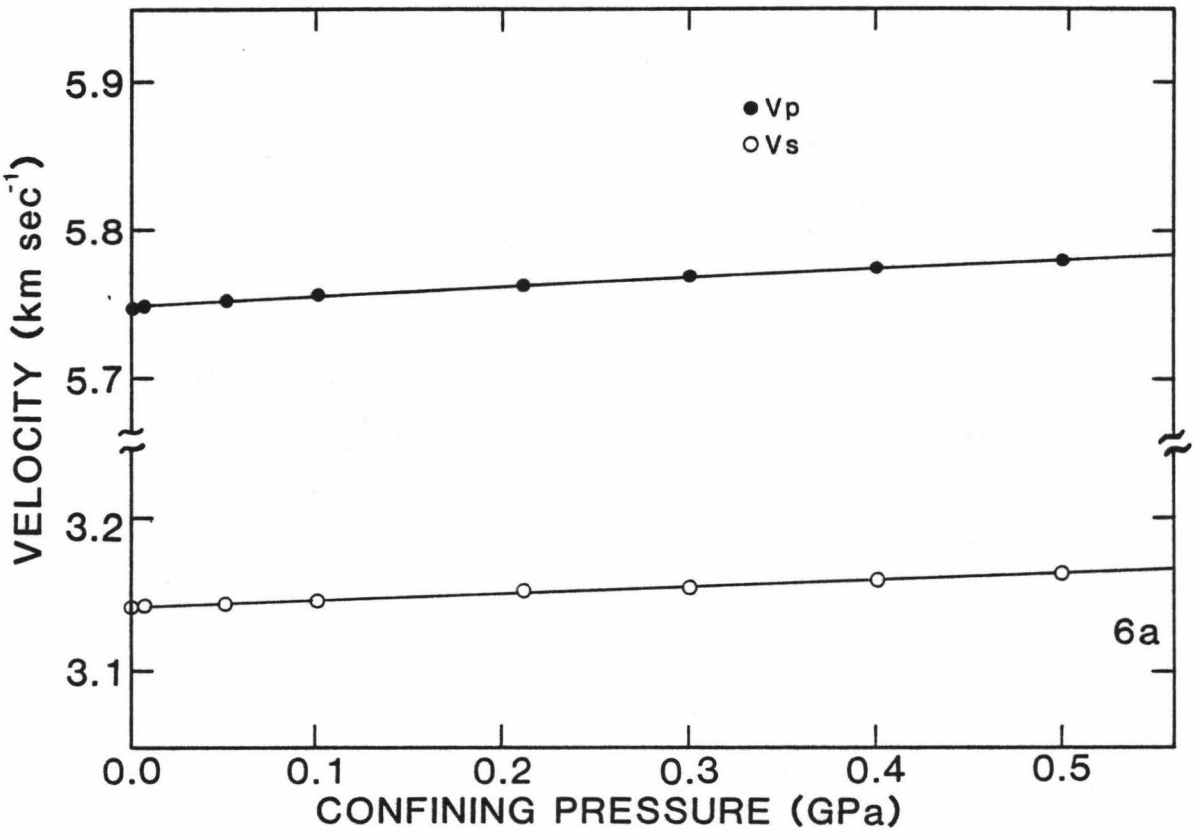
5.9
5.8
5.7
3.2
3.1
VELOCITY (km sec^{-1})
● Vp
○ Vs
6a
0.0
0.1
0.2
0.3
0.4
0.5
CONFINING PRESSURE (GPa)

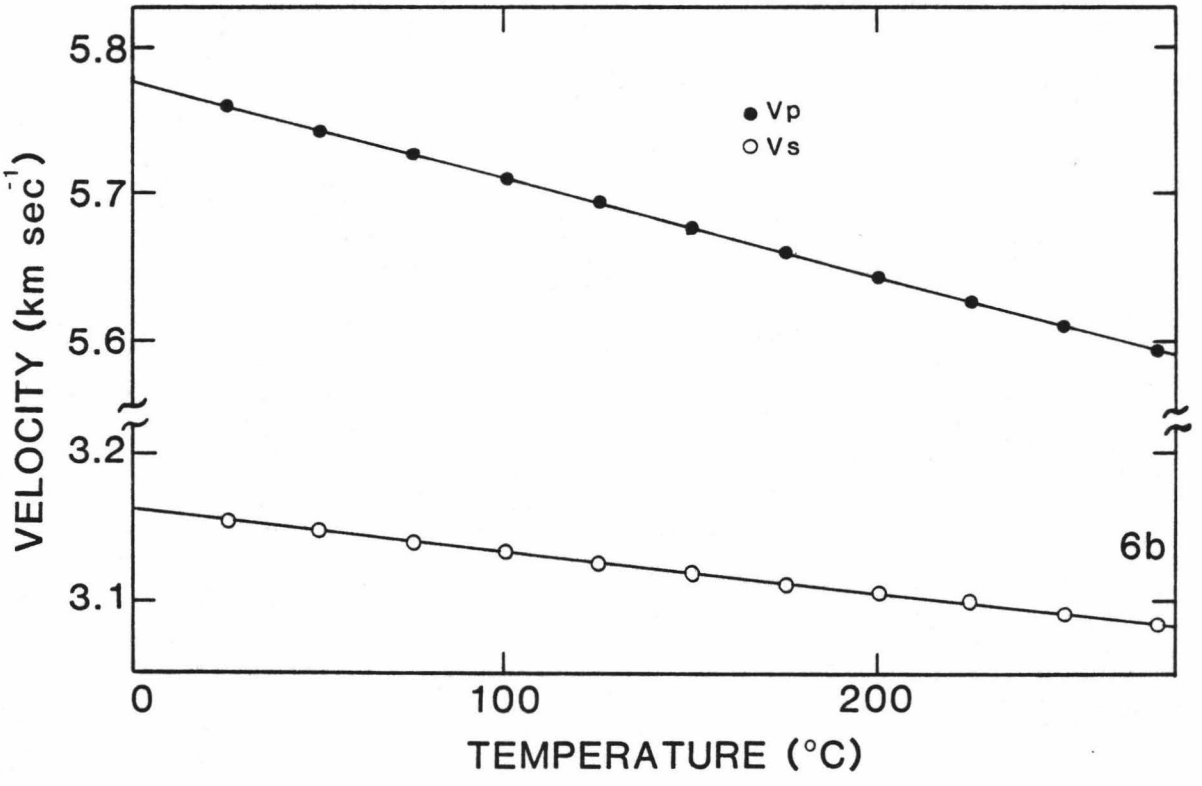
5.8
5.7
5.6
3.2
3.1
VELOCITY (km sec^{-1})
● Vp
○ Vs
6b
0
100
200
TEMPERATURE (°C)

length at 25° C and atmospheric presssure. The length ratio L_o/L was approximated by using Cook's (1957) formula:

$$\frac{L_o}{L} = 1 + \frac{1 + \Delta}{\rho_o} \int_0^P \frac{dP}{3V_p^2 - 4V_s^2} - \frac{1 + \Delta}{3} \int_{T_o}^T \alpha_1 \, dT$$

Δ, the adiabatic isothermal correction (dimensionless), is equal to $\alpha_v \gamma T$, where α_v is the volumetric thermal expansion coefficient, γ is the Gruneisen parameter, and T (°K) is absolute temperature. Since Δ is only 0.005 to 0.010 for gabbroic rocks (Manghnani et al., 1974), it was neglected. ρ_o (g cm^{-3}) is the initial bulk density of the sample. α_1 (cm $°C^{-1}$) is the linear thermal expansion coefficient, for gabbros it is $5.4 * 10^{-6}$ $°C^{-1}$ (Skinner, 1966), while for 303 stainless-steel it is approximately $17.28 * 10^{-6}$ $°C^{-1}$ (Kirby et al., 1972); T (°C) is temperature, T_o is 25° C; and P (GPa) is confining pressure.

After correcting the measured velocities for length changes and calibrating the pulse transmission equipment, the largest source of error in measuring V_p and V_s was the uncertainity of recognizing the first arrivals of the transmitted elastic waves. For the high pressure experiments, both V_p and V_s first arrivals were very sharp. Error is estimated to be 0.5% and 1.0%, respectively, while repeatability of velocities was within 0.1%. For the high temperature experiments V_p first arrivals were less definite while the V_s first arrivals were masked by heavy background noise. The error is estimated to be 1.0% for V_p and 1.5% for V_s while repeatability of velocities was within 0.5%.

3.2.4 Bulk Density

Wet and dry bulk densities of the core samples at atmospheric pressure and 25° C were calculated by the following equation:

$$\rho_i = \frac{4\, M_i}{\pi\, D^2\, L_o} \quad , \text{g cm}^{-3}.$$

ρ_i (g cm^{-3}) is the dry or wet bulk density, M_i (gm) is the dry or wet mass, D and L_o (cm) are the average diameter and length of the core samples. Dry masses were measured for core samples that were oven dried at 50° C for 12 hours. Wet masses were measured for cores that were saturated in distilled water as described earlier. Errors are estimated to be 0.5% due to fractures and isolated pores within the samples, inaccuracies due to averaging core dimensions, the accuracy of measuring equipment, and water evaporation from the core samples. The bulk densities were also corrected for dimension changes at high pressure and temperature by the relation:

$$\rho = \rho_o \left(\frac{L_o}{L} \right)^3 \quad , \text{g cm}^{-3}.$$

ρ_o is the initial bulk density and ρ is the bulk density at high pressure and temperature. L_o/L is the length ratio described previously.

3.2.5 Effective Porosity

The effective porosity of the core samples was calculated by the relation:

$$\phi = \frac{M_w - M_d}{\pi D^2 L_o \rho_w} * 100\%.$$

ϕ(%) is the effective porosity of the core samples, ρ_w is the density of distilled water at 25° C (1.00 g cm^{-3}). Errors, estimated to be 1 to 2%, are discussed in the bulk density section.

4. DISCUSSION OF EXPERIMENTAL RESULTS

4.1 V_p and V_s as Functions of Confining Pressure at 25° C

Uncorrected V_p and V_s that were measured as functions of confining pressure at 25° C in a vesicular metabasalt (OM-342a) are shown in Figure 7. The length corrected velocity data for all of the core samples to 0.3 (metabasalts), 0.5 (metadiabases), and 1.0 (gabbros and peridotites) GPa confining pressures are listed in Appendix A with their lithologies and ambient bulk densities. The length corrections for the velocity data were less than 0.5% at 1.0 GPa confining pressure.

As Birch (1960) has shown, V_p and V_s in rocks increase with increasing confining pressure. The rapid change of velocities below 0.15 GPa (Figure 7) is related to the closure of flat (low aspect ratio) microcracks within the sample (Birch, 1960). At higher confining pressure, flat cracks are essentially closed and velocities change linearly with changing pressure due to the intrinsic properties of the minerals and spherical pores that form the aggregate rock sample (Birch, 1960; Christensen and Salisbury, 1975). The application of hydrostatic confining pressure to the core sample is assumed to reproduce the <u>in situ</u> porosity and crack configuration of the core sample at depth in the oceanic crust.

The dry and saturated curves (Figure 7) demonstrate the effect of fluid phase water on V_p and V_s in a vesicular metabasalt. In the water saturated rock, the water becomes another phase component of the mineral and pore aggregate (Nur and Simmons, 1969). Because V_p is greater in water than in air, V_p below 0.2 GPa confining pressure is appreciably

Figure 7. Compressional (V_p) and shear (V_s) wave velocities as functions of confining pressure in a vesicular metabasalt (OM-342a) when dry and water saturated. (P_p) is pore pressure and (P) is external confining pressure on the core sample.

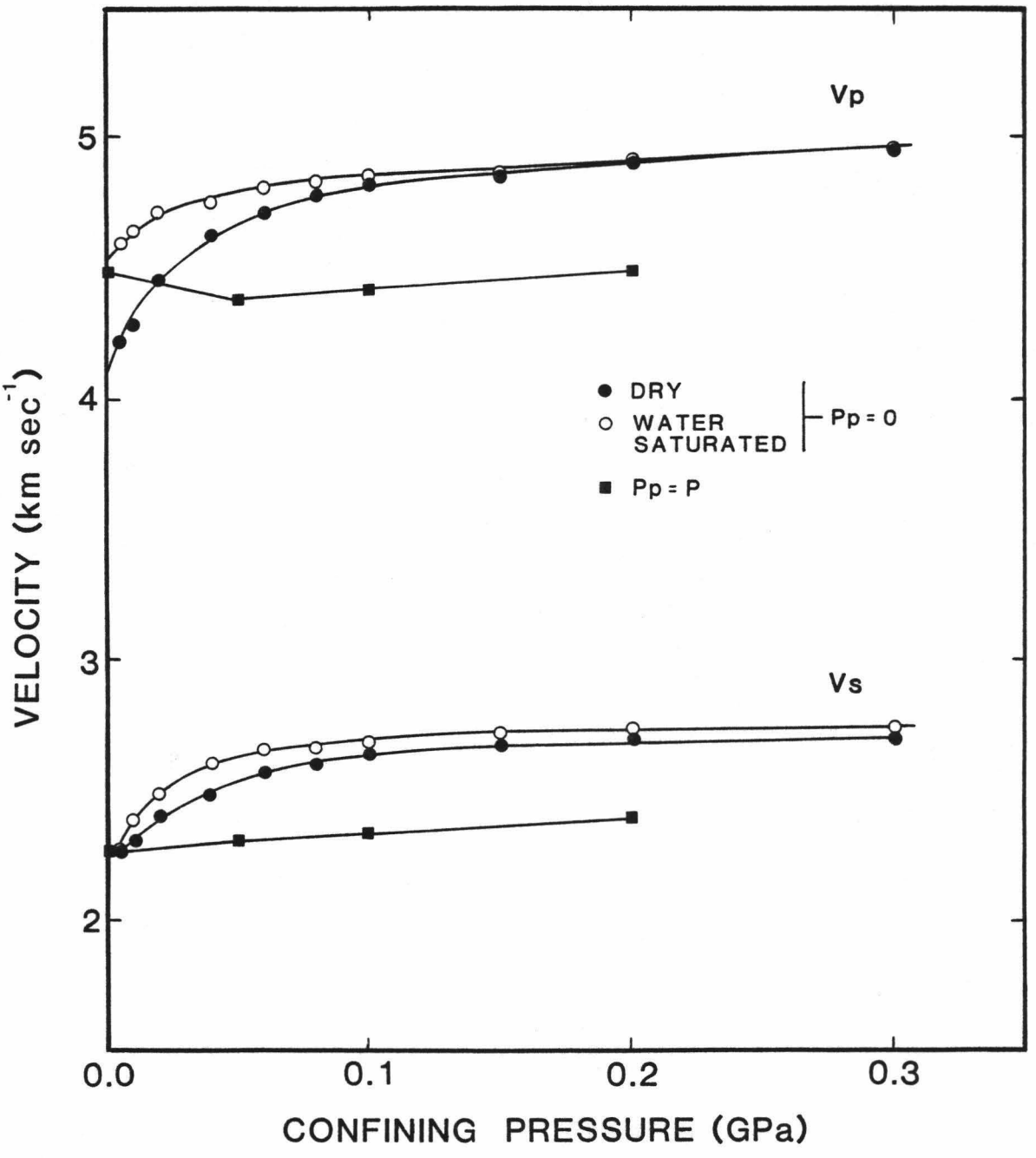
Vp
Vs
DRY
WATER SATURATED
Pp = 0
Pp = P
VELOCITY (km sec^{-1})
CONFINING PRESSURE (GPa)
5
4
3
2
0.0
0.1
0.2
0.3

greater in the water saturated sample; above 0.2 GPa V_p in the wet and dry samples is identical. Because shear waves travel neither in air nor water, V_s is essentially unaffected by water saturation.

Fluid phase water is present as seawater passively filling pores, joints, and fractures of the upper oceanic crust (Nur and Simmons, 1969; Christensen and Salisbury, 1975) and as hydrothermal fluids circulating to greater depths in the oceanic crust (Spooner, 1979; Christensen and Salisbury, 1975; Lister, 1972; Cann, 1979). These conditions are duplicated in the laboratory by saturating the metabasalts, metadiabases, and massive metagabbros of the Samail ophiolite as described earlier.

The effect of pressure on the fluid phase water (pore pressure) is also shown in Figure 7. When water that is saturating the core sample is not allowed to escape from the flat microcracks and pores of the rock as confining pressure increases, pore pressure (P_p) on the water is equivalent to the confining pressure (P) on the core sample. As a result the microcracks do not close and velocities remain essentially constant with changing confining pressure. However, when the water filling the microcracks and pores of the core sample can escape as confining pressure increases, pore pressure is less than confining pressure, microcracks close, and V_p and V_s vary according to the intrinsic properties of the core sample. Pore pressure within the oceanic crust probably varies between lithostatic and hydrostatic pressure (Brace, 1971; Christensen and Salisbury, 1975). These pore pressure conditions are approximated in the laboratory by sealing all

core samples from the pressure mediums and by placing screen wire between the copper jackets and the saturated cores as described earlier. The void spaces of the screen wire provide a zero-pressure reservoir for the pore fluids.

4.2 V_p and V_s as Functions of Temperature at 0.21 GPa Confining Pressure

The temperature dependence of V_p and V_s in a massive metagabbro (K2m1) and a cumulate gabbro (K9m1) to 300° C at 0.21 GPa confining pressure is shown in Figure 8. The data have been smoothed where velocity hysteresis (< 1.0%) was present and subsequently corrected for length changes as described earlier. Length corrections to the velocity data at 300° C were less than 0.5%

Velocity hysteresis is the difference between velocity values that are measured while increasing confining pressure or temperature and those values that are measured while decreasing confining pressure or temperature. To reduce velocity hysteresis in the high temperature experiments, each sample was subjected to three heating and cooling cycles at constant pressure; this procedure stabilizes the elastic behavior of rock samples by preventing the formation of new thermal cracks within the cycled temperature range (Ramananantoandro and Manghnani, 1978; Christensen, 1979; Yong and Wang, 1980).

Although temperatures at the ends of the samples were always within 0.1 to 0.5° C of each other, low temperatures at the center of the furnace created excessive temperature gradients along the length of the samples. The temperature gradients increased from 2° C cm^{-1} at 75° C to

Figure 8. Compressional (V_p) and shear (V_s) wave velocities as functions of temperature at 0.21 GPa confining pressure in a massive metagabbro (K2ml) and a cumulate gabbro (K9ml).

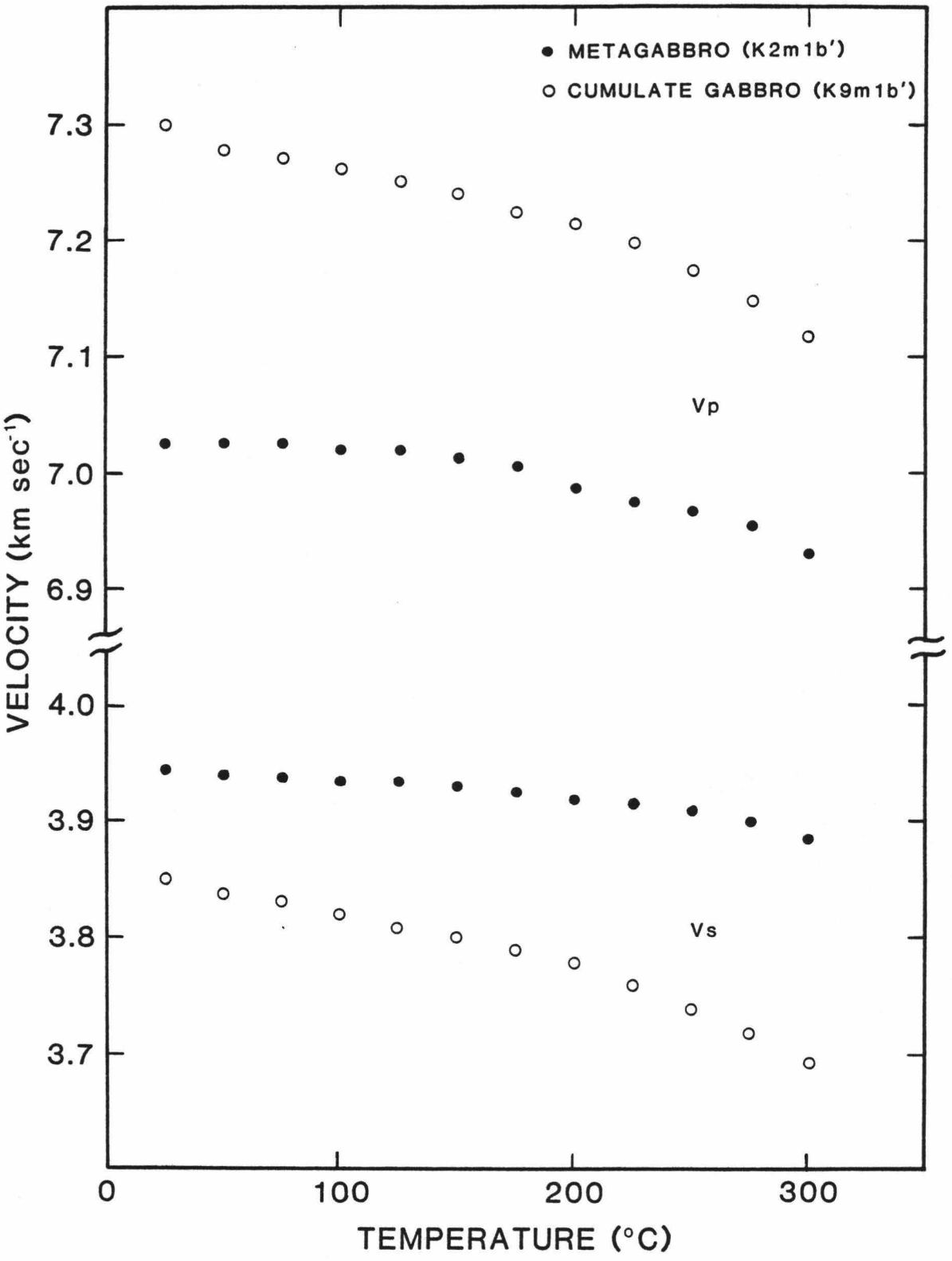
METAGABBRO (K2m1b')
CUMULATE GABBRO (K9m1b')
Vp
Vs
VELOCITY (km sec⁻¹)
7.3
7.2
7.1
7.0
6.9
4.0
3.9
3.8
3.7
0
100
200
300
TEMPERATURE (°C)

16^{o} C cm^{-1} at 300^{o} C. When the ends of the samples were 300^{o} C, their centers were 29^{o} C cooler. For this reason the data were used only to determine the temperature derivatives of the velocities. Because the velocities are plotted as functions of the highest measured temperatures, their temperature derivatives are minimum values.

In Figure 8 velocities are seen to decrease linearly as temperature increases from 25^{o} C to 200^{o} C. At temperatures above 200^{o} C, grain-boundary cracks formed by the differential thermal expansion of mineral grains overcome the confining pressure and cause velocities to decrease non-linearly (Christensen, 1979). Since metamorphic reactions and viscous flow at crustal temperatures and pressures over geologic time would prevent open grain-boundary cracks (Christensen, 1979), the linear sections probably represent the <u>in situ</u> effect of temperature on crustal gabbroic rocks.

Temperature derivatives of V_p and V_s for the gabbros, calculated by a least squares method for the linear portion of the velocity-temperature data are listed in Table 1. Birch (1958) found that for gabbros dV_p/dT values ranged widely from -3.8 to $-10.7 * 10^{-4}$ km sec^{-1} $^{o}C^{-1}$. Christensen (1979) found dV_p/dT for a Mid-Atlantic Ridge gabbro to be $-5.7 * 10^{-4}$ km sec^{-1} $^{o}C^{-1}$ between 25 and 300^{o} C at 0.2 GPa confining pressure. Kroenke et al. (1976) found dV_p/dT for a clinopyroxene-gabbro to be $-6.0 * 10^{-4}$ km sec^{-1} $^{o}C^{-1}$ from 25 to 100^{o} C at 0.3 GPa. Lin and Wang (1980), including the non-linear portion of their velocity-temperature data between 20 and 400^{o} C at 0.5 GPa, determined dV_p/dT for a hornblende-gabbro and an olivine-gabbro to be

TABLE 1

Comparison of Temperature Derivatives of V_p and V_s for Gabbroic Rocks ($* 10^{-4}$ km sec^{-1} $^oC^{-1}$)

Rock Type	Temperature Range (^oC)	Confining Pressure (GPa)	dV_p/dT	dV_s/dT	Reference
Diabase			-1.91 ± 0.36[a]	-1.18 ± 0.10[a]	
Transitional Gabbro			-4.41 ± 0.18[a]	-4.24 ± 0.08[a]	
High-Level Gabbro hb-cpx Gabbro (K2m1b′)	25-200	0.21	-1.91 ± 0.36	-1.18 ± 0.10	This study
Cumulate Gabbro ol-cpx Gabbro (K9m1b′)	25-200	0.21	-4.41 ± 0.18	-4.24 ± 0.08	This study
Gabbros			-3.8 to -10.7		Birch (1958)
Mid-Atlantic Ridge Gabbro	25-300	0.20	-5.70		Christensen (1979)
Papua ophiolite cpx-Gabbro	25-100	0.30	-6.00		Kroenke et al. (1976)
hb-Gabbro	20-400	0.50	-8.89		Lin and Wang (1980)
ol-Gabbro	20-400	0.50	-14.00		Lin and Wang (1980)
Norite	20-500	0.60	-1.73 ± 0.2	-1.49 ± 0.1	Kern and Richter (1981)
Peridotite	20-500	0.60	-4.94 ± 0.2[a]	-3.93 ± 0.3[a]	Kern and Richter (1981)

[a] Assumed temperature derivatives of V_p and V_s used in this study to adjust the velocities that were measured as functions of high pressure at 25° C for <u>in situ</u> temperatures.

-8.89 and $-14.0 * 10^{-4}$ km sec^{-1} $^{o}C^{-1}$, respectively. Likewise Kern and Richter (1981) used the non-linear section of their velocity-temperature data between 20 and 500° C at 0.6 GPa to calculate dV_p/dT and dV_s/dT values of -1.73 ± 0.2 and $-1.49 \pm 0.1 * 10^{-4}$ km sec^{-1} $^{o}C^{-1}$, respectively, for a norite. They were the first to measure dV_s/dT for rocks.

The temperature derivatives of V_p and V_s for the cumulate gabbro (K9ml) and the massive metagabbro (K2ml) appear to be within the range of experimentally determined values for other mafic rocks. Because the sample assemblies were gas-tight and the velocity-temperature curves were reproducible to within 1.0%, the dV_p/dT and dV_s/dT values that were determined for the massive metagabbro (K2ml) and the cumulate gabbro (K9ml) in this study are considered real.

The difference between the temperature derivatives of V_p and V_s for the two gabbros may be due to the differences in their olivine content and rock textures. The cumulate gabbro (K9ml) with the greater olivine content (6.0%) and only incipient alteration, has larger temperature derivatives of V_p and V_s than the metagabbro (K2ml) in which extensive alteration has completely replaced minor olivine with pseudomorphs of hematite and fibrous amphibole and clinopyroxene by uralite. Although Lin and Wang (1980) suggested that secondary minerals cause greater temperature derivatives of velocity, the data presented here suggest that olivine content is also an important factor. The data support Christensen's (1979) suggestion that rocks with euhedral mineral grains (e.g. the cumulate gabbro, K9ml, with euhedral plagioclase grains) have

greater temperature derivatives of velocity than rocks with anhedral, interlocking grains (e.g. the massive metagabbro, K2ml).

Table 1 lists the temperature derivatives of V_p and V_s that were used in this thesis to correct the measured velocities for <u>in situ</u> temperature effects. The sheeted dikes and high-level gabbros with anhedral grains and metamorphic assemblages were assumed to have temperature derivatives of V_p and V_s that are comparable to those of the massive metagabbro (K2ml). The transitional and layered gabbros with fresh olivine and euhedral plagioclase grains probably have temperature derivatives of V_p and V_s that are comparable to those of the cumulate gabbro (K9ml). The temperature derivatives of V_p and V_s that were used to correct the measured velocities for temperature effects in the harzburgite tectonites were assumed from Kern and Richter's (1981) data for a peridotite. Because temperature corrections are less than 1.0%, no attempt was made to correct the measured velocities in the Samail basalts.

4.3 <u>In Situ</u> V_p and V_s in the Samail Ophiolite

The measured V_p and V_s data, corrected for length changes, are presented in Appendix B for each core sample at the calculated <u>in situ</u> lithostatic confining pressure and temperature within the Samail ophiolite. Also listed are Poisson's ratio, bulk density, stratigraphic position, and lithology of each core sample. The velocities were determined from the velocity-pressure plots, discussed earlier, at the <u>in situ</u> lithostatic confining pressure on each rock sample. Lithostatic confining pressure was calculated by the relation:

$$P = (\rho' \; g \; Z * 10^{-10}) + 0.05 \quad , \text{GPa.}$$

P (GPa) is the lithostatic confining pressure, ρ' (g cm^{-3}) is the average bulk density of the overlying rocks (ρ' = 2.81 for the volcanic member, 2.86 for the sheeted dike complex, 2.96 for the high-level gabbro, 2.98 for the transitional gabbro, and 2.93 for the layered gabbro), g is acceleration due to gravity (980 cm sec^2), Z (cm) is the thickness of the overlying rock column, and 0.05 GPa is the average hydrostatic pressure due to seawater and sediments.

The velocities were then adjusted for <u>in situ</u> temperatures by the relation:

$$V_c = V + \left(\frac{dV}{dT}\right)(T - 25^{o}\ C) \quad , \text{km sec}^{-1}.$$

V_c is the <u>in situ</u> V_p or V_s, V is the velocity at 25° C that was determined from the velocity-pressure plots, dV/dT (km sec^{-1} $^{o}C^{-1}$) is the appropriate temperature derivative of V_p or V_s, and T is the <u>in situ</u> temperature. T was calculated assuming a constant geothermal gradient of 35° C km^{-1} in the Samail ophiolite before its detachment from the upper mantle.

Figures 9 and 10 present the <u>in situ</u> V_p, V_s, bulk density, effective porosity, and Poisson's ratio data for each core sample as functions of stratigraphic position, lithology, and metamorphic assemblages in the Samail ophiolite. Poisson's ratio is discussed later. The figures suggest that V_p, V_s, and bulk density continuously vary with depth in the Samail ophiolite. V_p, V_s, and bulk density

Figure 9. In situ compressional (V_p) and shear (V_s) wave velocities, bulk density (ρ), effective porosity (ϕ), and Poisson's ratio (σ) as functions of depth in the Wadi Gideah East section of the Samail ophiolite. V_p, V_s, and ρ have been corrected for length changes due to high temperature and pressure effects. The open circles are the values that were measured when pore pressure (P_p) was equivalent to confining pressure (P).

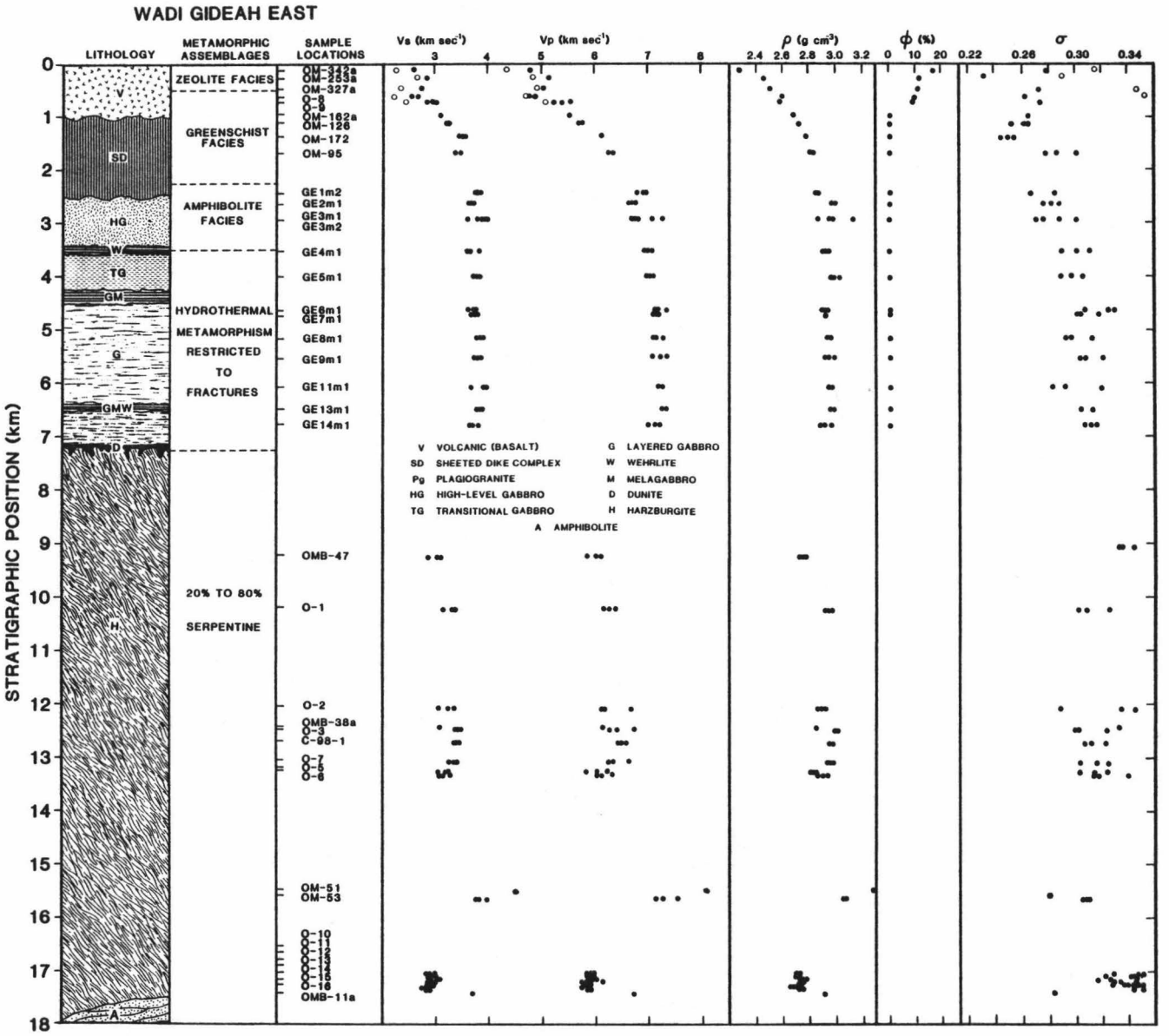
WADI GIDEAH EAST
LITHOLOGY
METAMORPHIC ASSEMBLAGES
SAMPLE LOCATIONS
Vs (km sec⁻¹)
Vp (km sec⁻¹)
ρ (g cm³)
ϕ (%)
σ
STRATIGRAPHIC POSITION (km)
ZEOLITE FACIES
GREENSCHIST FACIES
AMPHIBOLITE FACIES
HYDROTHERMAL METAMORPHISM RESTRICTED TO FRACTURES
20% TO 80% SERPENTINE
V VOLCANIC (BASALT)
SD SHEETED DIKE COMPLEX
Pg PLAGIOGRANITE
HG HIGH-LEVEL GABBRO
TG TRANSITIONAL GABBRO
A AMPHIBOLITE
G LAYERED GABBRO
W WEHRLITE
M MELAGABBRO
D DUNITE
H HARZBURGITE

Figure 10. In situ compressional (V_p) and shear (V_s) wave velocities, bulk density (ρ), and Poisson's ratio (σ) as functions of depth in the Wadi Kadir section of the Samail Ophiolite. V_p, V_s, and ρ have been corrected for length changes due to high temperature and pressure effects.

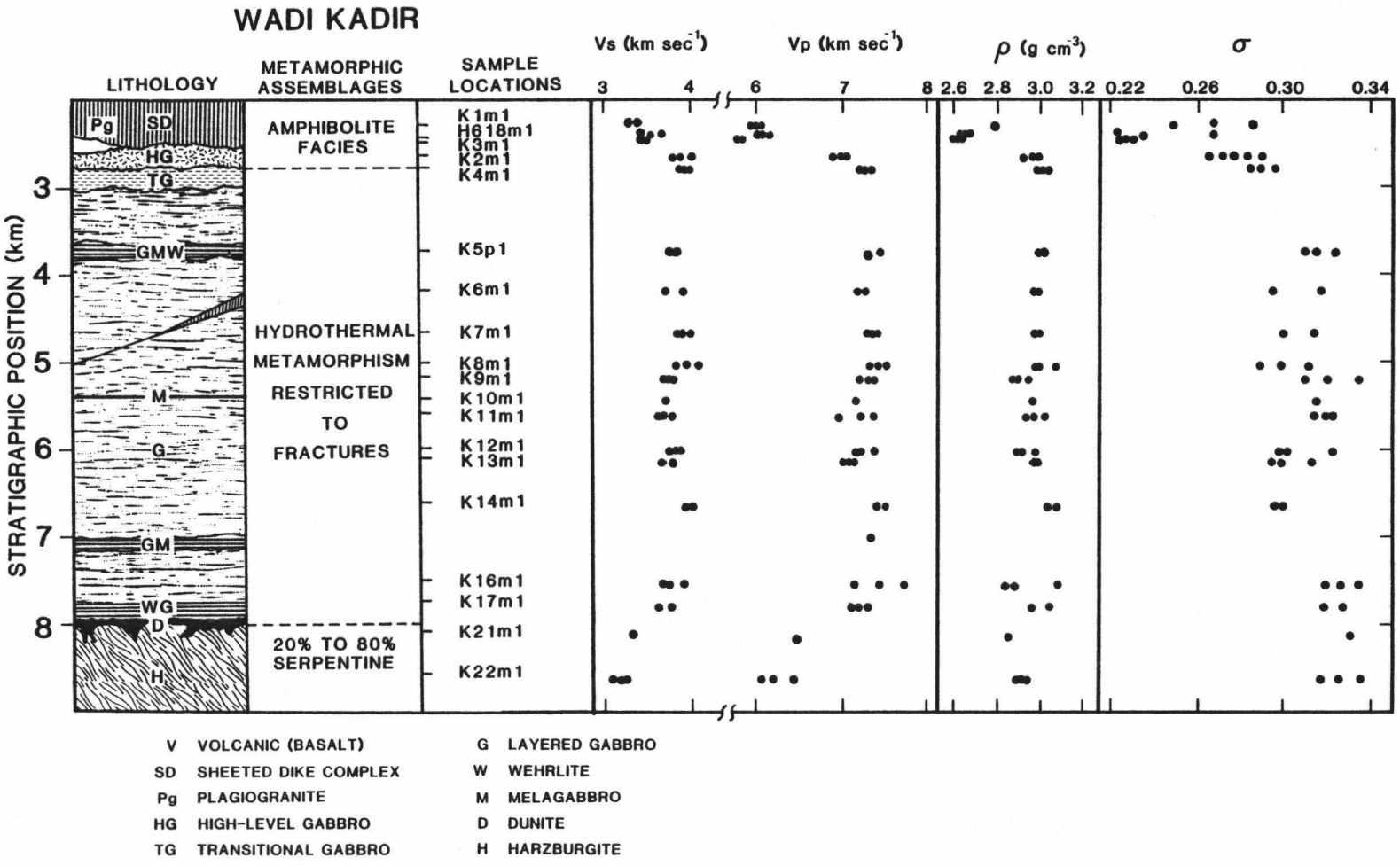
WADI KADIR
LITHOLOGY
METAMORPHIC ASSEMBLAGES
SAMPLE LOCATIONS
Vs (km sec⁻¹)
Vp (km sec⁻¹)
ρ (g cm⁻³)
σ
STRATIGRAPHIC POSITION (km)
Pg
SD
HG
TG
GMW
M
G
GM
WG
D
H
AMPHIBOLITE FACIES
HYDROTHERMAL METAMORPHISM RESTRICTED TO FRACTURES
20% TO 80% SERPENTINE
K1m1
H618m1
K3m1
K2m1
K4m1
K5p1
K6m1
K7m1
K8m1
K9m1
K10m1
K11m1
K12m1
K13m1
K14m1
K16m1
K17m1
K21m1
K22m1
V VOLCANIC (BASALT)
SD SHEETED DIKE COMPLEX
Pg PLAGIOGRANITE
HG HIGH-LEVEL GABBRO
TG TRANSITIONAL GABBRO
G LAYERED GABBRO
W WEHRLITE
M MELAGABBRO
D DUNITE
H HARZBURGITE

increase rapidly to depths of 3.0 to 3.5 km in the Wadi Kadir and Wadi Gideah East sections, respectively, and then slowly increase or remain constant to depths of 7.0 to 8.0 km. Due to the serpentenization of the harzburgite tectonites, major low velocity and low density discontinuities are apparent at the crust-mantle contact. Figures 9 and 10 demonstrate the effects of mineralogy (both metamorphic and igneous), bulk density, effective porosity, and lithostatic confining pressure on V_p and V_s in ancient oceanic crustal rocks. V_p, V_s, and bulk density trends through the sections parallel each other. Their relationship in each lithologic member of the Samail ophiolite is discussed below.

Volcanic member:

The velocity data for this member show considerable scatter due to the variable alteration and textures of the metabasalts. Generally, the member is characterized by initial low velocities that increase rapidly to 0.5 km depth, slowly increase for several hundred meters, and again increase to the base of the unit at a depth of 1.0 km. V_p and V_s vary from 4.8 and 2.6 km sec^{-1} to 5.5 and 3.1 km sec^{-1}, respectively, when pore pressure is zero; and from 4.4 and 2.3 km sec^{-1} to 5.5 and 3.1 km sec^{-1}, respectively, when pore pressure equals confining pressure. Effective porosity of the metabasalts, present as vesicles that are partially filled with secondary minerals (primarily calcite) and fractures, varies from 0.1 to 17.1%. The effective porosity also decreases with depth in the same general manner (Figure 9) that velocities increase with depth. Bulk density increases rapidly with depth from 2.28 to 2.68 g cm^{-3}.

Although V_p and V_s were measured in only six metabasalt samples from the Samail ophiolite, the data presented in Figure 11 suggest that effective porosity is an important factor controlling V_p and V_s in the metabasalts at the low lilthostatic confining pressures appropriate to the upper 0.5 km of the Samail ophiolite (0.05 to 0.07 GPa). The bulk density of the Samail metabasalts tends to increase as their effective porosity decreases (Figure 11b). V_p and V_s likewise tend to increase as the effective porosity of the metabasalts decreases (Figure 11a). Schreiber and Fox (1977) found that V_p and V_s at 0.1 GPa confining pressure in vesicular basalts from the Mid-Atlantic Ridge increased as the porosity of the basalts decreased. Furthermore they suggested that fluid pore pressure in the upper 0.5 km of the oceanic crust should significantly affect seismic velocities in oceanic basalts.

An attempt was made in this study to determine the effect of high pore pressure on V_p and V_s in the Samail metabasalts. The results, shown in Figure 11a, are inconclusive due to the large degree of scatter in the data, the small number of metabasalt samples, the limited range of the effective porosity of the metabasalts, and the low accuracy of the effective porosity measurements. Nevertheless, the data in Figure 11a suggest that V_p and V_s in the Samail metabasalts are as much as 9% and 13% lower, respectively, when pore pressure is equivalent to confining pressure than when pore pressure is less than confining pressure. These results support Spudich and Orcutt's (1980a) contention that porosity and pore pressure are two of the many poorly determined variables that control seismic velocities in the upper oceanic crust.

Figure 11. Compressional (V_p) and shear (V_s) wave velocities (Figure 11a) and mean bulk density (ρ)(Figure 11b) of the Samail basalts as functions of their effective porosity; when pore pressure (P_p) is zero and when pore pressure is equivalent to confining pressure (P).

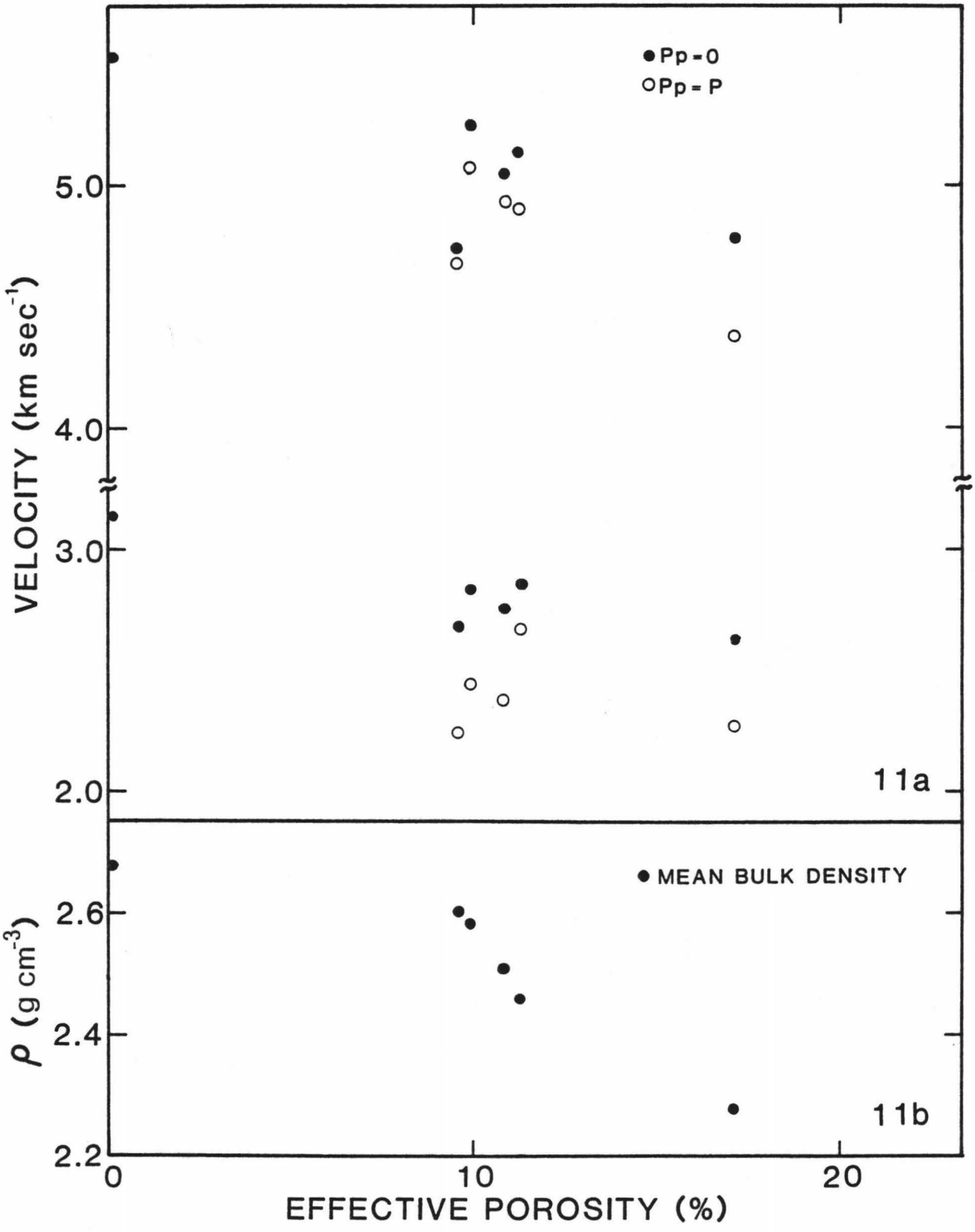
● Pp = 0
○ Pp = P
VELOCITY (km sec⁻¹)
5.0
4.0
3.0
2.0
11a
● MEAN BULK DENSITY
ρ (g cm⁻³)
2.6
2.4
2.2
11b
0
10
20
EFFECTIVE POROSITY (%)

Sheeted Dike complex:

V_p and V_s increase from 5.7 and 3.2 km sec^{-1} in the uppermost sheeted dikes to 6.9 and 3.8 km sec^{-1}, respectively, at their base. Birch (1961) showed that velocities in silicates (crustal rocks) with similar chemical compositions are linearly related to the bulk density of the rocks. Therefore velocities in the sheeted dikes increase downward due to increasing metamorphic grade (greenschist to lower amphibolite facies) and increasing bulk density (2.7 to 2.9 g cm^{-3}) of the metadiabases with depth. At the base of the sheeted dikes in the Wadi Kadir section V_p and V_s of less than 6.0 and 3.5 km sec^{-1}, respectively, are measured in the plagiogranites (K3m1 and H618m1) and the metadiabase (K1m1). These low values are caused by the presence of quartz in the plagiogranites (20% by modal percentage) and the metadiabase (4% by modal percentage).

Gabbro member:

In the gabbro member bulk density varies from approximately 2.9 g cm^{-3} in the high-level gabbro to 3.1 g cm^{-3} near the base of the layered gabbro at depths of 7.0 to 8.0 km. Within the same depth interval measured V_p values vary from 6.7 to 7.35 km sec^{-1} while V_s values vary from 3.8 to 4.0 km sec^{-1}.

A wide range of velocities are observed in the high-level gabbro unit. V_p that were measured in a metadiabase (GE3m2) and a massive metagabbro (GE2m1) from the contact zone marking the transition from metadiabases to massive metagabbros are lower (approximately 6.7 km sec^{-1}) than the average V_p of 7.0 km sec^{-1} that is observed in the

metagabbros below the contact zone. The low V_p is caused by the presence of quartz in the metadiabase (4% by modal percentage) and metagabbro (1% by modal percentage). The presence of quartz in these samples is probably related to the occurrence of intrusive late-stage differentiates near the sheeted dike-gabbro contact. In the high-level gabbro below the sheeted dike-gabbro contact zone, V_p and V_s increase with depth from 6.8 and 3.8 km sec^{-1} to 7.1 and 3.9 km sec^{-1}, respectively, due to the downward increasing bulk density (ρ = 2.8 to 3.0 g cm^{-3}) and metamorphic grade (lower to upper amphibolite facies) of the metagabbros.

In the transitional and layered gabbro units upper amphibolite facies assemblages are restricted to fractures and joints and bulk density is essentially constant (ρ = 2.9 to 3.0 g cm^{-3}) with depth. Therefore the variation of velocities with depth in the fresh cumulate gabbros is primarily controlled by the variation with depth of the relative content of the primary cumulus minerals in the samples. Petrographic modal analyses of the Samail rock samples are listed in Appendix C. The range of velocities that are shown in Figures 9 and 10 for each cumulate gabbro is caused by the velocity anisotropy of the rock samples.

Figure 12 shows: (1) the relative contents (by modal percentage) of hornblende, olivine, clinopyroxene, and plagioclase in the gabbro samples as functions of depth in the gabbro member, and (2) the relative effect of these minerals on the mean velocities and Poisson's ratio (discussed later) of the gabbro samples. This figure strikingly

Figure 12. Mean compressional (V_p) and shear (V_s) wave velocities and Poisson's ratio (σ) in the gabbro member of the Wadi Gideah East and Wadi Kadir sections of the Samail ophiolite. These values are plotted as functions of their stratigraphic position and major mineral content (by modal percentage); hb is hornblende, cpx is clinopyroxene, ol is olivine, and plag is plagioclase. Hornblende is the sum of igneous and metamorphic phases; the other minerals represent cumulus phases only.

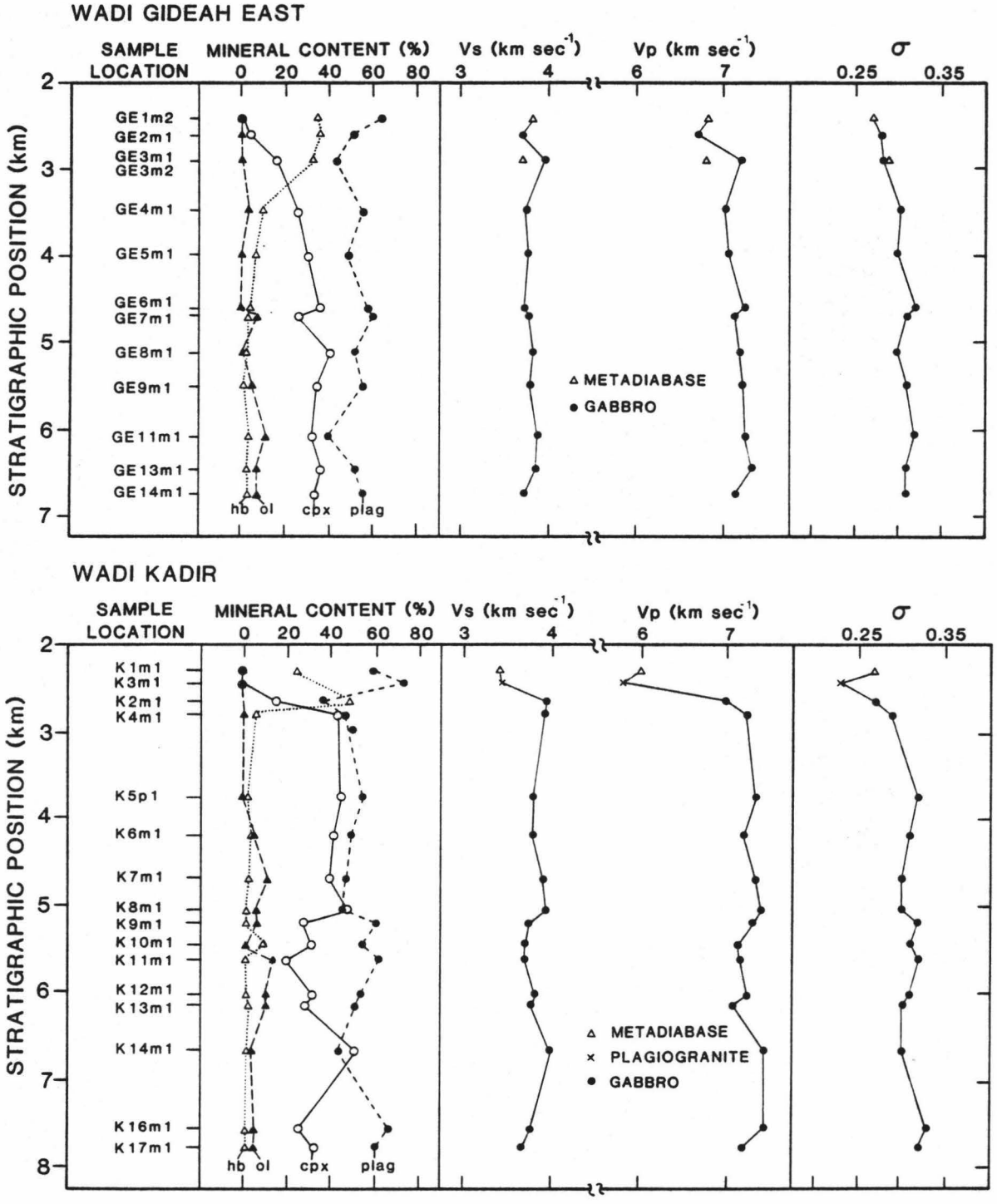
WADI GIDEAH EAST
SAMPLE LOCATION
MINERAL CONTENT (%)
0 20 40 60 80
Vs (km sec⁻¹)
3 4
Vp (km sec⁻¹)
6 7
σ
0.25 0.35
STRATIGRAPHIC POSITION (km)
2 3 4 5 6 7
GE1m2
GE2m1
GE3m1
GE3m2
GE4m1
GE5m1
GE6m1
GE7m1
GE8m1
GE9m1
GE11m1
GE13m1
GE14m1
hb ol cpx plag
△ METADIABASE
● GABBRO
WADI KADIR
SAMPLE LOCATION
MINERAL CONTENT (%)
0 20 40 60 80
Vs (km sec⁻¹)
3 4
Vp (km sec⁻¹)
6 7
σ
0.25 0.35
STRATIGRAPHIC POSITION (km)
2 3 4 5 6 7 8
K1m1
K3m1
K2m1
K4m1
K5p1
K6m1
K7m1
K8m1
K9m1
K10m1
K11m1
K12m1
K13m1
K14m1
K16m1
K17m1
hb ol cpx plag
△ METADIABASE
× PLAGIOGRANITE
● GABBRO

illustrates the mineralogical differences between the massive metagabbros and the underlying fresh cumulate gabbros. The metagabbro samples are characterized by abundant metamorphic hornblende (10 to 40%) that is predominantly present as amphibolite facies assemblages of uralite and green to brown hornblende replacing clinopyroxene grains. In the fresh cumulate gabbros only insignificant amounts of igneous and metamorphic hornblende are found. These mineralogical variations reflect the range of prevasive hydrothermal metamorphism in the ophiolite.

Figure 12 indicates that V_p and V_s in gabbroic rocks are not significantly affected by the presence of amphibolite facies assemblages. Olivine and plagioclase contents are seen to primarily control the relative V_p and V_s in the gabbro samples. When plagioclase content increases, V_p and V_s tend to decrease. High plagioclase content (56 to 65%) in the lower cumulate gabbros appears to cause the velocity inversion at the base of the layered gabbro. The overall increase of V_p and V_s with depth in the cumulate gabbros can be explained by the increase of olivine content with depth (0 to 8.0%) in the gabbro member.

Harzburgite Tectonites:

Except for harzburgite (OM-51), the peridotites in this study are extensively serpentenized (20 to 87%). Olivine is replaced by lizardite, clinochrysotile, brucite, magnetite, and talc (Boudier and Coleman, 1981). Harzburgite (OM-51) has only trace serpentine along grain boundaries.

Figure 13 shows that as the percentage of serpentine in the harzburgite tectonites decreases, V_p, V_s, and bulk density increase. The vertical bars indicate the range of V_p and V_s that were measured for each core sample while only mean bulk density is plotted. Due to the preferred orientation of olivine in these samples (discussed later), the range of velocities (velocity anisotropy) is great when core samples parallel the crystallographic directions of the aligned olivine grains.

Because harzburgite tectonite (OM-51) has no velocity anisotropy or serpentine, its measured V_p, V_s, and bulk density (8.14 km sec^{-1}, 4.52 km sec^{-1}, 3.29 g cm^{-3}, respectively) probably represent the average <u>in situ</u> values for unserpentenized upper mantle peridotites. The velocities and bulk density compare closely with those measured in the laboratory by Christensen (1966) for Hawaiian peridotites (V_p = 8.1 to 8.2 km sec^{-1}, V_s = 4.4 to 4.6 km sec^{-1}, and ρ = 3.29 g cm^{-3}) and those measured by Kroenke et al. (1976) for harzburgites from the Papua New Guinea ophiolite (V_p = 7.5 to 8.1 km sec^{-1}, V_s = 3.6 to 4.3 km sec^{-1}, and ρ = 3.16 to 3.23 g cm^{-3}). The velocities also fall within the range of values (V_p = 7.8 to 8.8 km sec^{-1}, V_s = 4.4 to 4.6 km sec^{-1}) measured by marine seismic refraction methods for the upper mantle (Fowler, 1978; Helmberger and Morris, 1970; Spudich and Orcutt, 1980b). Because serpentenization of the peridotite member of the Samail ophiolite probably occurred after its detachment from the upper mantle (Boudier and Coleman, 1981), the measured velocities and bulk density of harzburgite sample (OM-51) are used in the velocity-depth and bulk density profiles of the Ibra area of the Samail ophiolite.

Figure 13. Compressional (V_p) and shear (V_s) wave velocities and mean bulk density (ρ) as functions of the percentage of serpentine in the harzburgite tectonites of the Samail ophiolite.

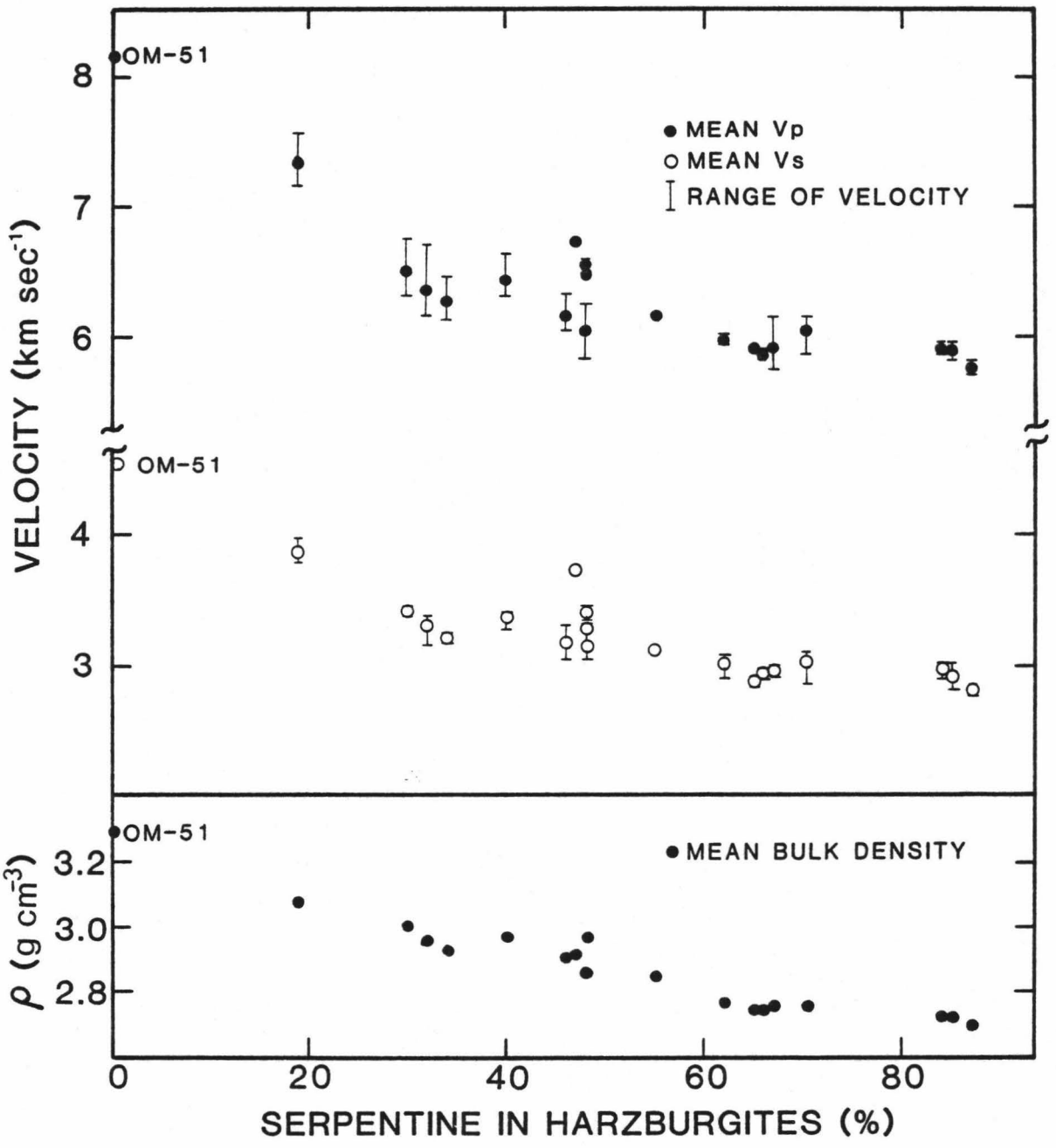
OM-51
8
7
6
MEAN Vp
MEAN Vs
RANGE OF VELOCITY
VELOCITY (km sec⁻¹)
OM-51
4
3
OM-51
3.2
3.0
2.8
MEAN BULK DENSITY
ρ (g cm⁻³)
0
20
40
60
80
SERPENTINE IN HARZBURGITES (%)

4.4 Poisson's Ratio in the Samail Ophiolite

Christensen (1966, 1972a) has shown that the ratio V_p/V_s, and thus Poisson's ratio (ρ), is a better indicator of rock types than the individual elastic parameters V_p or V_s. Poisson's ratio can also provide information on the physical properties of the oceanic crust such as pore pressure, degree of saturation, and effective porosity once the relationship between laboratory and seismically measured Poisson's ratios is determined (Nichols, 1977).

Birch (1961) showed that V_p and V_s in rocks, aggregates of highly anisotropic minerals and pores, could be described by the theory of isotropic elasticity. Poisson's ratio is therefore calculated for the Samail rocks from their <u>in situ</u> velocities by the equation (Birch, 1961):

$$2\sigma = \frac{\left(\frac{V_p}{V_s}\right)^2 - 2}{\left(\frac{V_p}{V_s}\right)^2 - 1}, \text{ dimensionless.}$$

Because this equation is strictly applied to isotropic materials, Poisson's ratio calculated for each rock core is an apparent value as is Poisson's ratio calculated for oceanic crustal rocks from marine seismic refraction data (Salisbury and Christensen, 1978).

Poisson's ratio for each core sample is plotted as a function of stratigraphic position and lithology in the Samail ophiolite in Figures 9 and 10. Within the upper 2.5 km of the Samail ophiolite Poisson's

ratio varies from 0.28 (when $P_p = 0$) and 0.35 (when $P_p = P$) for the metabasalts to a low value of 0.23 near the base of the sheeted dikes. Poisson's ratio generally increases with depth from 0.28 in the high-level gabbros to 0.33 at the gabbro-harzburgite tectonite contact. In the harzburgite tectonites Poisson's ratio exhibits a wide range of values (0.28 to 0.35) but no general trend is apparent. In the Samail ophiolite Poisson's ratio is affected by the effective porosity, pore pressure, and degree of alteration in the metabasalts; the major mineral content of the gabbros; and the percentage of serpentine in harzburgite tectonites. These factors and their effect on Poisson's ratio in the Samail ophiolite are examined below.

Hyndman and Drury (1976) and Hyndman (1979) found that Poisson's ratio at 0.1 GPa confining pressure decreased as the vesicular porosity of fresh deep sea basalts increased. Christensen and Salisbury (1972) found that Poisson's ratio at 0.1 GPa confining pressure increased as the degree of weathering increased in DSDP basalts. Poisson's ratio for the six metabasalts from the Samail ophiolite shows no strong dependence on their effective porosity (Figure 14a). Figure 14a therefore suggests that Poisson's ratio for the Samail metabasalts is affected by both their effective porosity and degree of alteration. Moreover, Poisson's ratio of 0.35 to 0.29 is calculated for the Samail metabasalts when pore pressure is equivalent to confining pressure. Because these values are significantly greater than those calculated when pore pressure is less than confining pressure, Poisson's ratio appears to depend on pore pressure in the metabasalts of the Samail ophiolite.

Figure 14. Poisson's ratio (σ) for the metabasalts and harzburgite tectonites of the Samail ophiolite.

Figure 14a. Poisson's ratio as a function of the effective porosity of the metabasalts: when pore pressure (P_p) is zero and when pore pressure is equivalent to confining pressure (P).

Figure 14b. Poisson's ratio as a function of the percentage of serpentine in the harzburgite tectonites.

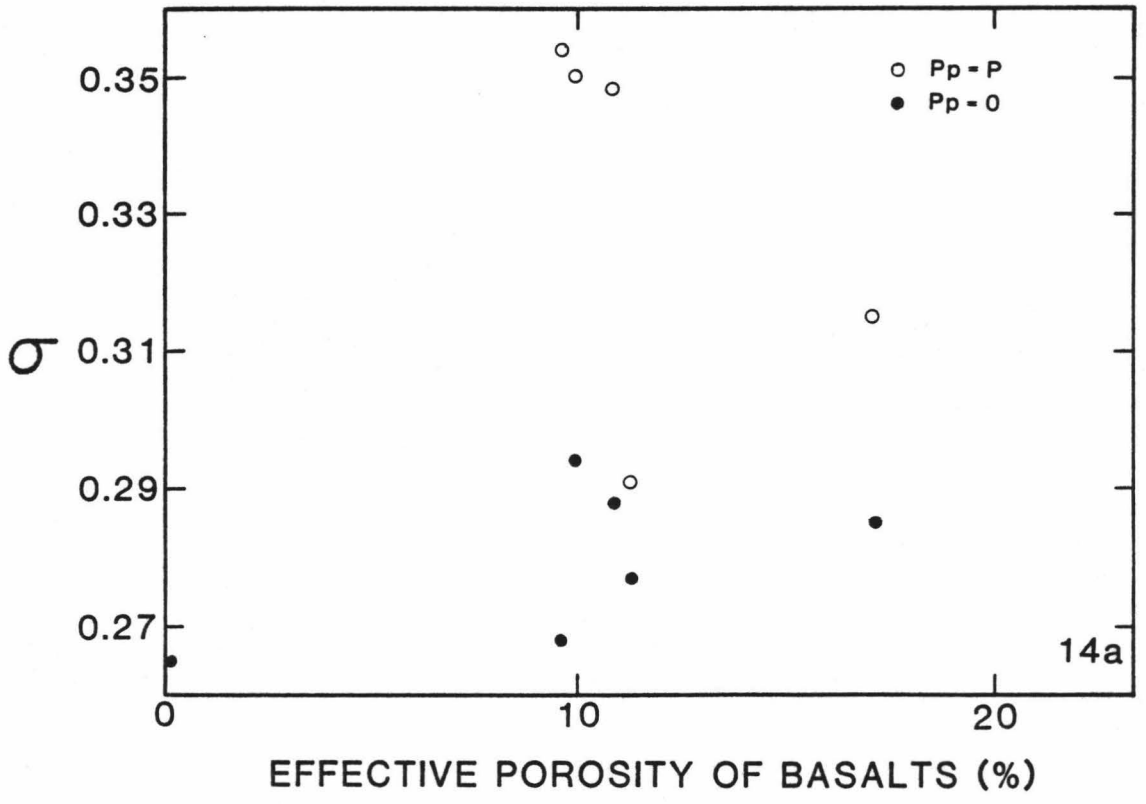
0.35
0.33
σ 0.31
0.29
0.27
0
10
20
Pp = P
Pp = 0
14a
EFFECTIVE POROSITY OF BASALTS (%)

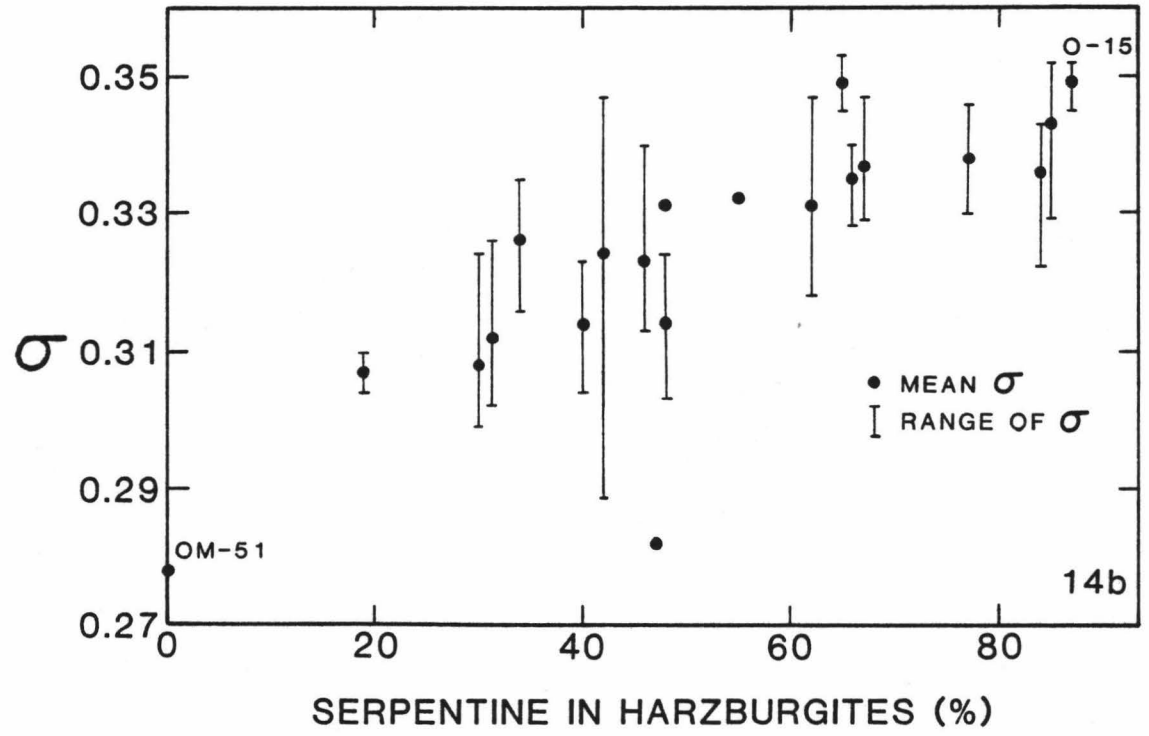
0.35
0.33
σ 0.31
0.29
0.27
0
20
40
60
80
O-15
OM-51
MEAN σ
RANGE OF σ
14b
SERPENTINE IN HARZBURGITES (%)

Poisson's ratio values that are calculated when pore pressure is equivalent to confining pressure are within the range of Poisson's ratio (0.30 to 0.40) that was calculated by Cheung (1978) for the uppermost 1.0 km of a section of oceanic crust near the Explorer Ridge. This comparison suggests that pore pressures within the upper 0.5 to 1.0 km of the oceanic crust may be equivalent to lithostatic confining pressures.

In Figure 12 the variation of Poisson's ratio with depth for the gabbros from the Wadi Kadir and Wadi Gideah East sections is correlated with the variation of the modal percentages of the primary mineral phases in the gabbros with depth. Poisson's ratio tends to increase as the plagioclase content of the gabbros increases. Low V_s in plagioclase results in the greater Poisson's ratio (Kern and Richter, 1981). The presence of quartz, characterized by low V_p and relatively high V_s (Salisbury and Christensen, 1978), causes the low value of Poisson's ratio (0.23) for the plagiogranites (K3ml and H618ml).

In Figure 14b Poisson's ratio is plotted as a function of the percentage of serpentine in the harzburgite tectonites of the Samail ophiolite. This figure shows that Poisson's ratio for the harzburgite tectonites increases from 0.28 to 0.35 as the percentage of serpentine in these rocks increases from 0% (sample OM-51) to 87% (sample O-15), respectively. Figure 14b suggests that Poisson's ratio for an upper mantle section of the Samail ophiolite that has undergone no <u>in situ</u> serpentenization is 0.28. This value of Poisson's ratio is comparable to the values measured by Sutton et al. (1971) for the upper mantle

beneath a section of the California continental rise (0.26 to 0.27) and within the range of values measured by Cheung (1978) for a section of the upper mantle near the Explorer Ridge (0.25 to 0.30). Comparison of the values of Poisson's ratio that have been measured in the oceanic upper mantle with Figure 14b suggests that serpentine comprises less than 20% of the upper mantle peridotites beneath the seismic Moho in some areas of the Pacific basin.

4.5 Velocity Anisotropy in the Samail Ophiolite

Velocity anisotropy (ΔV_p and ΔV_s) in rocks is caused by the dependence of V_p and V_s on their direction of propagation through rocks. Velocity anisotropy of the Samail rocks, defined as the maximum difference of V_p and V_s between the three mutually perpendicular cores from each rock sample, is calculated by the relation:

$$\Delta V = \frac{V_{max} - V_{min}}{V_{max}} \quad 100\%.$$

V_{max} is the maximum velocity that is measured in the three cores from each rock sample and V_{min} is the minimum measured velocity.

Velocity anisotropy and its causes are important geophysical parameters to determine for the Samail rocks because the lower oceanic crust (Christensen, 1966, 1972a) and the upper mantle (Hess, 1964; Raitt et al., 1969) exhibit seismic velocity anisotropy. Velocity anisotropy in rocks at high confining pressure is caused by the preferred orientation of minerals in the rocks and/or the compositional heterogeneity ($\Delta\rho$) of the rocks (Birch, 1961). Compositional

heterogeneity, the dependence of composition or bulk density on direction in a rock, is calculated for the Samail rocks by the relation:

$$\Delta\rho = \frac{\rho_{max} - \rho_{min}}{\rho_{max}} \quad 100\%.$$

ρ_{max} is the maximum <u>in situ</u> bulk density of the three rock cores and ρ_{min} is the minimum bulk density. In Figure 15 velocity anisotropy (both ΔV_p and ΔV_s) and compositional heterogeneity ($\Delta\rho$) of the Samail rocks are plotted as functions of depth in the Samail ophiolite. The ΔV_p, ΔV_s, and $\Delta\rho$ values of the Samail rocks are listed in Appendix B.

The data presented in Figure 15 suggest that velocity anisotropy in the Samail basalts and sheeted dikes is primarily controlled by the compositional heterogeneity of the metabasalts and metadiabases. Petrographic evidence indicating that the minerals in these rocks are not preferentially oriented supports this conclusion. $\Delta\rho$ in the Samail basalts (1.5 to 2.3%) is probably caused by the presence of oriented pores and open grain-boundary cracks that do not close under the low <u>in situ</u> confining pressures (0.05 to 0.07 GPa) on the metabasalts (Manghnani and Woollard, 1968). Low $\Delta\rho$ of the sheeted dikes (0 to 1.1%) corresponds to low ΔV_p (0.2 to 2.2%) and ΔV_s (0.3 to 2.9%) for the metadiabases.

ΔV_p and ΔV_s in the high-level gabbro samples do not exceed 3.0% although $\Delta\rho$ for a metagabbro (GE3ml) is 5.5%. This observation suggests that $\Delta\rho$ is not the primary factor controlling velocity anisotropy in the metagabbros. The insignificant velocity anisotropy of the massive

Figure 15. Velocity anisotropy (ΔV_p and ΔV_s) of the Wadi Gideah East (15a) and Wadi Kadir (15b) rock samples as functions of their stratigraphic position and compositional heterogeneity ($\Delta\rho$).

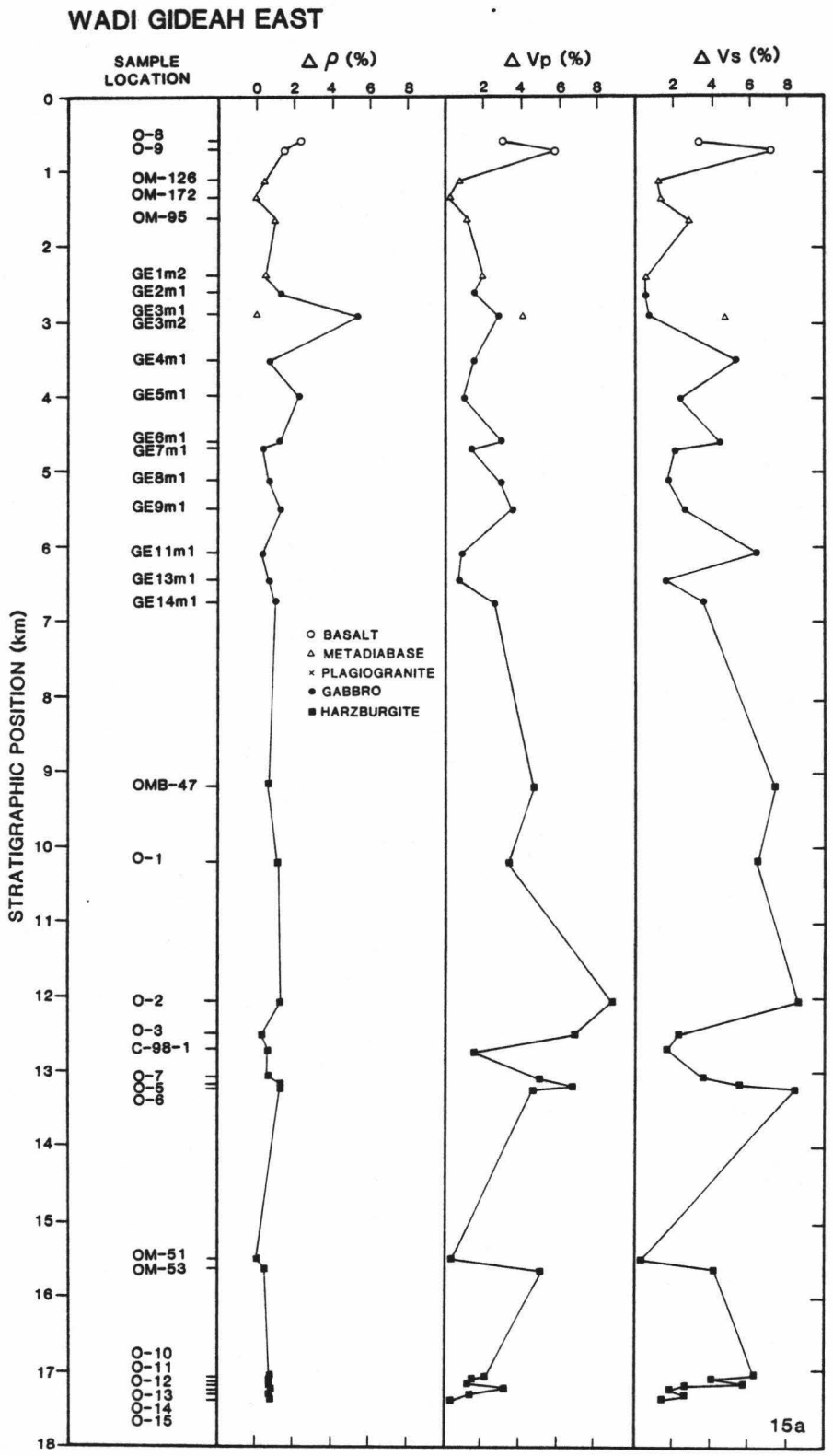
WADI GIDEAH EAST
SAMPLE LOCATION
Δ ρ (%)
Δ Vp (%)
Δ Vs (%)
STRATIGRAPHIC POSITION (km)
O-8
O-9
OM-126
OM-172
OM-95
GE1m2
GE2m1
GE3m1
GE3m2
GE4m1
GE5m1
GE6m1
GE7m1
GE8m1
GE9m1
GE11m1
GE13m1
GE14m1
OMB-47
O-1
O-2
O-3
C-98-1
O-7
O-5
O-6
OM-51
OM-53
O-10
O-11
O-12
O-13
O-14
O-15
BASALT
METADIABASE
PLAGIOGRANITE
GABBRO
HARZBURGITE
15a

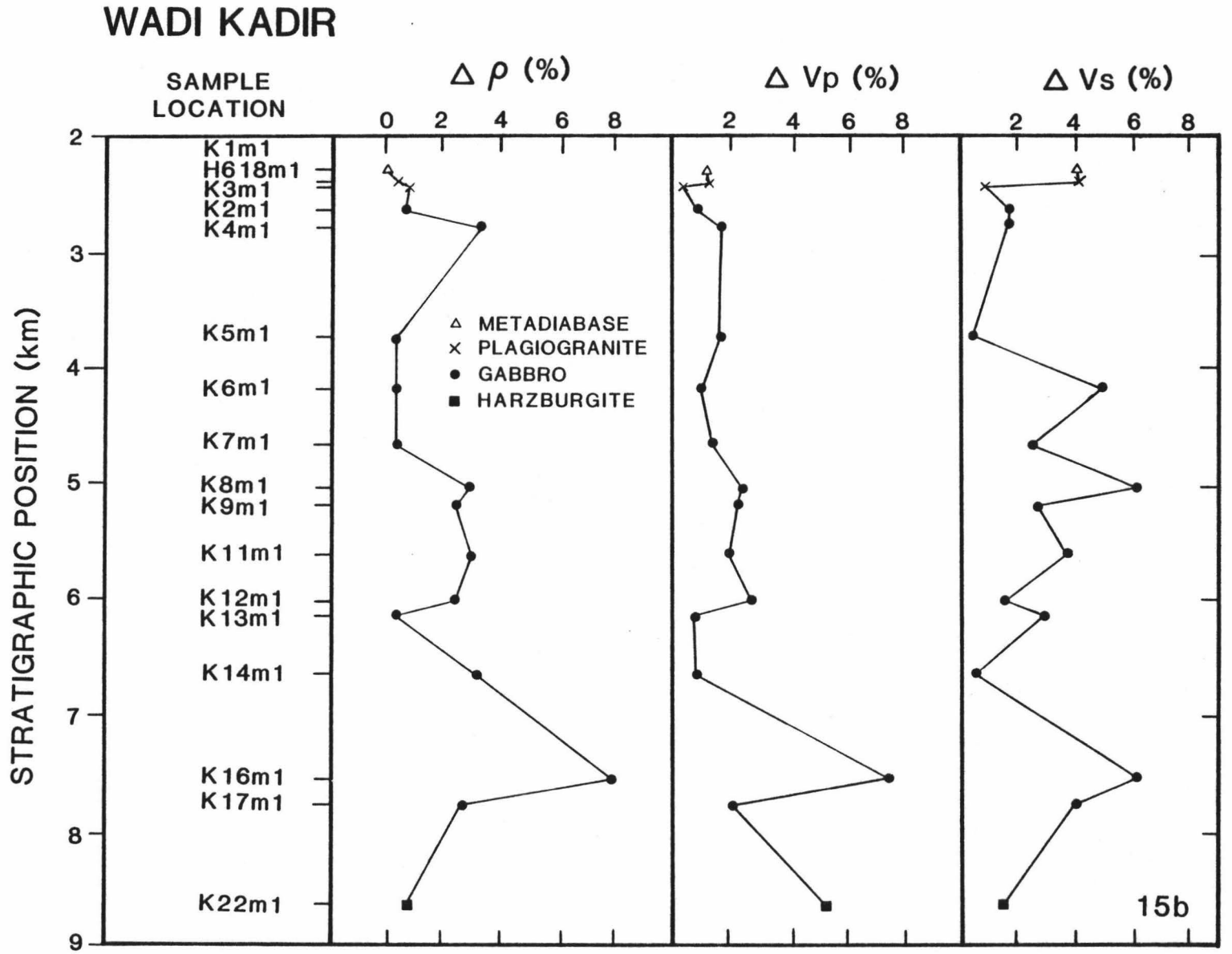
WADI KADIR
SAMPLE LOCATION
Δ ρ (%)
Δ Vp (%)
Δ Vs (%)
0 2 4 6 8
2 4 6 8
2 4 6 8
STRATIGRAPHIC POSITION (km)
2
3
4
5
6
7
8
9
K1m1
H618m1
K3m1
K2m1
K4m1
K5m1
K6m1
K7m1
K8m1
K9m1
K11m1
K12m1
K13m1
K14m1
K16m1
K17m1
K22m1
METADIABASE
PLAGIOGRANITE
GABBRO
HARZBURGITE
15b

metagabbros results from the random orientation of the igneous phases of clinopyroxene, plagioclase, and minor olivine and the replacement phases of uralite and brown hornblende in these rocks.

Due to cumulate layering, $\Delta\rho$ values for the layered gabbros are significant (0.3 to 7.8%). Surprisingly, ΔV_p only exceeds 4.0% in the cumulate olivine-clinopyroxene gabbro (K16m1) with a value of 7.5%. This observation suggests that $\Delta\rho$ is not the major factor controlling ΔV_p in the cumulate gabbros. ΔV_s, on the other hand, exceeds 4.0% in many cases, reaching a maximum of 6.5% for the cumulate olivine-clinopyroxene gabbro (GE11m1). This observation suggests that ΔV_s has a greater dependence on $\Delta\rho$ than ΔV_p.

The preferred orientation of tabular plagioclase grains with their long axes randomly oriented in a plane parallel to the cumulus textures is the major cause of ΔV_p and ΔV_s in the cumulate gabbros. This orientation of the plagioclase grains results in the statistical alignment of their [010] axes perpendicular to the horizontal textures (Christensen and Salisbury, 1975). The [010] axis of plagioclase is the fast direction for V_p while being the slow direction for V_s (Salisbury and Christensen, 1978). The layered gabbros of the Samail ophiolite therefore display significant velocity anisotropy when velocities are measured perpendicular to the cumulus textures of the rocks. Insignificant velocity anisotropy is measured parallel to the cumulus textures.

The petrographic evidence that the harzburgite tectonites of the Samail ophiolite are compositionally isotropic is supported by the low

$\Delta\rho$ values of 0 to 1.5% measured for these rocks. The high values of ΔV_p and ΔV_s (0 to 8.8%) measured for the harzburgite tectonites are therefore caused by the preferentially aligned olivine grains in the rocks.

From seven harzburgites (OMB-47, C-98-1, 0-1 to 0-3, 0-5, and 0-6), cores `a´ were cut parallel to the [100] axes of the olivine grains, the fast direction for $V_p$ and $V_s$ in olivine (Verma, 1960). Cores `b´ and `c´ were cut parallel to either the [001] or [010] axes. ΔV_p for these samples ranges from 1.5 to 8.7% while ΔV_s ranges from 1.8 to 8.7%. For the unoriented samples, ΔV_p ranges from 0.4 to 5.1% while ΔV_s ranges from 0.4 to 6.4%. The greater ΔV_p and ΔV_s values for the oriented samples indicate the major influence of aligned olivine grains on velocity anisotropy in the harzburgite tectonites. However, the wide range of values for these samples indicates that the directional dependence of velocities is masked by serpentine and other accessory minerals (orthophyroxene) (Christensen, 1966).

4.6 Velocity-Density Systematics of the Samail Ophiolite

Birch (1961) and Simmons (1964) have shown that V_p and V_s in rocks of similar chemical composition are linearly related to the bulk density of the rocks. The mean atomic weight ($\bar{M}$), a measure of the chemical composition of rocks, is calculated for representative Samail rocks from their chemical analyses by the relation (Birch, 1961):

$$M = \left(\frac{\Sigma X_i}{m_i} \right)^{-1}, \text{ dimensionless.}$$

X_i is the proportion by weight of oxide `i' and m_i is the mean atomic weight of the oxide. The major chemical analyses and $\overline{M}$ values of representative Samail rocks are listed in Appendix D.

In Figure 16 the mean V_p and V_s that were measured in all of the Samail rock samples are plotted versus the mean bulk density of the rocks. The scatter that is seen in the velocity data for the metadiabases and gabbros is caused by variations in the $\overline{M}$ values and calcium oxide [CaO] contents (9.1 to 17.8%) of the rocks (Birch, 1961; Simmons, 1964; Manghnani et al., 1974). Nevertheless, since the $\overline{M}$ values for the rocks in this study only vary from 20.6 to 22.1 (i.e. $\overline{M} \sim 21$), the velocity-density data in Figure 16 can be adequately described by linear equations of the form $V = a(\overline{M}) + b\rho$. The experimentally determined parameters, $a(\overline{M})$ and b, and data statistics for two lines that were determined by a least squares method for both V_p and V_s data are listed in Table 2. The heavy, solid lines (Figure 16) are determined for all velocity data of the Samail rocks except for the anomalously low velocities of the serpentenized harzburgite tectonites; the heavy, dashed lines are determined for all of the Samail velocity data. The lighter solid and dashed lines were determined by Christensen and Salisbury (1975) for the laboratory measured velocities in oceanic rocks that had been drilled or dredged from the oceanic basement. The velocity measurements were made by several researchers at 0.1 GPa confining pressure and room temperature. The solid line was determined for all published velocity data of oceanic rocks except for the velocities in serpentenites and vesicular basalts; the dashed lines were

Figure 16. Mean compressional (V_p) and shear (V_s) wave velocities versus the mean bulk density (ρ) of the Samail ophiolite samples.

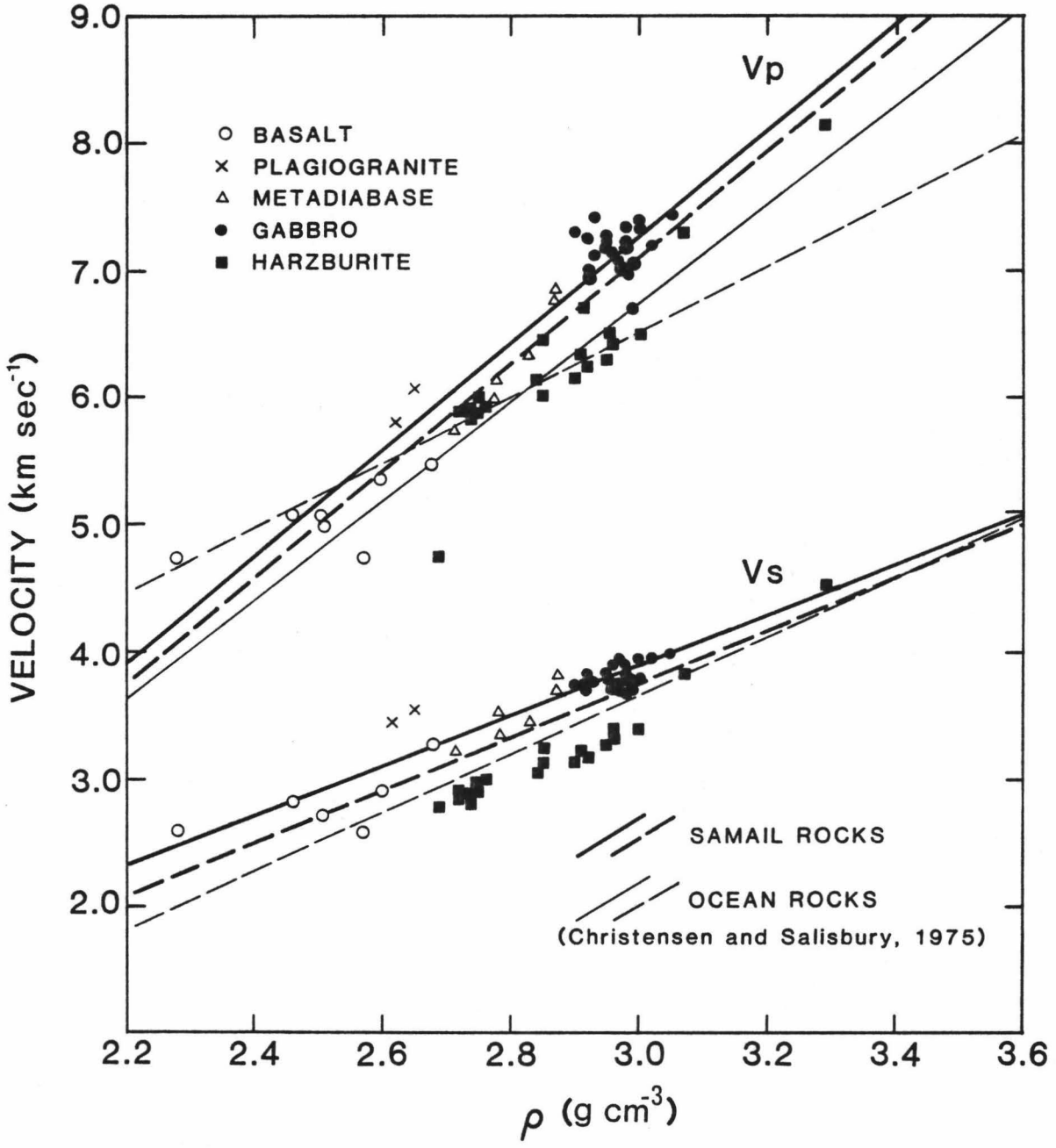
9.0
8.0
7.0
6.0
5.0
4.0
3.0
2.0
VELOCITY (km sec^{-1})
Vp
Vs
BASALT
PLAGIOGRANITE
METADIABASE
GABBRO
HARZBURITE
SAMAIL ROCKS
OCEAN ROCKS
(Christensen and Salisbury, 1975)
2.2
2.4
2.6
2.8
3.0
3.2
3.4
3.6
ρ (g cm^{-3})

TABLE 2

Regression Line Parameters for the Velocity-Density Systematics of the Samail Ophiolite and Oceanic Rocks

Solution	Confining Pressure (GPa)	n	a (km sec^{-1})	b (km sec^{-1}/g cm^{-3})	$\bar{M}$	Reference
			$V_p = a(\bar{M}) + b$			
All rocks of Samail ophiolite except serpentenized harzburgites	0.05–0.6	37	-5.17 ± 0.67	4.15 ± 0.23	20.87–22.11	This study
All rocks of Samail opliolite	0.05–0.6	57	-5.08 ± 0.74	4.06 ± 0.26	20.57–22.11	This study
All oceanic rocks except serpentenites and vesicular basalts	0.1	215	-4.92	3.89		Christensen and Salisbury (1975)
All oceanic rocks	0.1	386	-1.18	2.57		Christensen and Salisbury (1975)
			$V_s = a(\bar{M}) + b$			
All rocks of Samail ophiolite except serpentenized harzburgites	0.05–0.6	37	-2.03 ± 0.35	1.97 ± 0.12	20.87–22.11	This study
All rocks of Samail ophiolite	0.05–0.6	57	-2.55 ± 0.55	2.10 ± 0.199	20.57–22.11	This study
All oceanic rocks except serpentenites and vesicular basalts	0.1	175	-3.50	2.39		Christensen and Salisbury (1975)
All oceanic rocks	0.1	213	-3.22	2.32		Christensen and Salisbury (1975)

`n´ is the number of data points; $a(\bar{M})$ is the slope of the line solution; `b´ is the y-intercept of the line; $\bar{M}$ is the mean atomic weight.

determined for all of the published velocity data of oceanic rocks. The parameters for these lines are also listed in Table 2.

Despite the difference in temperature and pressure conditions, the velocity-density systematics of the Samail rocks agree with those presented by Christensen and Salisbury (1975) for oceanic crustal rocks. This indicates that the velocity-density systematics for the rocks of the Samail ophiolite can be used to estimate the bulk density of oceanic crustal rocks from marine seismic refraction data.

4.7 Velocity-Depth Profile of the Samail Ophiolite

By combining the average measured velocities and the stratigraphic columns of the Wadis Kadir and Gideah East sections, the general stratigraphic section and velocity-depth profile of the southeastern part of the Samail ophiolite (Ibra area) are developed (Figure 17). The average bulk density and Poisson's ratio profiles are also shown.

The mafic crustal section of the Samail ophiolite in the Ibra area varies in thickness from 7.0 to 8.1 km over a horizontal distance of 5.0 km (Hopson et al., 1981). The volcanic member and sheeted dike complex show a uniform thickness of 1.0 and 1.5 km, respectively. The gabbro member varies from 4.5 to 5.6 km in thickness; the high-level gabbro varies from 0.2 to 1.0 km in thickness, the transitional gabbro varies from 0.36 to 0.80 km in thickness, and the layered gabbro varies from 2.5 to 5.0 km in thickness.

The velocity, bulk density, and Poisson's ratio profiles that are presented in Figure 17 are drawn to represent the average variation of these values with depth in the Samail ophiolite while it was a section

Figure 17. The general stratigraphic column and velocity-depth (V_p and V_s), bulk density (ρ), and Poisson's ratio (σ) profiles of the Samail ophiolite in the Ibra area. The plotted points represent mean values. The best-fit profiles are based on the relative abundance of each lithology in the Samail ophiolite and the average values of V_p, V_s, ρ, and σ. The lines are dashed where there is insufficient data.

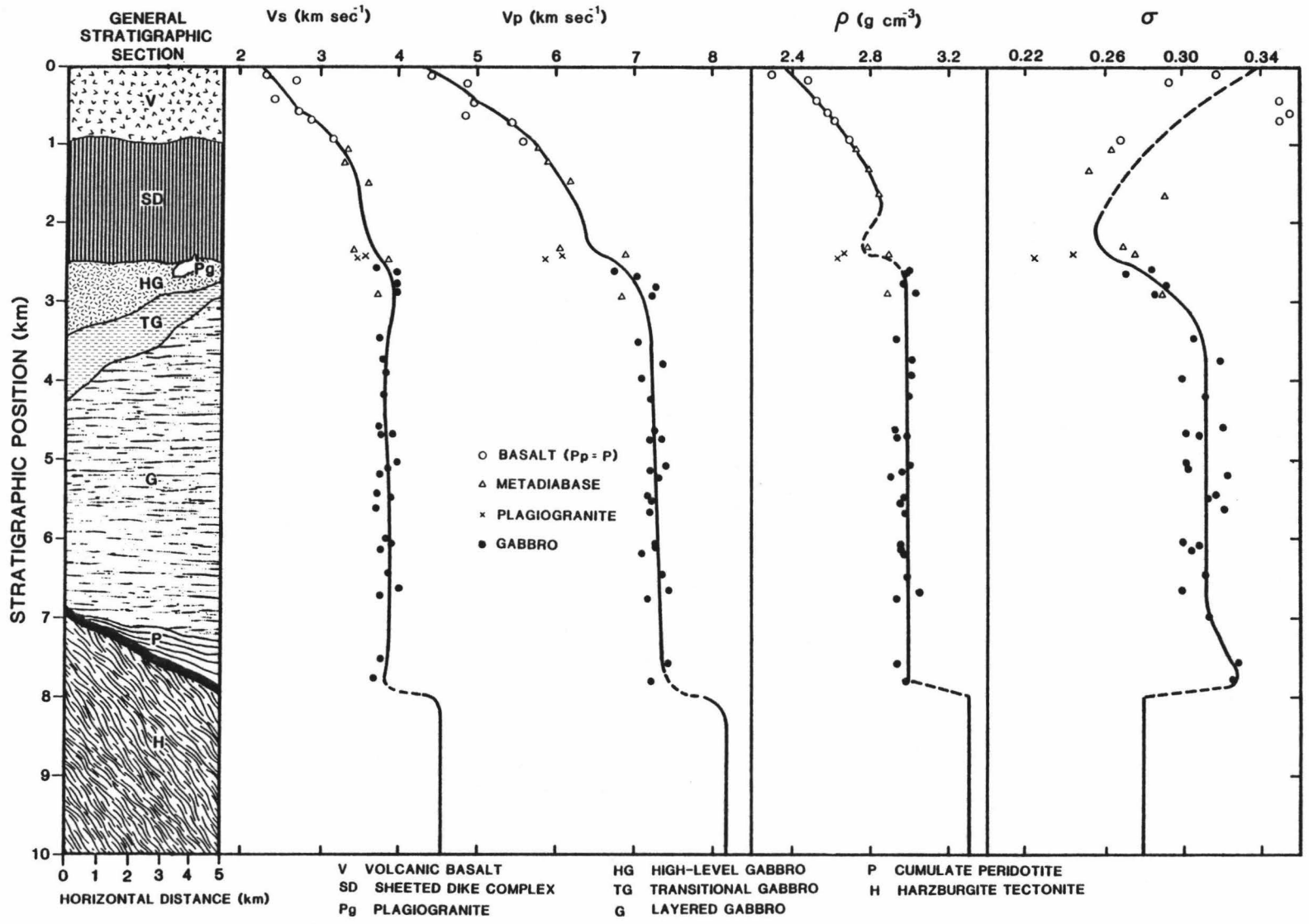
GENERAL STRATIGRAPHIC SECTION
Vs (km sec⁻¹)
Vp (km sec⁻¹)
ρ (g cm⁻³)
σ
STRATIGRAPHIC POSITION (km)
HORIZONTAL DISTANCE (km)
V
SD
Pg
HG
TG
G
P
H
BASALT (Pp = P)
METADIABASE
PLAGIOGRANITE
GABBRO
V VOLCANIC BASALT
SD SHEETED DIKE COMPLEX
Pg PLAGIOGRANITE
HG HIGH-LEVEL GABBRO
TG TRANSITIONAL GABBRO
G LAYERED GABBRO
P CUMULATE PERIDOTITE
H HARZBURGITE TECTONITE

of Tethyan oceanic crust. The best-fit profiles are based on the relative abundance of each lithology in the ophiolite and on the mean values of velocity, bulk density, and Poisson's ratio of the rock samples used in this study.

Because pore pressures within the uppermost oceanic basalts are probably equivalent to the lithostatic confining pressures on the rocks (Spudich and Orcutt, 1980a), velocities and Poisson's ratio (V_p = 4.4 to 5.0 km sec^{-1}, V_s = 2.3 to 2.6 km sec^{-1}, σ = 0.29 to 0.35) in the metabasalt samples that were measured and calculated at this condition are shown in the uppermost 0.5 km of the Samail ophiolite. At a depth of 0.5 km, the V_p and V_s velocity-depth profiles are marked by a change to higher velocity gradients. These higher velocity gradients are caused primarily by decreasing effective porosity, increasing metamorphic grade (zeolite to lower greenschist facies), and decreasing pore pressure (isolated pores) in the metabasalts.

Between depths of 0.5 and 2.5 km, V_p increases from 5.2 to 6.35 km sec^{-1} while V_s more slowly increases from 3.2 to 3.5 km sec^{-1}. The high velocity gradients ($\sim$0.7 sec^{-1}) for both V_p and V_s are caused by downward increasing metamorphic grade (greenschist to amphibolite facies) and lithologic changes (vesicular metabasalts grading to massive metabasalts and metadiabases) that result in downward increasing bulk density (2.55 to 2.90 g cm^{-3}) in the Samail ophiolite. Poisson's ratio decreases rapidly to 0.25. The high velocity gradients terminate near the base of the sheeted dikes where intrusive, late-stage differentiates and/or the widespread occurrence of quartz in metadiabases and

metagabbros near the sheeted dike-gabbro contact depress velocities. Although V_p and V_s in the late-stage differentiates are low ($V_p \sim 6.0$ km sec^{-1}, $V_s \sim 3.4$ km sec^{-1}) a velocity inversion is not shown at the sheeted dike-gabbro contact due to the discontinuous distribution and insignificant volume of the late-stage differentiates.

Below the base of the sheeted dikes, V_p and V_s increase rapidly due to the presence of amphibolite facies assemblages and high density metagabbros. This rapid velocity increase causes the distinctive velocity discontinuities in the V_p and V_s profiles at a depth of 2.5 km. V_p increases to 7.1 km sec^{-1}, V_s increases to 3.9 km sec^{-1}, and Poisson's ratio increases to 0.31 at the base of the high-level gabbro due to downward increasing metamorphic grade (lower to upper amphibolite facies) and decreasing extent of metamorphism in the metagabbros.

Below the high-level gabbro a low velocity gradient (0 to 0.04 sec^{-1}) in the transitional and layered gabbros is caused by the increase of olivine content with depth in the cumulate gabbros. V_p increases from 7.1 to 7.35 km sec^{-1} while V_s slightly decreases or remains constant (V_s = 3.8 to 3.9 km sec^{-1}). Poisson's ratio remains constant (σ = 0.31) in the fresh cumulate gabbros as does bulk density (ρ = 3.10 g cm^{-3}).

Although the basal cumulate peridotites (interlayered wehrlites, melagabbros, and dunites) and cumulus dunite at the base of the layered gabbro unit were not sampled in this study, representative velocity values for these ultramafic rocks are assumed from previously published data and denoted by the dashed line segments at depths of 7.0 to 8.0 km

in Figure 17. Christensen (1966), Salisbury and Christensen (1978), and Christensen and Smewing (1981) found that V_p and V_s in cumulate peridotites varied from 7.3 and 3.85 km sec^{-1} to 8.1 and 4.5 km sec^{-1}, respectively. The high velocities were caused by the high olivine content (> 20%) of the rocks while the wide range of velocities was caused by the variation of serpentine content in the rock samples and the variation of rock types. With less than 10% serpentine, V_p and V_s in the basal cumulus dunite can exceed 8.0 and 4.5 km sec^{-1}, respectively, according to Christensen (1966).

The assumed V_p and V_s values for the basal cumulate peridotites suggest that they comprise a thin (0 to 0.6 km thick) crust-mantle transition zone in which lower crustal velocities (V_p = 7.35 km sec^{-1}, V_s = 3.9 km sec^{-1}) increase to upper mantle velocities (V_p > 8.0 km sec^{-1}, V_s > 4.5 km sec^{-1}). When the cumulate peridotites are not present and cumulate gabbros are in contact with the basal cumulus dunite, such as seen in the Wadi Gideah East section, a first order velocity discontinuity will occur at the layered gabbro-cumulus dunite contact. Upper mantle velocities that mark the seismic Moho may occur anywhere within the cumulate peridotites. Therefore, the exact stratigraphic position of the seismic Moho in the Samail ophiolite is undetermined. In contrast, the petrologic Moho occurs stratigraphically below the seismic Moho at the cumulus dunite-harzburgite tectonite contact.

Because serpentenization of the harzburgite tectonites in the Samail ophiolite probably occurred following the detachment of the

ophiolite from the upper mantle (Boudier and Coleman, 1981), V_p and V_s of 8.1 and 4.5 km sec^{-1}, respectively, that were measured in an unserpentenized harzburgite tectonite (OM-51) are assumed to represent the average velocities for the unserpentenized upper mantle section of the Samail ophiolite. These velocities are also assumed to vary as much as 9.0% due to the velocity anisotropy of the harzburgite tectonites.

Figure 17 shows that both the primary igneous petrology of the Samail ophiolite and the subsequent hydrothermal metamorphism of the rocks determine the velocity structure of the ophiolite to depths of 2.5 km. Below depths of 2.5 km, V_p and V_s are primarily controlled by the igneous petrology of the gabbroic rocks in the Samail ophiolite.

4.8 Comparison Between the Velocity-Depth Profiles of the Samail and Other Ophiolites

In Table 3 are listed the range of V_p, V_s, bulk density, and Poisson's ratio values that were measured in this study for the major rock types of the Samail ophiolite. Also listed but not corrected for temperature effects are the range of the same values that have been measured for comparable lithologies from the Ming's Bight ophiolite, Newfoundland (Peterson et al., 1974); the Papua New Guinea ophiolite, Papua New Guinea (Kroenke et al., 1976); and several western United States ophiolites (Christensen, 1978). The range of values that were measured for the Samail ophiolite is consistent with the range of values that have been measured for the other ophiolites.

In Figure 18 the V_p profile of the Ibra area of the Samail ophiolite (Ibra profile) is compared to V_p profiles of the Pt. Sal

TABLE 3

Comparison of the Laboratory Measured Elastic and Physical Properties of Rocks from Ophiolites

Physical Properties	Papua[a] Ophiolite	Ming's Bight[b] Ophiolite	U.S.[c] ophiolites	Samail[d] Ophiolite
Basalt				
ρ ($g\ cm^{-3}$)			2.70-2.74	2.28-2.68
V_p ($km\ sec^{-1}$)			5.43-5.88	4.37-5.53
V_s ($km\ sec^{-1}$)			2.98-3.40	2.27-3.13
σ (dimensionless)			0.25-0.29	0.27-0.35
Metadiabase				
ρ		2.90-3.20		2.71-2.87
V_p		6.10-6.90		5.74-6.85
V_s				3.26-3.82
σ				0.25-0.29
Metagabbro				
ρ			2.72-3.04	2.92-3.02
V_p			6.38-7.13	6.71-7.24
V_s			3.58-3.79	3.70-3.96
σ			0.27-0.31	0.27-0.30
Gabbro				
ρ	2.81-3.06	2.90-3.20	2.84-3.01	2.92-3.05
V_p	7.09-7.59	6.10-7.80	6.43-7.34	7.07-7.43
V_s	3.71-3.98		3.76	3.66-3.97
σ	0.31-0.33		0.29	0.30-0.33

[a] Measured by Kroenke et al. (1976) at 0.20 to 0.30 GPa confining pressure

[b] Measured by Peterson et al. (1974) at 0.15 GPa confining pressure

[c] Measured by Christensen (1979) at 0.1 GPa confining pressure

[d] Measured in this study at *in situ* confining pressures

Figure 18. Comparison between the laboratory measured velocity-depth profiles of the Pt. Sal, the Bay of Islands (BOI), the northern part of the Samail (Northern Samail), and the Ibra area of the Samail (Ibra profile) ophiolites.

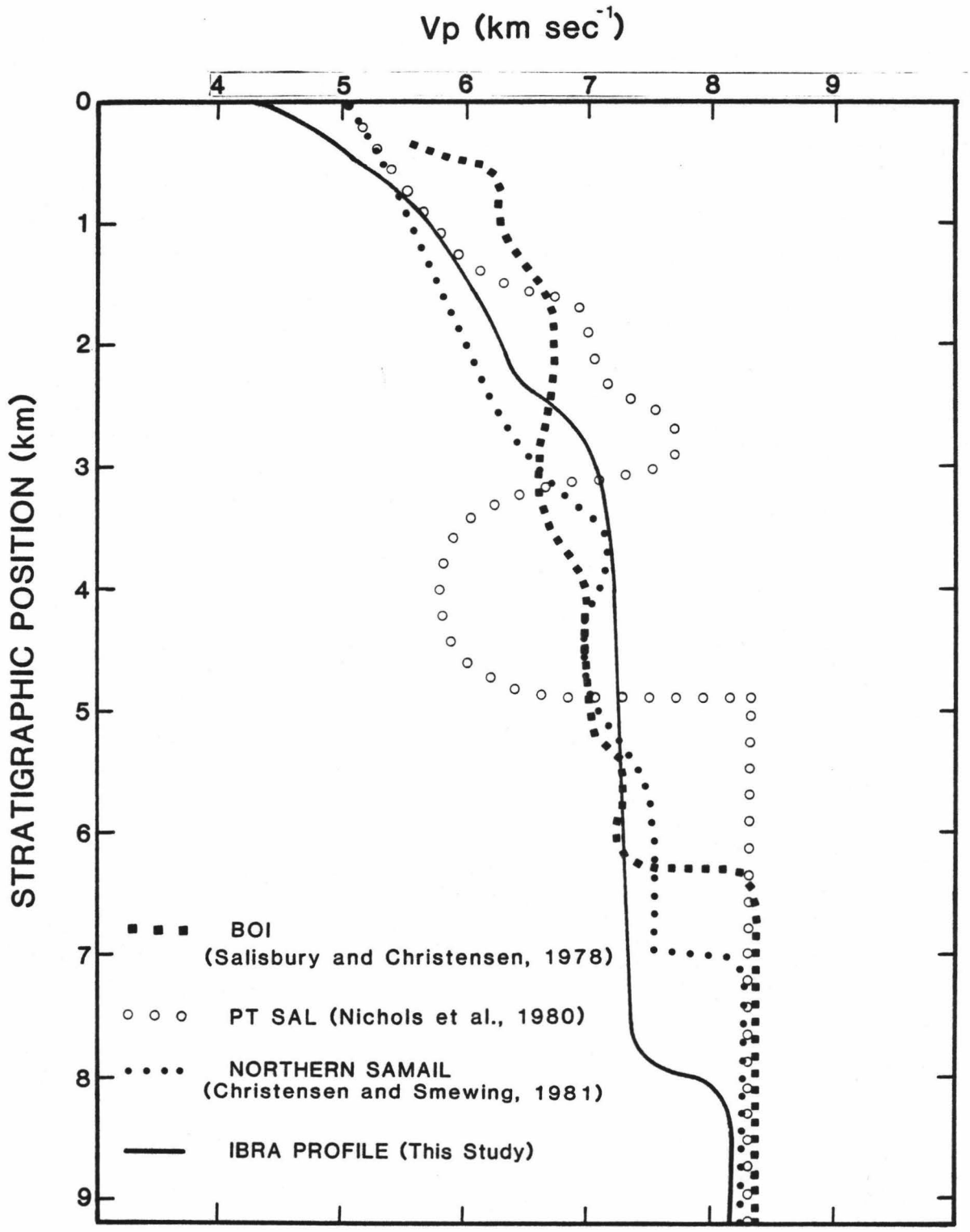
Vp (km sec^{-1})
4
5
6
7
8
9
0
1
2
3
4
5
6
7
8
9
STRATIGRAPHIC POSITION (km)
BOI
(Salisbury and Christensen, 1978)
PT SAL (Nichols et al., 1980)
NORTHERN SAMAIL
(Christensen and Smewing, 1981)
IBRA PROFILE (This Study)

ophiolite, California (Nichols et al., 1980); the Bay of Islands (BOI profile) ophiolite, New Foundland (Salisbury and Christensen, 1978); and the northern part of the Samail (Northern Samail profile) ophiolite (Christensen and Smewing, 1981). Note that only the Ibra profile has been adjusted for temperature at depth; V_p values that were measured at 25° C in the lower cumulate gabbros were adjusted by 1.5 to 2.0% for temperatures (~250° C) at 7.0 km depth. The comparison between the velocity-depth profiles of the ophiolites illustrates some of the major problems that are present when one tries to develop a model of oceanic crust based on an ophiolite.

As with many exposed ophiolites throughout the world, the Pt. Sal ophiolite is stratigraphically incomplete, tectonically disrupted, and thin compared to the seismic velocity structure of oceanic crust. Basalts, sills and dikes, cumulate gabbros, and basal cumulate peridotites comprise the thin (~3.0 km thick), highly weathered, mafic crustal section of the Pt. Sal ophiolite. This thin crustal section overlies extensively serpentenized upper mantle peridotites. In comparison the relatively fresh mafic crustal sections of the BOI and the Samail ophiolites are 6.0 to 8.0 km thick, respectively. Therefore a comparison between the Pt. Sal and the Ibra profiles illustrates the seismic differences between ophiolites with thin and thick and with highly weathered and relativley fresh crustal sections, respectively.

The Pt. Sal and Ibra profiles have similar V_p values to a depth of 1.0 km and below depths of 7.0 km. Between depths of 1.0 and 7.0 km the profiles show distinctly different shapes and V_p values. V_p of 7.8 km

sec^{-1} at a depth of 3.0 km in the Pt. Sal profile is caused by the occurrence of cumulate peridotites in the Pt. Sal ophiolite at this depth. Cumulate peridotites in which V_p is assumed to be 7.8 km sec^{-1} occur in the Samail ophiolite at a depth of 7.0 km. Because Nichols et al. (1980) assumed that the uppermost mantle below the thin crustal section of the Pt. Sal ophiolite was partially serpentenized while <u>in situ,</u> a low velocity layer ($V_p \sim$ 5.5 km sec^{-1}) exists in the Pt. Sal profile between depths of 3.0 and 5.0 km. Because the upper mantle peridotites were probably serpentenized following detachment of the Samail ophiolite (Boudier and Coleman, 1981), no low velocity layer is shown in the Ibra profile. Moreover, the depth to upper mantle velocities ($V_p >$ 8.0 km sec^{-1}) is significantly less in the Pt. Sal profile (< 5.0 km) than in the Ibra profile (~7.0 to 8.0 km).

The differences between the Pt. Sal and the Ibra profiles are caused by the differences in lithologic structure and degree of weathering in the ophiolites. These differences probably represent some of the variations that are present in oceanic crust. The Pt. Sal ophiolite may represent a section of thin oceanic crust that formed in a small, short-lived magma chamber at a slow spreading ridge or in a back arc basin and was underlain by a layer of partially serpentenized upper mantle peridotite (Hopson, 1981). The Samail ophiolite, in contrast, represents a section of thick oceanic crust that probably formed in a large, long-lived magma chamber at a fast spreading mid-ocean ridge (Pallister and Hopson, 1981) and was underlain by unserpentenized upper mantle peridotites.

The Ibra and BOI profiles display a similar range of velocities with upper mantle velocities occurring at similar depths in both profiles (6.0 to 8.0 km). The obvious differences between the two profiles are: (1) velocities in the upper 3.0 km of the BOI profile are greater than those in the Ibra profile, and (2) velocities increase smoothly with depth in the Ibra profile while distinctive velocity discontinuities are prominent features in the BOI profile.

The BOI ophiolite probably represents a section of thick (~6.0 km) oceanic crust that formed at a moderately fast spreading (3 to 5 cm yr^{-1}, half-rate) mid-ocean ridge 45 m.y. before its obduction onto the American continental margin. By comparison the Samail ophiolite represents a section of thick (7.0 to 8.0 km) oceanic crust that formed 4 to 8 m.y. before its obduction onto the Arabian continental margin.

Kempner and Gettrust (1981b) suggested that the differences in the velocity structures of the Samail and BOI ophiolites are caused by the difference in their formation-to-emplacement ages. They concluded that the oceanic crust ages through a process of hydrothermal metamorphism and low temperature weathering. As a result they suggested that young crust (< 10 m.y.) with a smoothly varying velocity-depth profile will age to old crust (> 30 m.y.) with a velocity-depth profile that is characterized by distinct velocity discontinuities.

The comparison between the Ibra, the BOI, and the Pt. Sal profiles shows that an ophiolite and its velocity-depth profile must by cautiously used to develop a model of oceanic crust. The spreading rate, formation-to-emplacement age, and tectonic provenance of the

ophiolite and the section of the oceanic crust must be similar to insure a valid comparison between the two.

In Figure 18 a velocity-depth profile for the Ibra area of the Samail ophiolite (this study) is also compared to a velocity-depth profile for the northern part of the Samail ophiolite. The Northern Samail profile was developed by Christensen and Smewing (1981) from their laboratory measured velocities in rocks from the northern part of the Samail ophiolite.

As expected, several similarities are noted between the two profiles:

(1) The range of V_p that was measured in the rock samples from different parts of the ophiolite and in different laboratories are similar.

(2) V_p increases rapidly with depth in the upper 2.5 to 3.0 km of both profiles and then increases slowly to depths of 7.0 to 8.0 km.

(3) Upper mantle V_p of 8.1 to 8.2 km sec^{-1} are encountered at depths of 7.0 to 8.0 km in both profiles. In the Northern Samail profile the boundary marking the change from lower crustal velocities to upper mantle velocities appears as a first order discontinuity. In the Ibra profile the assumed V_p for the cumulate peridotites suggest that the transition from lower crustal V_p to upper mantle V_p occurs over a vertical distance of 0 to 0.6 km.

(4) Both profiles show a velocity discontinuity or high velocity gradient between depths of 2.5 km (Ibra profile) and 3.5 km (Northern Samail profile). In both areas of the Samail ophiolite this velocity

discontinuity marks the contact between the sheeted dike complex and the high-level gabbro. The difference in stratigraphic position for the discontinuity is caused by the variation of the thickness of the sheeted dike complex from the northern part of the ophiolite (~2.0 km) to the Ibra area (~1.5 km). Christensen and Smewing (1981) have suggested that the velocity discontinuity in the Northern Samail profile marks the "layer 2-layer 3" seismic velocity boundary in the Samail ophiolite.

Some differences are also apparent between the two profiles:

(1) V_p in the Northern Samail profile is lower than V_p in the Ibra profile between depths of 0.6 and 3.5 km. The lower V_p in the Northern Samail profile is caused by the greater thickness of the sheeted dike complex in the northern part of the Samail ophiolite. Due to the greater thickness of the dike complex, lower bulk density and metamorphic grade occur at deeper stratigraphic positions in the northern part of the Samail ophiolite than in the Ibra area. The lower bulk density and metamorphic grade result in lower V_p at deeper stratigraphic positions in the Northern Samail profile.

(2) A velocity inversion between depths of 4.0 to 5.0 km in the Northern Samail profile is not seen in the Ibra profile. In the northern part of the Samail ophiolite, plagiogranites at depths of 4.0 to 5.0 km cause the velocity inversion (Christensen and Smewing, 1981). The occurrence of plagiogranites and quartz-rich metadiabases and metagabbros near the sheeted dike-gabbro contact at a depth of 2.5 km in the Ibra area of the Samail ophiolite depresses V_p but probably does not cause a velocity inversion.

(3) In the Ibra profile between depths of 3.5 and 8.0 km, V_p increases smoothly while in the Northern Samail profile a high velocity gradient is noted at a depth of 5.6 km. Christensen and Smewing (1981) have suggested that this high velocity gradient marks the appearance of basal cumulate peridotites in the northern section of the Samail ophiolite. Furthermore, they have suggested that this velocity gradient marks the "layer 3A-layer 3B" seismic velocity boundary in the Samail ophiolite. The basal cumulate peridotites found in the Ibra area of the Samail ophiolite appear to comprise a thin (0 to 0.6 km thick) transition zone from lower crustal to upper mantle velocities.

The differences between the Ibra and Northern Samail profiles reflect actual variations in the lithologic structure of the ophiolite over distances of several hundred kilometers. They also represent different interpretations of the measured velocity data. Christensen and Smewing (1981) concluded that the seismic velocity structure of the Samail ophiolite is "remarkably similar to that of the oceanic crust and upper mantle". This conclusion lends support to the following discussion in which the velocity-depth profile of the Ibra area of the Samail ophiolite is compared with the seismic velocity structures of normal oceanic crust as defined by Christensen and Salisbury (1975) and a velocity-depth function for a section of oceanic crust that formed 4.5 m.y. ago at the East Pacific Rise.

5. RELATIONSHIP BETWEEN THE SAMAIL OPHIOLITE AND THE OCEANIC CRUST

The major assumption of this study is that the Samail ophiolite is a fragment of Tethyan oceanic crust. Before a petrologic-seismic model of contemporary oceanic crust can be presented that is based on the petrology and velocity structure of the Samail ophiolite, the Samail ophiolite must be shown to be comparable with contemporary oceanic crust of similar thickness, age, and spreading rate. In the following discussion the relationship between the Samail ophiolite and contemporary oceanic crust is established by: (1) the comparison between the seismic velocity structures of the Samail ophiolite and normal oceanic crust as defined by Christensen and Salisbury (1975), and (2) the comparison between the velocity-depth profile of the Samail ophiolite (Ibra area) and the velocity-depth function for a section of oceanic crust that formed at the East Pacific Rise. To facilitate these comparisons the seismic velocity structure and petrologic models of the oceanic crust are introduced below.

5.1 Marine Seismic Refraction Studies and Interpretations

5.1.1 Seismic Velocity Structure of the Oceanic Crust

Due to its inaccessibility, the oceanic crust more than 0.6 km below the sediment-basement interface is defined by its velocity structures as developed from marine seismic reflection-refraction data. As marine seismic refraction methods, instruments, and data analysis techniques have improved, the seismic velocity structure of the oceanic crust has evolved from the simple two-layer model of Ewing et al. (1950)

to the velocity gradient models of Kennett and Orcutt (1976) and Spudich and Orcutt (1980b); as the seismic velocity structures of the oceanic crust are better constrained they tend to converge to the laboratory determined velocity structures of ophiolites.

Resolution of the velocity structure of the oceanic crust is limited by the wavelength of the seismic waves that are employed in marine seismic refraction surveys. Using classical explosion seismology techniques with poor structural resolution due to wide shot spacings (2.0 to 2.5 km) and straight line solutions to first arrival travel-time data, Hill (1957) and Raitt (1963) detected only three refracting "layers" (termed layers 1,2, and 3) in the oceanic crust. To develop his three-layer seismic velocity structure of average oceanic crust, Raitt (1963) assumed: (1) that the oceanic crust is horizontally layered, (2) that the measured velocities are constant in each homogeneous layer, and (3) that velocity of the layers always increases with depth.

Sutton et al. (1971), Hussong (1972), and Houtz and Ewing (1976), using ASPER (Airgun and Sonobuoy Precision Echo-Recorder) and OBS (Ocean Bottom Seismometer) techniques which incorporate high shot densities, expendable sonobuoys, phase correlation between traces, and second arrival data to achieve better structural resolution, have added more detail to the seismic velocity structure of the oceanic crust. Sutton et al. (1971) found that "layer 2" often has a low velocity cap (V_p = 2.5 to 3.8 km sec^{-1}) while oceanic "layer 3" appears to have a high velocity (V_p = 7.1 to 7.7 km sec^{-1}) basal crustal layer (average

thickness of 3.0 km) throughout the Pacific. Houtz and Ewing (1976) suggested that "layer 2" may have three distinct sublayers ("layer 2A" with V_p = 3.64 km sec^{-1}, "layer 2B" with V_p = 5.19 km sec^{-1}, and "layer 2C" with V_p = 6.09 km sec^{-1}) that vary in thickness and distribution with crustal spreading rate, age, and tectonic provenance. Hussong (1972) demonstrated that the seismic velocity structure of the oceanic crust varies throughout the Pacific.

Christensen and Salisbury (1975) averaged classical explosion and airgun-sonobuoy refraction data from main ocean basins and determined the mean seismic velocity structures of normal oceanic crust (Figure 19). They defined normal oceanic crust as oceanic crust that formed at least 40 m.y. ago in a main ocean basin and is not associated with fracture zones, offridge rises, plateaus, intraplate volcanism, or linear island chains.

Their classical seismic velocity structure of oceanic crust, developed from explosion refraction data, consists of three layers. "Layer 1" is a thin veneer, 0.66 ± 0.90 km thick, of sediments in which V_p is 2.20 ± 0.31 km sec^{-1}; in "layer 2", 1.71 km thick, V_p is 5.07 ± 0.63 km sec^{-1}; in "layer 3", 4.86 ± 1.42 km thick, V_p is 6.69 ± 0.26 km sec^{-1}, V_s is 3.75 ± 0.03 km sec^{-1}, and Poisson's ratio is 0.28.

They identified two oceanic crustal types from airgun-sonobuoy refraction data (Figure 19). In Type I crust, "layer 3" is divided into a low velocity (V_p = 6.4 km sec^{-1}) refractor ("layer 3A") with an average thickness of 1.0 km that is underlain by a higher velocity

Figure 19. Seismic velocity structures of normal oceanic crust (after Christensen and Salisbury, 1975). The 3-layer structure is the seismic velocity structure as seen by classical explosion seismology refraction techniques. Types I and II are interpreted from airgun-sonobuoy refraction data. (V_p) and (V_s) represent compressional and shear wave velocities (km sec^{-1}), respectively; (t) is thickness of each layer in kms; and (σ) is Poisson's ratio.

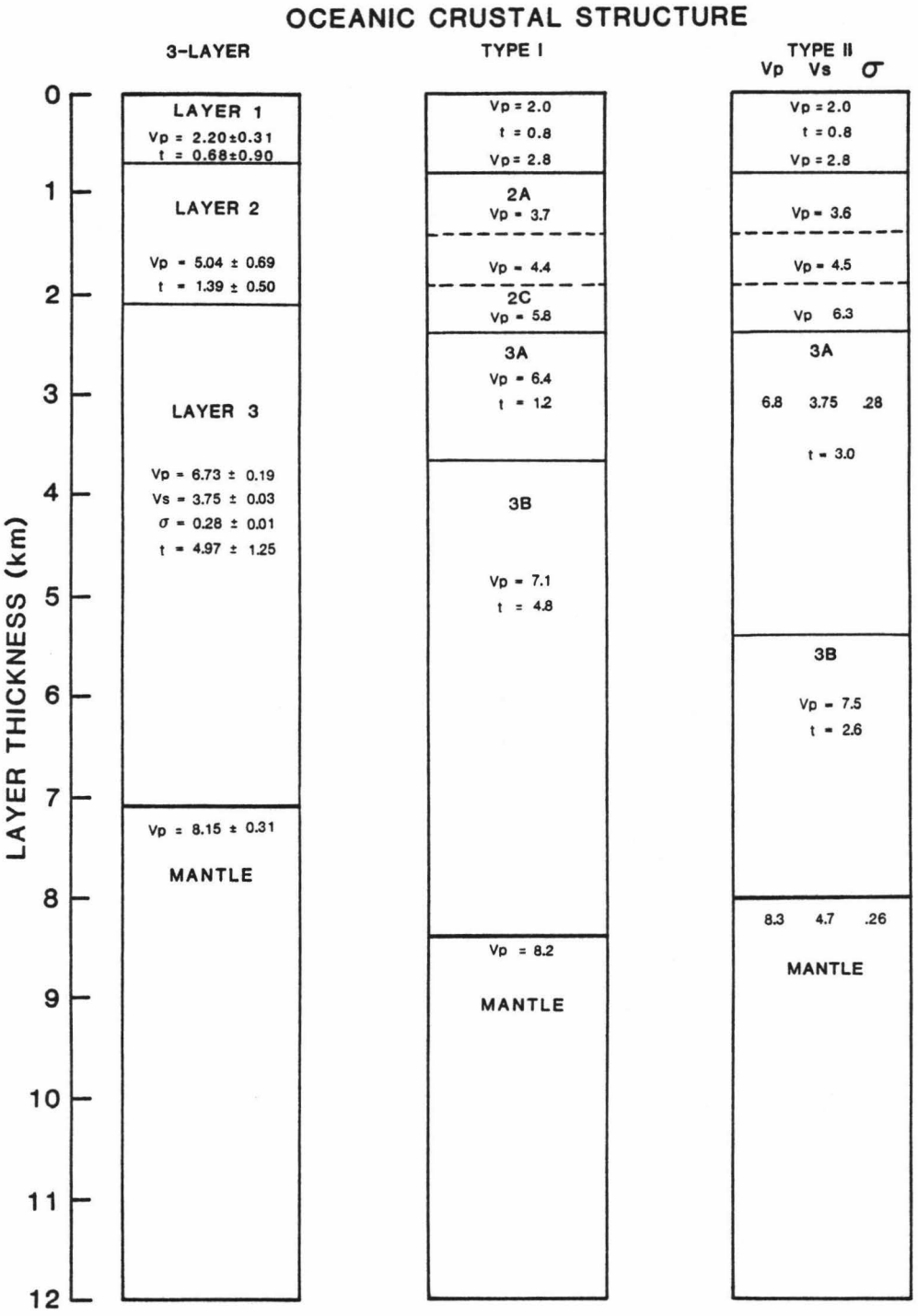
OCEANIC CRUSTAL STRUCTURE
3-LAYER
TYPE I
TYPE II
Vp Vs σ
LAYER THICKNESS (km)
0
1
2
3
4
5
6
7
8
9
10
11
12
LAYER 1
Vp = 2.20±0.31
t = 0.68±0.90
LAYER 2
Vp = 5.04 ± 0.69
t = 1.39 ± 0.50
LAYER 3
Vp = 6.73 ± 0.19
Vs = 3.75 ± 0.03
σ = 0.28 ± 0.01
t = 4.97 ± 1.25
Vp = 8.15 ± 0.31
MANTLE
Vp = 2.0
t = 0.8
Vp = 2.8
2A
Vp = 3.7
Vp = 4.4
2C
Vp = 5.8
3A
Vp = 6.4
t = 1.2
3B
Vp = 7.1
t = 4.8
Vp = 8.2
MANTLE
Vp = 2.0
t = 0.8
Vp = 2.8
Vp = 3.6
Vp = 4.5
Vp 6.3
3A
6.8 3.75 .28
t = 3.0
3B
Vp = 7.5
t = 2.6
8.3 4.7 .26
MANTLE

(V_p = 7.1 km sec^{-1}) refractor ("layer 3B") with an average thickness of 5.0 km. In Type II crust, "layer 3" is divided into two refractors of equal thickness (~3.0 km). The upper refractor ("layer 3A") with V_p of 6.8 km sec^{-1} overlies a lower refractor ("layer 3B") with V_p of 7.5 km sec^{-1}.

The Type I crustal model was developed from second arrival amplitude information and extended marine seismic refraction profiles. The Type II crustal model was developed from ASPER data. The ASPER technique, which uses phase coherence between traces and not amplitude information, often yields mantle V_p greater than 8.3 km sec^{-1} and thicker oceanic crustal sections. Christensen and Salisbury (1975) suggested that the differences between the two oceanic types can be attributed to local structural and petrologic heterogeneity. Kempner (1981) suggested that the apparent differences reflect the differences in shot densities and interpretative techniques.

Kennett and Orcutt (1976) and Spudich and Orcutt (1980a, 1980b), using synthetic seismograms to model arrival times, amplitudes, and waveforms of marine reflection-refraction data, have suggested that velocities vary smoothly and continuously with depth in the oceanic crust. Although the results of Spudich and Orcutt (1980b) generally support the earlier seismic velocity structures of the oceanic crust, they found that the high velocity basal crustal layer ("layer 3B") of Sutton et al. (1971) may be an artifact of the ASPER data analysis techniques. With their refined data analysis techniques Spudich and Orcutt (1980b) have found that the detailed seismic velocity structures

of crustal "layers 2 and 3" and the crust-mantle transition zone appear to vary regionally: lateral heterogeneity of the crust is exhibited by structural variations, extreme variability of V_s, and missing mantle reflections between adjacent refraction stations. They and Salisbury and Christensen (1978) and Nichols et al. (1980) have suggested that fine seismic velocity details such as low velocity layers, velocity gradients, and small velocity changes are probably present within the oceanic crust but are usually undetected by the marine seismic refraction techniques that are presently used.

There are several complications to the seismic velocity structure of the oceanic crust. One complication is the presence of seismic velocity anisotropy (ΔV_p) in oceanic "layer 3" and the upper mantle. Christensen (1972b) suggested that ΔV_p in "layer 3" is statistically fastest by a maximum of 4% when measured parallel to ridge crests. ΔV_p in the upper mantle is commonly detected (Hess, 1964; Raitt et al., 1969) with values of 8.0 to 10.0% where V_p is fastest when measured perpendicular to ridge crests. Christensen (1972b) suggested that the preferentially oriented hornblende grains in amphibolites of "layer 3" causes the ΔV_p that may occur in that layer. Christensen and Salisbury (1979) and Peselnick and Nicolas (1978) showed that strain aligned olivine grains in peridotite tectonites could explain the measured ΔV_p in the upper mantle.

The oceanic crust also appears to vary structurally with age, spreading rate, and tectonic provenance. Not only does the oceanic crust appear to age from young crust with seismic velocity structures

that are characterized by smoothly varying velocity gradients to old crust with distinctly layered seismic velocity structures (Kempner and Gettrust, 1981b), but "layer 3" and the total oceanic crust also appear to thicken with age (Moores and Jackson, 1974; Christensen and Salisbury, 1975). Moores and Jackson (1974), using marine seismic refraction data, suggested that the thickness of oceanic "layers 3A and 3B" decrease and increase, respectively, as the spreading rate of the oceanic crust increases. Modeling the temperature distribution beneath an oceanic ridge with a magma chamber, Sleep (1975), Kuznir and Bott (1976), and Kuznir (1980) suggested that the existence and width of a magma chamber and the thickness of a dike complex beneath a spreading ridge depend on the half-spreading rate of the oceanic crust. Furthermore, Christensen and Salisbury (1975) suggested that the crustal structures of fracture zones, offridge rises, linear island chains, troughs, trenches, and back arc basins are all different.

5.1.2 Petrologic Models of the Oceanic Crust

Petrologic models that attempt to explain the seismic velocity structures of the oceanic crust have been proposed. The models are based on dredge haul samples, DSDP cores, and ophiolites.

To explain the abundance of serpentinites that were dredged from mid-ocean ridges and trenches, Hess (1962) proposed that "layer 3" of the oceanic crust is composed of partially serpentenized peridotites. Hess (1962) suggested that the partially serpentenized peridotites are generated at ridge crests by the hydration of exposed upper mantle peridotites down to the 500^{o} C isotherm in the crust. With continued

spreading the partially serpentenized peridotites are carried laterally beneath the oceanic crust and away from the ridge crest. This model explained the seismic Moho as the fossilized hydration boundary (a gradational boundary) between fresh and partially serpentenized upper mantle peridotites.

Clague and Straley (1977) and Nichols et al. (1980), using the laboratory measured velocities in rocks from ophiolites, suggested that "layer 3" is composed of massive and cumulate metagabbros, partially serpentenized cumulate peridotites, and a layer of partially serpentenized peridotite tectonites of the upper mantle. They suggested that in situ serpentenization of the upper mantle occurs beneath thin crustal sections due to penetration of the crustal sections by seawater. Furthermore they implied that: (1) the seismic Moho is a gradational boundary between partially serpentenized and fresh upper mantle peridotites, and (2) "layer 3" of the oceanic crust thickens with age due to continued downward serpentenization of the upper mantle with time.

Other authors reject the idea of an oceanic "layer 3" that is composed of serpentenites. Cann (1968) argued that the restricted range of V_p that was seismically measured in "layer 3" required a uniform degree of serpentenization in the proposed peridotites of the lower oceanic crust. He considered such a uniform degree of serpentenization unlikely and suggested instead that "layer 3" is composed of metagabbros. Christensen and Salisbury (1975) compared laboratory measured velocities and calculated Poisson's ratio of rocks dredged from

the ocean floor and taken from ophiolites to those values that had been seismically measured in the oceanic crust. From this comparison they suggested that oceanic "layer 3" is composed of metagabbros overlying fresh gabbros and other rocks.

The composition of "layer 3B", the high velocity basal layer of Sutton et al. (1971), is also speculative. Based on their velocity measurements in rocks from the Ming's Bight ophiolite, Newfoundland, Peterson et al. (1974) suggested that "layer 3B" is composed of fresh gabbro, cumulate gabbro, or cumulate peridotite. Salisbury and Christensen (1978), using their velocity-depth profile of the BOI ophiolite, suggested that "layer 3B" is marked by the first appearance of cumulus phase olivine in cumulate gabbros of "layer 3".

5.2 Comparison Between the Seismic Velocity Structures of the Oceanic Crust and the Samail Ophiolite

The smoothly and continuously varying velocity-depth profile of the Samail ophiolite can be directly compared to the velocity gradient models of oceanic crust; it can not be compared to the discretely layered seismic velocity structures of normal oceanic crust. For this reason the classical explosion and airgun-sonobuoy seismic velocity structures of the Samail ophiolite are inferred from its velocity-depth profile by the method of Salisbury and Christensen (1978). The seismic velocity structures of the Samail ophiolite are developed by assuming that routine marine seismic refraction surveys, using classical explosion and airgun-sonobuoy techniques, are conducted over a section of oceanic crust that is petrologically and structurally equivalent to

the Samail ophiolite. It is also assumed that: (1) only the most distinct first and second arrival data are used to determine the layered seismic velocity structures of the Samail ophiolite, and (2) the most distinct arrivals are head waves that have been critically refracted at rock boundaries that are marked by strong velocity gradients or velocity discontinuities.

If a routine marine seismic refraction survey employing classical explosion seismology techniques were conducted over the Samail ophiolite, only three distinct basement refractors would be detected below a thin layer of oceanic sediments ("layer 1"). The classical, three-layer seismic velocity structure of the Samail ophiolite would consist of a shallow, low velocity layer that extends 2.5 km beneath the sediments, a 6.9 km sec^{-1} layer between depths of 2.5 and 8.0 km, and a 8.1 km sec^{-1} layer below depths of 8.0 km. This three-layer seismic velocity structure of the Samail ophiolite, presented in column D of Figure 20, can be correlated with the lithology and metamorphic assemblages of the Samail ophiolite that are presented in layered format in columns A and B of Figure 20.

The shallow, low velocity refractor ($V_p \sim 5.7$ km sec^{-1}, $V_s \sim 3.3$ km sec^{-1}) would consist of extrusive basalts that grade to sheeted dikes. Due to the large range of velocities in the metabasalts and the poor resolution of velocity structure afforded by classical explosion refraction techniques, the assumed seismic velocities represent an average value for the shallow refractor.

Figure 20. Comparison between the seismic velocity structures of normal oceanic crust and the Samail ophiolite. Columns A, B, and C present the lithology, metamorphic assemblages, and the measured compressional (V_p) and shear (V_s) wave velocities (km sec^{-1}) and Poisson's ratio (σ), respectively, of the Samail ophiolite in layered format. Column D is the inferred seismic veloctiy structure of the Samail ophiolite as seen by classical explosion seismology refraction techniques; column H as seen by airgun-sonobuoy refraction techniques. The dashed lines in column H mark the occurrence of V_p that is characteristic of oceanic "layers 2C and 3B", respectively. Columns E, F, and G are the seismic velocity structures of normal oceanic crust (after Christensen and Salisbury, 1975) as discussed in Figure 19. (t) is the thickness of each layer in kms. The heavy line indicates the seismic Moho.

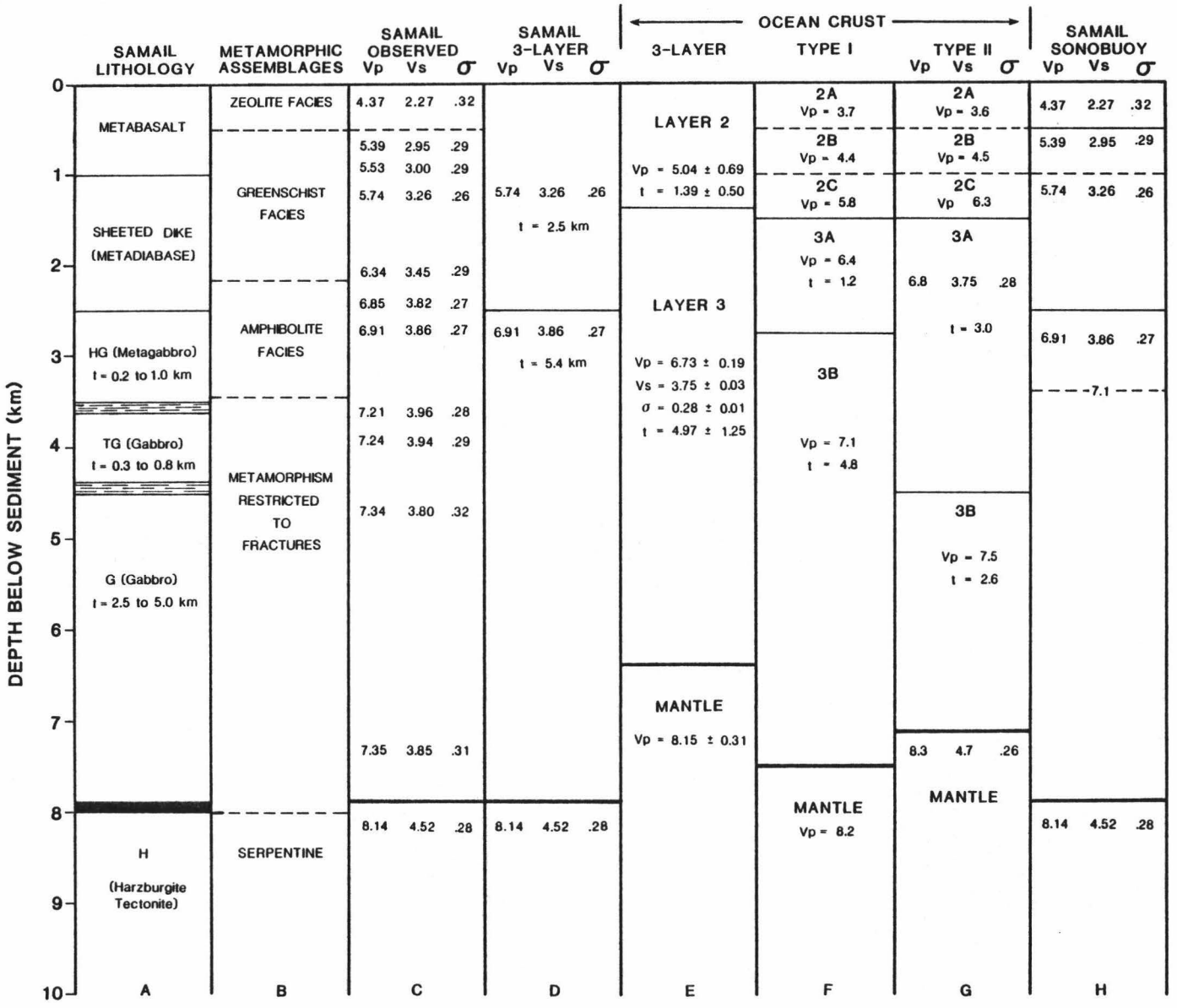
DEPTH BELOW SEDIMENT (km)
0
1
2
3
4
5
6
7
8
9
10
SAMAIL LITHOLOGY
METABASALT
SHEETED DIKE (METADIABASE)
HG (Metagabbro) t = 0.2 to 1.0 km
TG (Gabbro) t = 0.3 to 0.8 km
G (Gabbro) t = 2.5 to 5.0 km
H (Harzburgite Tectonite)
A
METAMORPHIC ASSEMBLAGES
ZEOLITE FACIES
GREENSCHIST FACIES
AMPHIBOLITE FACIES
METAMORPHISM RESTRICTED TO FRACTURES
SERPENTINE
B
SAMAIL OBSERVED
Vp Vs σ
4.37 2.27 .32
5.39 2.95 .29
5.53 3.00 .29
5.74 3.26 .26
6.34 3.45 .29
6.85 3.82 .27
6.91 3.86 .27
7.21 3.96 .28
7.24 3.94 .29
7.34 3.80 .32
7.35 3.85 .31
8.14 4.52 .28
C
SAMAIL 3-LAYER
Vp Vs σ
5.74 3.26 .26
t = 2.5 km
6.91 3.86 .27
t = 5.4 km
8.14 4.52 .28
D
OCEAN CRUST
3-LAYER
LAYER 2
Vp = 5.04 ± 0.69
t = 1.39 ± 0.50
LAYER 3
Vp = 6.73 ± 0.19
Vs = 3.75 ± 0.03
σ = 0.28 ± 0.01
t = 4.97 ± 1.25
MANTLE
Vp = 8.15 ± 0.31
E
TYPE I
2A
Vp = 3.7
2B
Vp = 4.4
2C
Vp = 5.8
3A
Vp = 6.4
t = 1.2
3B
Vp = 7.1
t = 4.8
MANTLE
Vp = 8.2
F
TYPE II
Vp Vs σ
2A
Vp = 3.6
2B
Vp = 4.5
2C
Vp 6.3
3A
6.8 3.75 .28
t = 3.0
3B
Vp = 7.5
t = 2.6
8.3 4.7 .26
MANTLE
G
SAMAIL SONOBUOY
Vp Vs σ
4.37 2.27 .32
5.39 2.95 .29
5.74 3.26 .26
6.91 3.86 .27
7.1
8.14 4.52 .28
H

Distinct first arrivals of headwaves that would be critically refracted at the high velocity gradient at a depth of 2.5 km in the Samail ophiolite, would indicate an intermediate velocity refractor at this depth. Because the headwaves travel only in the top of the refractor (in the massive metagabbros) V_p of 6.9 km sec^{-1} and V_s of 3.9 km sec^{-1} would be detected. Because low velocity gradients (< 0.1 sec^{-1}) below a depth of 2.5 km would not produce distinct first arrivals, this refractor would extend to depths of 7.0 to 8.0 km. The high velocities that were assumed for the cumulate peridotites would not be detected because these rocks form a layer that is less than 1.0 km thick; less than the seismic wavelengths employed in explosion seismology refraction techniques. Therefore this intermediate velocity refractor would consist of massive metagabbros that overlie fresh cumulate gabbros and peridotites.

Likewise distinct first arrivals of headwaves that would be critically refracted at the crust-mantle seismic velocity discontinuity would indicate a deep refractor (below 8.0 km) in which V_p of 8.1 km sec^{-1} and V_s of 4.5 km sec^{-1} would be measured. This refractor would consist of a thin layer of cumulus dunite that caps a thick layer of harzburgite tectonites. The velocity anisotropy of the harzburgite tectonites of the Samail ophiolite would be seismically detected because: (1) the thickness of the layer of cumulus dunite ($\sim$0.1 km) is much less than the seismic wavelengths employed in explosion seismology techniques, and (2) the laterally isotropic cumulate peridotites would comprise the base of the intermediate velocity refractor.

This three-layer seismic velocity structure of the Samail ophiolite is compared with the classical seismic velocity structure of normal oceanic crust as summarized by Christensen and Salisbury (1975) and presented in column F of Figure 20. The three refractors of the Samail ophiolite appear to correlate with the three constant velocity "layers" of normal oceanic crust. V_p and Poisson's ratio values for the three refractors of the Samail ophiolite and the thickness of the intermediate velocity refractor of the ophiolite are within one standard deviation of normal crustal values. Although the thickness of the shallow low velocity refractor of the Samail ophiolite (2.5 km) is greater than the thickness of "layer 2" of normal oceanic crust (1.39 ± 0.5 km), the thickness of the refractor in the ophiolite is within the range of thicknesses (1.0 to 2.5 km) measured by Raitt (1963) for oceanic "layer 2". V_s of 3.3 km sec^{-1} in the shallow refractor of the ophiolite is within the range of V_s (2.50 to 3.55 km sec^{-1}) measured by Sutton et al. (1971) in oceanic "layer 2". V_s of 3.9 km sec^{-1} in the intermediate velocity refractor of the ophiolite, although greater than V_s of normal oceanic crust (3.75 ± 0.03 km sec^{-1}) is within the measured range of V_s for oceanic "layer 3" (3.55 to 3.88 km sec^{-1}) as compiled by Christensen and Salisbury (1975). Also the presence of velocity anisotropy (ΔV_p and ΔV_s = 0.4 to 9.0%) in the harzburgite tectonites of the Samail ophiolite is within the range of seismic velocity anisotropy that has been measured in the upper mantle (ΔV_p = 8 to 10%) with classical seismic refraction techniques by Hess (1964) and Raitt et al. (1969).

The comparison between the three-layer seismic velocity structures of the Samail ophiolite and normal oceanic crust suggests that the seismic velocity structures can be correlated. The shallow, low velocity refractor of the Samail ophiolite appears to represent a thick oceanic "layer 2"; the intermediate velocity refractor of the ophiolite corresponds to oceanic "layer 3"; and the high velocity refractor below depths of 8.0 km in the Samail ophiolite corresponds to the oceanic upper mantle.

If a routine seismic marine refraction survey employing airgun-sonobuoy techniques were conducted over the Samail ophiolite, the four-layer seismic velocity structure that would be observed in the ophiolite is shown in column H of Figure 20. The airgun-sonobuoy and classical seismic velocity structures of the Samail ophiolite differ in one aspect. With the increased structural resolution of the airgun-sonobuoy techniques that is afforded by high shot densities and second arrival data analysis, an additional low velocity refractor (V_p = 4.4 km sec^{-1}, V_s = 2.3 km sec^{-1}, and σ = 0.32) of pillowed metabasalts would be detected in the Samail ophiolite. This shallow refractor would cap the seismic velocity structure of the ophiolite and extend 0.5 km below the oceanic sediments. Arrivals of headwaves that would be criticaly refracted at the minor velocity discontinuity at a depth of 0.5 km in the Samail ophiolite would indicate a discrete refractor at this depth in which V_p of 5.4 km sec^{-1}, V_s of 3.0 km sec^{-1}, and Poisson's ratio of 0.29 would be measured. This refractor would extend to a depth of 2.5 km below the oceanic sediments and would be

composed of low-porosity metabasalts that grade to sheeted dikes. Due to the lack of high velocity gradients in the cumulate gabbros, only the "layer 3" and upper mantle refractors would be detected below depths of 2.5 km in the Samail ophiolite. The seismic velocity structure that would be determined for the lower crustal section of the Samail ophiolite when using airgun-sonobuoy techniques is therefore identical to the classical seismic velocity structure of the ophiolite below depths of 2.5 km.

The airgun-sonobuoy seismic velocity structure of the Samail ophiolite, presented in column H of Figure 20, is compared with the Type I and Type II seismic velocity structures of normal oceanic crust that are shown in columns F and G of Figure 20. The correlation between the airgun-sonobuoy seismic velocity structures of the Samail ophiolite and normal oceanic crust is not as apparent as the correlation between the classical seismic velocity structures of normal oceanic crust and the Samail ophiolite.

V_p of the two refractors within the uppermost 2.5 km of the Samail ophiolite are greater than V_p in "layers 2A and 2B" of normal oceanic crust (3.6 to 3.7 km sec^{-1} and 4.4 to 4.5 km sec^{-1}, respectively). However, Houtz and Ewing (1976), using airgun-sonobuoy refraction data from the Reykajanes Ridge, the Atlantic, and the Pacific basins, found that V_p in oceanic "layer 2B" ranges from 4.8 to 6.3 km sec^{-1}; V_p of 5.4 km sec^{-1} in the refractor between depths of 0.5 and 2.5 km in the Samail ophiolite is within this range. Also the relatively high V_p values (V_p > 4.37 km sec^{-1}) that were measured in this study in the uppermost

basalts of the Samail ophiolite between depths of 0 to 0.5 km are probably not representative of the V_p values in the uppermost oceanic crust (discussed later). Nevertheless, because pillowed to massive basalts are commonly recovered in DSDP cores, the uppermost refractor of the Samail ophiolite is known to correspond to "layer 2A" of the oceanic crust.

It is suggested that seismically distinct refractors corresponding to oceanic "layers 2C and 3B" would not be interpreted from airgun-sonobuoy refraction data for the Samail ophiolite. Because velocities increase smoothly with depth between 0.5 and 2.5 km in the Samail ophiolite, a sufficiently high velocity gradient that would support a simple headwave or interference headwave (Spudich and Orcutt, 1980b) at an appropriate depth for the "layer 2B-layer 2C" seismic velocity boundary does not occur in the Samail ophiolite. Likewise a high velocity gradient that would mark the "layer 3A-layer 3B" seismic velocity boundary does not occur between depths of 3.0 and 8.0 km in the ophiolite. As a result the changes in velocities that occur within these regions would be correctly attributed to velocity gradients in "layer 2B" and "layer 3" (Salisbury and Christensen, 1978).

"Layer 2C and 3B" refractors are not consistently observed in the oceanic crust when using airgun-sonobuoy seismic refraction techniques. Houtz and Ewing (1976) noted the lack of arrivals from oceanic "layer 2C" in Atlantic crust less than 50 m.y. old. Spudich and Orcutt (1980b) suggested that oceanic "layer 3B" is not a widespread feature of the lower oceanic crust, while Christensen and Salisbury (1975) and Kempner

and Gettrust (1981a) suggested that a seismically distinct oceanic "layer 3B" is most often found in mature oceanic crust. However the failure to detect distinct "layer 2C and 3B" refractors in a section of oceanic crust does not necessarily indicate that these refractors or at least seismic velocities that are characteristic of these refractors do not occur in the section of oceanic crust. With high frequency seismic sources and much more densely spaced seismic refraction data, the seismic velocity structures of the oceanic "layers 2 and 3" would be better defined (Spudich and Orcutt, 1980b).

In this study rock velocity data was determined at approximately 250 m intervals with depth in the Samail ophiolite. As a result, laboratory measured V_p values of 5.7 to 6.3 km sec^{-1}, values that are close to those that have been measured in oceanic "layer 2C" by Houtz and Ewing (1976), occur in the sheeted dikes of the Samail ophiolite below a depth of 1.0 km. Likewise, laboratory measured V_p values of 7.1 to 7.35 km sec^{-1} that correspond to the V_p values that were measured in oceanic "layer 3B" by Sutton et al. (1971) occur in the fresh cumulate gabbros of the Samail ophiolite below depths of 3.5 km. Dashed lines in column H indicate the stratigraphic positions of these characteristic velocities in the Samail ophiolite. This comparison suggests that the airgun-sonobuoy seismic velocity structure of the Samail ophiolite is comparable to the seismic velocity structure of of Type I oceanic crust.

The comparisons between the classical explosion and airgun-sonobuoy seismic velocity structures of the Samail ophiolite and normal oceanic crust demonstrate that the Samail ophiolite is comparable to average

oceanic crust. To establish a more definite relationship between the Samail ophiolite and contemporary oceanic crust, the velocity-depth profile of the Samail ophiolite is compared below with the velocity gradient model of a section of oceanic crust that formed at the East Pacific Rise.

In Figure 21 the V_p profile of the Samail ophiolite is compared with the velocity gradient model (ROSE profile) of a section of oceanic crust that formed 4.5 m.y. ago at the East Pacific Rise (Kempner and Gettrust, 1981a). This velocity-depth function generates synthetic seismograms that correlate closely with the OBS reflection-refraction data that was collected during the ROSE (Rivera Ocean Seismic Experiment) project near the East Pacific Rise (Kempner and Gettrust, 1981a). The ROSE profile, a perturbed model of the velocity-depth profile that was developed by Manghnani et al. (1981) for the Ibra-Muscat section of the Samail ophiolite, fits the stratigraphic limits of the ophiolite as described by Hopson et al. (1981).

The similarities of the V_p structure in the Samail ophiolite and the section of contemporary oceanic crust are exciting. Not only are V_p values similar but the seismic velocity gradients are nearly identical above a depth of 2.0 km (~ 1.0 sec^{-1}) and below a depth of 3.0 km (< 0.1 sec^{-1}). Late-stage differentiates occur at a depth of 2.5 km in the Ibra area of the Samail ophiolite and depress V_p in this region. Kempner and Gettrust (1981a) suggested that the minor velocity inversion in the ROSE profile may also signify late-stage differentiates at a depth of 3.5 km in the section of Pacific crust. The difference of

Figure 21. Comparison between the velocity gradient model (ROSE profile) for a section of 4.5 m.y. old oceanic crust near the East Pacific Rise (after Kempner, 1981) and the veloctiy-depth profile of the Samail ophiolite. (V_p) represents compressional wave velocity.

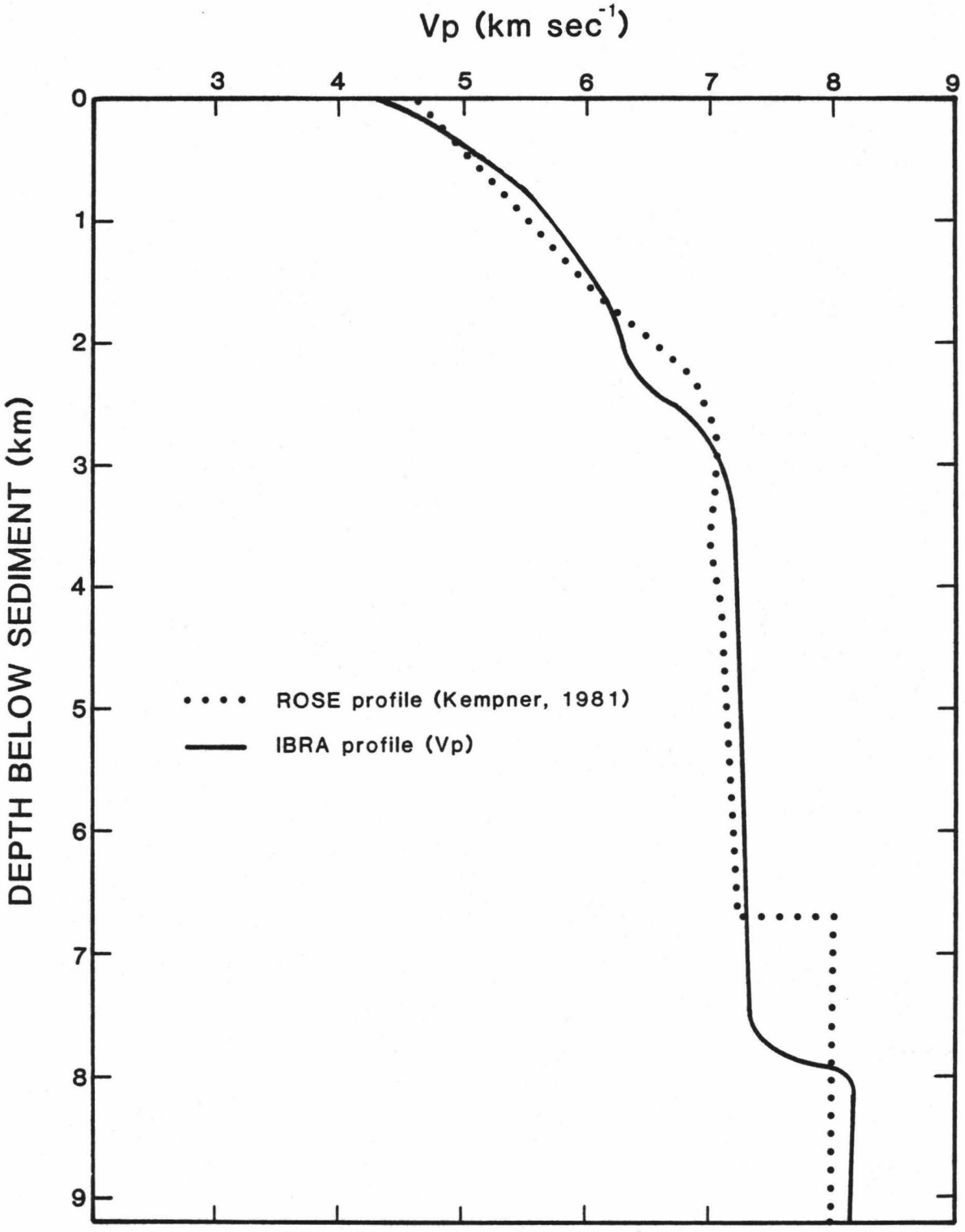
Vp (km sec^{-1})
3
4
5
6
7
8
9
0
1
2
3
4
5
6
7
8
9
DEPTH BELOW SEDIMENT (km)
ROSE profile (Kempner, 1981)
IBRA profile (Vp)

stratigraphic position for the low velocity regions in the two profiles (± 1.0 km) is no greater than the lateral variability displayed within the Samail ophiolite. Upper mantle V_p of 8.0 to 8.1 km sec^{-1} occurs at similar depths in both profiles (7.0 to 8.0 km). This observation indicates similar crustal thicknesses for the Samail ophiolite and the section of Pacific crust. The crust-mantle contact is a first order V_p discontinuity in the 4.5 m.y. old oceanic crust, and a thin transition zone in the Samail ophiolite. Kempner (1981) and Kempner and Gettrust (1981a) concluded that the velocity-depth profile of the Samail ophiolite (Ibra-Muscat area) is consistent with seismic reflection-fraction data for a section of 4.5 m.y. old oceanic crust that formed at the fast-spreading ($\sim$5 cm yr^{-1}, half-rate) East Pacific Rise. Furthermore, they suggested that the Samail ophiolite is a "seismically acceptable" model for young oceanic crust.

6. A PETROLOGIC-SEISMIC MODEL OF YOUNG AND THICK OCEANIC CRUST

The inferred classical explosion and airgun-sonobuoy seismic velocity structures of the Samail ophiolite are comparable to those of normal oceanic crust. Kempner and Gettrust (1981a) concluded that the velocity-depth profile of the Samail ophiolite is consistent with OBS reflection-refraction data for a section of oceanic crust that formed 4.5 m.y. ago at the East Pacific Rise. Moreover, they suggested that the Samail ophiolite, a fragment of Tethyan oceanic crust, is indeed a "seismically acceptable" model of young oceanic crust. For these reasons the Samail ophiolite and its laboratory measured velocity-depth profile are used as a petrologic-seismic model of young (4 to 8 m.y.) and thick (7.0 to 8.0 km) oceanic crust that formed in a large, long-lived magma chamber at a moderate-to-fast spreading (3 to 5 cm yr^{-1}, half-rate) mid-ocean ridge.

In Figure 22, the petrology of the modeled oceanic crust and its characteristic <u>in situ</u> V_p, V_s, bulk density, and Poisson's ratio profiles are shown. This petrologic-seismic model describes a section of oceanic crust that is distant from anomalous features such as fracture zones, island arcs, subduction zones, or intraplate volcanism. Below, the model is explained by seismic layers. The lateral and vertical variability of the model is emphasized. Layer 1 (oceanic sediments) is not discussed.

Figure 22. A petrologic-seismic model of young and thick oceanic crust. (V_p) and (V_s) represent compressional and shear wave velocities, respectively; (ρ) is the bulk density of the crustal lithologies; and (σ) is Poisson's ratio. The profiles present the average values that may be observed in the oceanic crust while the shading represents the range of values. The dashed lines indicate insufficient data. The seismic Moho, marking the occurrence of $V_p > 8.0$ km sec^{-1}, may occur at any stratigraphic position within the basal cumulate peridotites. In the model the deepest probable position of the seismic Moho is shown at the lithologic contact between basal cumulate peridotites and crustal cumulus dunite.

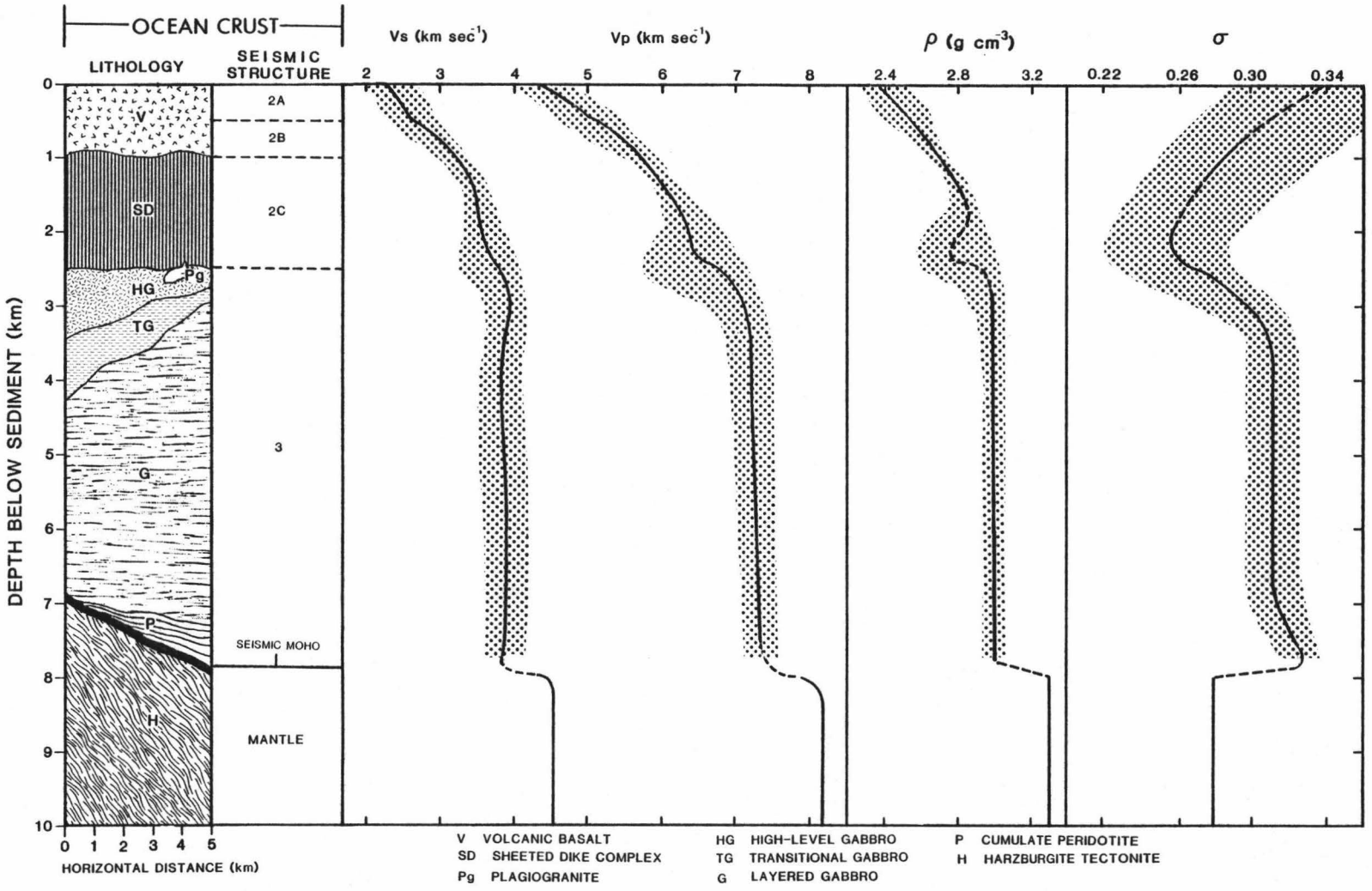
OCEAN CRUST
LITHOLOGY
SEISMIC STRUCTURE
Vs (km sec⁻¹)
Vp (km sec⁻¹)
ρ (g cm⁻³)
σ
2A
2B
2C
3
SEISMIC MOHO
MANTLE
V
SD
Pg
HG
TG
G
P
H
DEPTH BELOW SEDIMENT (km)
HORIZONTAL DISTANCE (km)
V VOLCANIC BASALT
SD SHEETED DIKE COMPLEX
Pg PLAGIOGRANITE
HG HIGH-LEVEL GABBRO
TG TRANSITIONAL GABBRO
G LAYERED GABBRO
P CUMULATE PERIDOTITE
H HARZBURGITE TECTONITE

The velocity-depth profile of the Samail ophiolite, the veolcity-depth function for a section of young oceanic crust near the East Pacific Rise, and the seismic velocity model of young and thick oceanic crust presented in Figure 22 show that seismic velocities continuously and smoothly vary with depth in young oceanic crust. Except for possible "layer 2A-layer 2B" and "layer 2-layer 3" seismic velocity boundaries, the seismic velocity structure of young and thick oceanic crust is not characterized by strong velocity gradients or velocity discontinuities. Nevertheless, due to convention, the petrologic-seismic model is discussed by seismic velocity "layers" with the understanding that discrete, constant velocity layers, as such, are not present in the model of young oceanic crust.

6.1 Layer 2

"Layer 2" of the crustal model is generally composed of extrusive basalts and sheeted dikes and may extend to a depth of 2.5 km below the oceanic sediments. The high velocity gradients ($\sim$1.0 km sec^{-1}) that characterize this region are caused by the combined effects of decreasing basalt porosity, increasing metamorphic grade, and changing lithology that result in increasing bulk density with depth. Sublayers "2A, 2B, and 2C" mark the regions where each of these factors primarily affects seismic velocities. The wide range of seismic velocities that are observed for oceanic "layer 2" is an indication of the lateral heterogeneity of this region (Schreiber and Fox, 1976).

DSDP cores from oceanic crust less than 10 m.y. old indicate that oceanic "layer 2A" consists of pillowed and massive basalts to zeolite facies metabasalts. The lowest velocities (V_p = 4.4 km sec^{-1}, V_s = 2.3 km sec^{-1}) and highest Poisson's ratio (σ = 0.29 to 0.35) of the crustal model occur in "layer 2A". In young oceanic crust that formed at a fast spreading ridge, this region has an average thickness of 0.5 to 0.7 km (Houtz and Ewing, 1976).

The low seismic velocities (V_p = 3.7 km sec^{-1}, V_s = 2.2 km sec^{-1}) that are characteristic in "layer 2A" of the oceanic crust were not measured in the metabasalt samples from the Samail ophiolite and have not been observed in basalt samples from other ophiolites (Peterson et al., 1974; Salisbury and Christensen, 1978; Nichols et al., 1980) or in basalt samples from the oceanic crust (Hyndman and Drury, 1976). This observation indicates that the seismic velocities of "layer 2A" are controlled by large scale fractures and pores, and pore pressure conditions that are not duplicated in laboratory rock samples (Schreiber and Fox, 1976; Spudich and Orcutt, 1980a). The high Poisson's ratio (σ = 0.31 to 0.38) and low seismic velocities in "layer 2A" of young oceanic crust suggest that porosity is in the form of cracks, fissures, breccia, talus, and rubble (Hyndman, 1979).

In young crust these pores and fractures are probably interconnected with each other and the overlying seawater such that pore pressure is at least equal to hydrostatic pressure (Spudich and Orcutt, 1980b). As observed in a vesicular metabasalt from the Samail ophiolite (see Figure 7), high pore pressure substantially reduces V_s relative to

V_p in a water saturated rock and subsequently causes a high Poisson's ratio for the rock. As a consequence Poisson's ratio is modeled as greater than 0.31 for the uppermost (0 to 0.5 km) basalts of young oceanic crust.

Higher velocities (V_p > 4.0 km sec^{-1}, V_s > 2.5 km sec^{-1}) and lower Poisson's ratio (σ = 0.31) that are commonly observed in "layer 2B" occur below a depth of 0.5 km in the crustal model. The greenschist facies metabasalts of this region are characterized by downward decreasing porosity and permeability (Salisbury et al., 1980). Due to decreased permeability, fluids filling open cracks and pores are no longer interconnected to the overlying seawater and, subsequently, pore pressures in the metabasalts probably vary between lithostatic and hydrostatic pressures (Brace, 1971). As a result velocities increase rapidly with depth as lithostatic confining pressure on the low-porosity basalts increases (see Figure 7). Consequently, the "layer 2A-layer 2B" seismic velocity boundary is modeled as a real structural feature of young oceanic crust. This seismic velocity boundary marks the gradational changes from porous to low-porosity metabasalts, from zeolite to greenschist facies assemblages, and from pore pressures equivalent to lithostatic confining pressures to pore pressures less than lithostatic confining pressures. These gradational boundaries may or may not coincide, they may be poorly defined (Spudich and Orcutt, 1980a), and they may change with time as hydrothermal metamorphism and low temperature alteration affect the rocks.

The lack of a distinct velocity discontinuity between depths of 0.5 to 2.5 km in the velocity-depth profile of the Samail ophiolite suggests that a "layer 2C" refractor in young oceanic crust will be difficult to detect using standard marine seismic refraction techniques. Nevertheless V_p of 5.7 to 6.4 km sec^{-1}, the range of V_p values that have been observed in oceanic "layer 2C" (Houtz and Ewing, 1976), were measured in the metadiabase samples from the Samail ophiolite. Therefore "layer 2C", when detected in marine seismic refraction studies of the oceanic crust, is modeled as a sheeted dike or dike and sill complex (Nichols et al., 1980) of greenschist to lower amphibolite facies metadiabases. The "layer 2B-layer 2C" seismic velocity boundary will, therefore, mark the minor lithologic change from low-porosity metabasalts to massive metadiabases. In this region V_p and V_s range from 5.7 to 6.4 km sec^{-1} and 3.25 to 3.8 km sec^{-1}, respectively, while Poisson's ratio ranges from 0.27 to 0.31. When "layer 2C" is not detected in young oceanic crust by marine seismic refraction techniques, the sheeted dike complex comprises the lower stratigraphic section of a thick "layer 2B". Discontinuous bodies of late-stage differentiates may intrude the base of the sheeted dikes.

6.2 Layer 3

In general, oceanic "layer 3" is modeled as a variably thick unit of massive metagrabbros (hydrothermally metamorphosed to the amphibolite facies) that overlie fresh cumulate gabbros and basal cumulate peridotites. In the model of young and thick oceanic crust it is assumed, based on petrological and geochemical evidence from the Samail

ophiolite (Boudier and Coleman, 1981; Gregory and Taylor, 1981), that the basal cumulate peridotites of the lower oceanic crust and peridotite tectonites of the upper mantle undergo only localized in situ serpentenization near a spreading ridge. Therefore, no low velocity layer of widely serpentenized upper mantle peridotites is included in "layer 3" of the model.

In the massive metagabbros at the top of the "layer 3" region, V_p widely ranges from 6.4 to 7.1 km sec^{-1} while V_s ranges from 3.6 to 3.9 km sec^{-1} and Poisson's ratio ranges from 0.27 to 0.31. Lower "layer 3" is characterized by a restricted range of velocities (V_p = 7.1 to 7.35 km sec^{-1}, V_s = 3.8 to 3.9 km sec^{1}) and Poisson's ratio (σ = 0.32 to 0.27) while velocity gradients beneath the metagabbros are less than 0.1 sec^{-1}.

The "layer 2-layer 3" seismic velocity boundary, as suggested by Nichols (1977), probably occurs as a high velocity gradient extending over a few hundred meters in depth. In the model this boundary occurs 2.5 km beneath the oceanic sediments where V_p increases rapidly from 6.4 to 7.0 km sec^{-1} in less than 500 meters. This high velocity gradient marks the contact between low density (< 2.9 g cm^{-3}) sheeted dikes and high density (> 2.9 g cm^{-3}) massive metagabbros, the appearance of intrusive plagiogranites and associated quartz-rich metadiabases and metagabbros near the contact, and the appearance of amphibolite facies assemblages. This interpretation of the "layer 2-layer 3" seismic velocity boundary is supported by Nichols et al. (1980).

The lack of a distinct velocity discontinuity or strong velocity gradient between depths of 3.0 to 7.0 km in the velocity-depth profile of the Samail ophiolite suggests that seismically distinct "layer 3A" and "layer 3B" refractors are not a widespread feature in young oceanic crust. Synthetic seismograms of marine seismic reflection-refraction data for sections of young oceanic crust support this conclusion (Spudich and Orcutt, 1980b; Kempner and Gettrust, 1981a).

Although the basal cumulate peridotites of the Samail ophiolite were not sampled in this study, it is suggested that a thin layer-set of interlayered cumulate peridotites (wehrlites, melagabbros, and minor troctolites) at the base of young and thick oceanic crust comprises a thin (< 1.0 km) crust-mantle transition zone. Within this zone, at depths of 6.4 to 7.4 km beneath the oceanic sediments, velocities that are observed in the lower oceanic crust (V_p = 7.1 to 7.35 km sec^{-1}, V_s = 3.8 to 3.9 km sec^{-1}) increase to those that are observed in the upper mantle (V_p > 8.00 km sec^{-1}, V_s > 4.50 km sec^{-1}) while Poisson's ratio decreases from 0.29 to 0.28. In support of this model, Talwani et al. (1981), using seismic Moho reflection data, concluded that the crust-mantle transition zone is abrupt, only several hundred meters thick, in young and old Pacific oceanic crust. Spudich and Orcutt (1980b) also stated that the crust-mantle transition zone is usually observed to be about 1.0 km thick in the oceanic crust while Kempner and Gettrust (1981a) suggested a thickness of only 0.5 km for the crust-mantle transition zone near the East Pacific Rise.

The seismic Moho marks the occurrence of upper mantle velocities in the young and thick oceanic crust. Due to the high olivine content of the basal cumulate peridotites, upper mantle velocities may be observed at any stratigraphic position within the crust-mantle transition zone. The petrologic Moho occurs stratigraphically lower at the lithologic contact between the crustal cumulus dunite and peridotite tectonites of the upper mantle.

The upper mantle is seismically modeled as a thin layer ($\sim$ 0.1 km) of crustal cumulus dunite overlying a thick and homogeneous (chemically and petrologically) layer of depleted harzburgite and dunite tectonites. The upper mantle displays seismic velocity anisotropy (ΔV_p and ΔV_s = 8.0 to 10.0%) due to the preferentially aligned, recrystallized olivine grains in the harzburgite tectonites. Petrofabric studies of harzburgite tectonites from the Samail ophiolite suggest that the [100] axes of the olivine grains, the fast direction for V_p and V_s in olivine, are aligned nearly parallel to the spreading direction of the crust and less than 15° from the horizontal (Boudier and Coleman, 1981). The velocity anisotropy of the upper mantle peridotites will be detected in marine seismic refraction surveys because: (1) most of the laterally isotropic cumulate peridotites (the crust-mantle transition zone) seismically comprise the base of oceanic "layer 3"; and (2) the crustal cumulus dunite that caps the harzburgite tectonites is much thinner than the seismic wavelengths that are characteristic of marine seismic refraction techniques. As a result the laterally isotropic cumulus dunite will not be "seen" by the seismic waves.

6.3 Implications of the Petrologic-Seismic Model

The petrologic-seismic model of young and thick oceanic crust that is presented in Figure 22 has several important implications for oceanic crust and for oceanic "layer 3" in particular. The most significant implication is that the Samail ophiolite can be used as a model for young and thick oceanic crust. This conclusion is based on the observation that the velocity-depth profile of the Samail ophiolite is consistent with the seismic velocity structures of normal oceanic crust and with marine reflection-refraction data for a section of oceanic crust near the East Pacific Rise (Kempner and Gettrust, 1981a).

Another implication of the model is that fresh cumulate gabbros comprise the major portion of oceanic "layer 3" in young and thick oceanic crust that is generated at a moderate-to-fast spreading mid-ocean ridge. A layer of massive metagabbros ($\sim$1.0 km thick), representing a sandwich horizon between cumulate gabbros and sheeted dikes, caps the cumulate gabbros and marks the upper "layer 3" of oceanic crust while a thin layer of cumulate peridotites (< 1.0 km thick) marks the base of "layer 3". The model is consistent with the conclusions of Cann (1968) and Christensen and Salisbury (1975) who suggested that the lower oceanic crust ("layer 3") consists of metagabbros, gabbros, and other rock types.

As shown by the model the thickness of individual rock units and the overall total thickness of the oceanic crustal section can vary significantly in lateral distances of only a few kilometers. According to the model (Figure 22), the greatest degree of lateral variability

occurs in oceanic "layer 3". Spudich and Orcutt (1980b) and Furukawa et al. (1981) have suggested from seismic reflection-refraction data that the structure of the lower oceanic crust does indeed display significant lateral heterogeneity over distances of only several kilometers.

Also seismic velocities in the model are shown to smoothly increase with depth in young and thick oceanic crust such that discrete "layer 2C, 3A, and 3B" refractors are not easily detected by standard marine seismic refraction techniques. The detection of these refractors in older oceanic crust (Sutton et al., 1971; Christensen and Salisbury, 1975) implies that young crust with seismic velocity structures that smoothly vary with depth may age to older crust with seismic velocity structures that are characterized by velocity discontinuities or strong velocity gradients that are distinct at seismic wavelengths (Kempner and Gettrust, 1981b).

The model demonstrates that the seismic velocity structure of "layer 2" in young and thick oceanic crust is controlled by both the primary igneous petrology (metabasalts and metadiabases) and the subsequent metamorphic assemblages (zeolite to lower amphibolite facies) in the rocks. In young oceanic crust the metamorphic assemblages are modeled as high temperature phases that result from pervasive high temperature hydrothermal metamorphism of the rocks very soon after their formation at a spreading ridge (Gregory and Taylor, 1981).

Hydrothermal metamorphism of the massive metagabbros (upper "layer 3") to the amphibolite facies does not appear to affect V_p and V_s in these rocks while hydrothermal metamorphism to the upper amphibolite

facies is probably restricted to fractures and joints within the cumulate gabbros of lower "layer 3". Therefore the seismic velocity structure in young and thick oceanic crust below 2.5 km is primarily controlled by the igneous petrology of "layer 3".

With increasing age and distance from a spreading ridge, the seismic velocity structure of oceanic "layer 2" may change. The porosity of the basalts and metabasalts of this region will decrease due to the infilling of cracks and pores with sediments and/or secondary minerals (Salisbury et al., 1980). With decreasing porosity of the metabasalts, seismic velocities in this region will tend to increase to those that are seismically measured in "layer 2B" (Houtz and Ewing, 1976; Salisbury et al., 1980). As a result "layer 2A" will appear to thin with age and finally disappear (Houtz and Ewing, 1976).

Retrograde metamorphism of the rocks in "layer 2", caused by low temperature hydrothermal metamorphism of the oceanic crust distant from a spreading ridge, may cause the zeolite-greenschist facies boundary at a depth of 0.5 km in "layer 2" to migrate downward until it coincides with the lithologic contact between low-porosity metabasalts and massive metadiabases. The coincident lithologic and metamorphic boundaries may cause a seismically distinct velocity gradient or velocity discontinuity at 1.0 km depth below the oceanic sediments such that a "layer 2B-layer 2C" seismic velocity boundary would be easily detected by marine seismic refraction techiques. The "layer 2A-layer 2B" seismic velocity boundary would probably not be affected by the lowering of the zeolite-greenschist facies boundary because effective porosity and pore

pressure affect velocities more than metamorphic assemblages at the low lithostatic confining pressures on the metabasalts in the upper 0.5 km of the oceanic crust (Schreiber and Fox, 1977).

Low temperature hydrothermal metamorphism in "layer 3" may result in retrograde metamorphism of the massive metagabbros to the greenschist facies with little additional alteration of the underlying cumulate gabbros (amphibolite facies metamorphics restricted to joints and fractures). The difference in metamorphic grade between the two gabbro units may cause a seismically distinct velocity gradient at the massive metagabbro-cumulate gabbro contact such that discrete "layer 3A" (greenschist facies metagabbros) and "layer 3B" (amphibolite facies cumulate gabbros) refractors would be observed in older oceanic crust by seismic refraction techniques. Therefore hydrothermal metamorphism may be an important factor controlling the seismic velocity structure of "layer 3" in older oceanic crust. Stern and Elthon (1979) have proposed a similar model of hydrothermal metamorphism in oceanic crust that was based on petrologic evidence from Chilean ophiolites. Kempner and Gettrust (1981a), using synthetic seismograms to model seismic reflection-refraction data of old and young sections of fast-spreading oceanic crust, have proposed a similar process to explain the apparent aging of oceanic crust.

The failure to sample the basal cumulate peridotites of the Samail ophiolite prevents a definite observation on their status in young and thick oceanic crust. Nevertheless, the velocities that were assumed in this study suggest that the basal cumulate peridotites comprise a thin

(0 to 0.6 km) crust-mantle transition zone in which lower "layer 3" velocities increase to upper mantle velocities. Christensen and Smewing (1981), using their velocity values for cumulate peridotite samples from the northern part of the Samail ophiolite, suggested that the peridotites comprise a seismically distinct "layer 3B" in young oceanic crust. They arrived at this conclusion despite the observation that the thickness of the basal cumulate peridotites in both the Ibra area and the northern part of the Samail ophiolite and in other ophiolites is always less than 1.0 km; substantially less than the average thickness of "layer 3B" (~3.0 km) that was measured by Sutton et al. (1971) in older oceanic crust and less than the limits of structural resolution (~1.0 km) afforded by airgun-sonobuoy seismic refraction techniques (Spudich and Orcutt, 1980b).

Support for the model presented in this study is supplied by Kempner (1981). Using synthetic seismograms to model reflection-refraction data for a section of 4.5 m.y. old oceanic crust, he suggested that a seismically distinct "layer 3B" does not occur in young oceanic crust. Furthermore he suggested that "layer 3B", when detected in older oceanic crust, corresponds to a crustal region in which V_p is 7.1 km sec^{-1}. In the model presented in Figure 22, a region in which V_p is equal to or greater than 7.1 km sec^{-1} correlates with the thick layer of fresh, cumulate olivine-pyroxene gabbros.

Although the model of young and thick oceanic crust can provide insight into several of the problems regarding "layer 3" of the oceanic crust, the model does not explain the seismic velocity anisotropy that

may occur in "layer 3" (Christensen, 1972b) nor does it explain the apparent thickening of oceanic "layer 3" with age.

Significant velocity anisotropy (ΔV_p = 1 to 8%) was measured in the cumulate gabbros of the Samail ophiolite while the massive metagabbros were essentially isotropic (ΔV_p = 0 to 2%). Velocity anisotropy was present in the cumulate gabbros because V_p was greatest when it was measured perpendicular to the cumulate layering of the gabbros (in core `a´); ΔV_p that was measured parallel to the cumulate layering was insignificant. Since cumulate layering in the Samail ophiolite was less than 15° from horizontal when it was a section of Tethyan oceanic crust (Pallister and Hopson, 1981), horizontal velocity anisotropy in the Samail ophiolite and the gabbro samples from the ophiolite is insignificant. Seismic velocity anisotropy in oceanic "layer 3", if measured by marine seismic refraction techniques, is a measurement of the horizontal seismic velocity anisotropy in the rocks of the lower oceanic crust. The massive metagabbro and cumulate gabbro samples from the Samail ophiolite and the petrologic-seismic model of oceanic crust presented in Figure 22 indicate that horizontal seismic velocity anisotropy, if it exists in oceanic "layer 3", is not caused by preferentially oriented minerals in the rocks of that region as has been suggested by Christensen (1972b). It is therefore suggested that geologic structures such as faults parallel to ridge crests and extending down through the massive metagabbros may cause the possible seismic velocity anisotropy of oceanic "layer 3".

The model of young and thick oceanic crust also provides no mechanism by which oceanic "layer 3" may thicken with age. No evidence of offridge intrusions into the cumulate gabbros is seen in the Samail ophiolite. This process was proposed by Christensen and Salisbury (1975) to explain the apparent seismic thickening of "layer 3" with age. Geochemical and petrologic evidence indicate that hydrothermal seawater only locally penetrated the upper mantle peridotites of the Samail ophiolite (Gregory and Taylor, 1981). As a result in situ serpentenization of the upper mantle beneath the thick crustal section of the Samail ophiolite probably did not occur (Boudier and Coleman, 1981). Clague and Straley (1977) and Nichols et al. (1980) suggested that thickening of oceanic "layer 3" could be explained by the downward serpentenization of the uppermost mantle beneath thin oceanic crust. Evidence from the Samail ophiolite therefore suggests that either (1) "layer 3" of thick oceanic crust does not thicken with age, or (2) in situ serpentenization of the lower crust and uppermost mantle in thick oceanic crust that is older than 4 to 8 m.y. may cause the apparent seismic thickening of oceanic "layer 3". Kempner (1981) has noted that in situ serpentenization of approximately 1.0 km of the lower oceanic crust and upper mantle may occur in thick oceanic crust that is between 10 and 30 m.y. old.

7. SUMMARY AND CONCLUSIONS

Geological (Glennie et al., 1974; Hopson et al., 1981) geochemical (Pallister and Knight, 1981), and geophysical (Manghnani and Coleman, 1981; Christensen and Smewing, 1981; Manghnani et al., in prep.) evidence indicate that the Samail ophiolite, Oman, is a well-preserved fragment of thick oceanic crust that formed at a Tethyan mid-ocean ridge 4 to 8 m.y. before its obduction onto the Arabian continental margin (Coleman, 1981). Before the Samail ophiolite can be used as a model for young and thick oceanic crust the relationship between the Samail ophiolite and contemporary oceanic crust must first be determined.

Because the oceanic crust is defined by its seismic velocity structure, V_p, V_s, and bulk density (ρ) of the major rock types in the Ibra area of the Samail ophiolite were measured in the laboratory at <u>in situ</u> lithostatic confining pressures and water saturation conditions. The measured velocities were then adjusted for temperature effects at depth in the Samail ophiolite. Poisson's ratio (σ) for the rocks was calculated from the final adjusted velocities. The range of these values (V_p = 4.4 to 8.1 km sec^{-1}, V_s = 2.3 to 4.5 km sec^{-1}, ρ = 2.28 to 3.29 g cm^{-3}, σ = 0.23 to 0.35) are within the range of values that have been measured in equivalent rocks from other ophiolites.

A velocity-depth profile of the Samail ophiolite in the Ibra area of the Oman Mountains is developed from the measured V_p, V_s, and known stratigraphic position of the rock samples. Three- and four-layer seismic velocity structures of the ophiolite that are inferred from its velocity-depth profile are consistent with the classical explosion and

airgun-sonobuoy seismic velocity structures of normal oceanic crust. Synthetic seismograms that were developed from a slightly perturbed version of the ophiolite's velocity-depth and bulk density profiles correlate closely with V_p seismic reflection-refraction data for a section of oceanic crust that formed 4.5 m.y. ago at the East Pacific Rise (Kempner and Gettrust, 1981a). Because the Samail ophiolite is seismically comparable with normal oceanic crust and a particular section of oceanic crust, a detailed petrologic-seismic model of young (4 to 8 m.y.) and thick (7.0 to 8.0 km) oceanic crust that formed at a moderate-to-fast spreading (3 to 5 cm yr^{-1}, half-rate) mid-ocean ridge is presented in Figure 22. To develop this model three assumptions are made.

(1) The major assumption is that lithologies found within the Samail ophiolite are equivalent to those of contemporary oceanic crust. This assumption is supported by dredge haul samples (Christensen and Salisbury, 1975), by DSDP samples, and, more recently, by in situ crustal sampling with deep submersibles (Thompson et al., 1981). Nevertheless, this model and others developed by the comparison of oceanic crustal seismic velocities with laboratory measured velocities in rock samples from ophiolites must be rigorously considered non-unique until it is proven that only rocks present within an ophiolite can satisfy the measured seismic properties of the oceanic crust (Spudich et al., 1978).

(2) Another assumption is that magma chamber and hydrothermal metamorphism processes at a Tethyan spreading ridge are comparable to

those that are operating at contemporary spreading ridges. These processes, described by Abbotts (1980), Pallister and Hopson (1981), and Gregory and Taylor (1981) for the Samail ophiolite, were responsible for the igneous petrology and the subsequent hydrothermal metamorphism of the Samail ophiolite. These two factors, in turn, control the seismic velocity structure of the Samail ophiolite and, by inferrence, the contemporary oceanic crust. The relationship between contemporary and Tethyan spreading ridge processes has not been determined.

(3) Finally it is assumed that modification of the velocity structure of the fragment of Tethyan oceanic crust (the Samail ophiolite) ceased once the crustal section was obducted onto the Arabian continental margin. Kempner and Gettrust (1981a) have argued that this assumption is valid for the Samail ophiolite.

In the model velocities are seen to increase rapidly (~ 1.0 sec^{-1}) and smoothly with depth in "layer 2" and slowly (< 0.1 sec^{-1}) in "layer 3" such that "layer 2C, 3A, and 3B" refractors are not seismically distinct in young oceanic crust. A distinct "layer 2-layer 3" seismic velocity boundary is caused by the lithologic contact between low density sheeted dikes and high density massive metagabbros, the presence of late-stage differentiates and quartz-rich rocks near the massive metagabbro-sheeted dike contact, and the appearance of amphibolite facies assemblages near the contact. A less distinct "layer 2A-layer 2B" seismic velocity boundary at approximately 0.5 km below the oceanic sediments is caused by the gradational changes from: (1) porous to low-porosity metabasalts, (2) zeolite to greenschist

facies assemblages, and (3) pore pressures equivalent to lithostatic confining pressures to pore pressures less than lithostatic confining pressures. "Layer 2A" consists of pillowed and massive basalts and metabasalts with zeolite facies assemblages. "Layer 2B" consists of low-porosity metabasalts and massive metadiabases that are hydrothermally metamorphosed to the greenschist facies. "Layer 3" consists of amphibolite facies massive metagabbros (~1.0 km thick) that overlie fresh cumulate gabbros (3.5 to 4.0 km thick) and cumulate peridotites. A basal layer of cumulate peridotites appears to comprise a thin (0 to 0.6 km) crust-mantle transition zone. Velocities that are characteristic in the upper mantle may occur within this transition zone and mark the seismic Moho. The petrologic Moho occurs beneath the seismic Moho at the lithologic contact between a thin layer of crustal cumulus dunite and harzburgite tectonites of the upper mantle.

This model has several implications for young and thick oceanic crust and for oceanic "layer 3" in particular. The model indicates that fresh cumulate gabbros comprise the major portion of "layer 3". A layer of massive metagabbros cap the unit of cumulate gabbros while a thin layer of basal cumulate peridotites occur at the base of "layer 3". The model also indicates that the thickness of individual rock units in the oceanic crust can vary significantly in lateral distances of only a few kilometers with the greatest degree of variability occurring in oceanic "layer 3".

Most significantly the model indicates that seismic velocities in "layer 2" of young oceanic crust are controlled by the primary igneous petrology and subsequent, high temperature metamorphic assemblages in the rocks (zeolite to lower amphibolite facies). In the lower oceanic crust, seismic velocities are primarily controlled by the igneous petrology of the gabbros of "layer 3". Retrograde, hydrothermal metamorphism may be an important factor contolling the seismic velocity structure of "layer 3" in oceanic crust formed more than 10 m.y. ago (Kempner and Gettrust, 1981a).

The petrologic-seismic model of oceanic crust presented in this study is not meant to describe all of the world's ocean basins where different spreading-ridge processes are creating oceanic crust of significantly different lithologic structures. This model may adequately describe oceanic crust that formed 4 to 8 m.y. ago in a large, long-lived magma chamber beneath a moderate-to-fast spreading (3 to 5 cm yr^{-1}, half-rate) mid-ocean ridge. Because the structural variations observed in ophiolites may reflect the range of oceanic crustal structures, similar studies of all stratigraphically complete and geologically constrained (age, spreading rate, and tectonic province reasonably determined) ophiolites may provide petrologic interpretations for marine seismic refraction data from all of the oceans' crust.

APPENDIX A

V_p AND V_s IN THE SAMAIL OPHIOLITE SAMPLES TO 0.3, 0.5, AND 1.0 GPa CONFINING PRESSURES AT 25° C

TABLE 4

Compressional (V_p) and Shear (V_s) Wave Velocities in the Samail Ophiolite Samples to 0.3, 0.5, and 1.0 GPa Confining Pressures at 25°C

Sample No. and Rock Type	Core	Ambient ρ g cm^{-3}	Velocity (km sec^{-1}) Pressure (GPa) .005 Vp	.005 Vs	.05 Vp	.05 Vs	.1 Vp	.1 Vs	.2 Vp	.2 Vs	.3 Vp	.3 Vs	.5 Vp	.5 Vs	1.0 Vp	1.0 Vs
O-8	a	2.54	4.38	2.24	4.70	2.53	4.82	2.64	4.95	2.71	5.01	2.73				
Pillow	b	2.57	4.53	2.35	4.84	2.62	4.97	2.73	5.09	2.78	5.15	2.79				
Basalt	c	2.60	4.44	2.37	4.70	2.61	4.84	2.71	4.96	2.78	5.01	2.81				
	mean	2.57	4.45	2.32	4.75	2.59	4.88	2.53	5.00	2.76	5.06	2.77				
O-9	a	2.58	4.76	2.53	5.16	2.78	5.29	2.88	5.38	2.95	5.41	2.99				
Pillow	b	2.60	5.24	2.82	5.48	3.00	5.60	3.09	4.70	3.15	5.75	3.18				
Basalt	c	2.62	5.00	2.72	5.30	2.93	5.41	2.96	5.50	2.99	5.58	3.02				
	mean	2.60	5.00	2.69	5.32	2.91	5.43	2.97	5.53	3.03	5.58	3.06				
OM-342 Pillow Basalt	a	2.28	4.55	2.31	4.78	2.61	4.84	2.68	4.89	2.72	4.94	2.72				
OM-253 Pillow Basalt	a	2.46	5.03	2.78	5.12	2.84	5.16	2.88	5.20	2.93	5.24	2.95				
OM-327 Pillow Basalt	a	2.51	4.56	2.47	4.97	2.71	5.13	2.82	5.25	2.92	5.29	2.95				
OM-162 Massive Basalt	a	2.68	5.45	3.05	5.51	3.11	5.55	3.14	5.63	3.17	5.70	3.20				
GElm2	a	2.85	6.74	3.82	6.79	3.83	6.81	3.84	6.83	3.85	6.84	3.85	6.85	3.86	6.89	3.87
Diabase	b	2.87	6.78	3.80	6.89	3.81	6.94	3.82	7.02	3.83	7.07	3.83	7.12	3.84	7.24	3.85
	c	2.87	6.73	3.83	6.78	3.83	6.80	3.84	6.83	3.85	6.84	3.85	6.87	3.86	6.94	3.87
	mean	2.86	6.75	3.82	6.82	3.83	6.85	3.83	6.89	3.84	6.92	3.85	6.95	3.85	7.02	3.87

TABLE 4. (Continued) Compressional (V_p) and Shear (V_s) Wave Velocities in the Samail Ophiolite Samples to 0.3, 0.5, and 1.0 GPa Confining Pressures at 25°C

Sample No. and Rock Type	Core	Ambient ρ g cm^{-3}	Velocity (km sec^{-1}) Pressure (GPa) .005		.05		.1		.2		.3		.5		1.0	
			Vp	Vs	Vp	Vs	Vp	Vs	Vp	Vs	Vp	Vs	Vp	Vs	Vp	Vs
GE3m2	a	2.87	6.72	3.58	6.77	3.61	6.79	3.63	6.82	3.65	6.84	3.66	6.86	3.68	6.92	3.69
Diabase	b	2.87	6.70	3.76	6.76	3.78	6.78	3.80	6.81	3.82	6.83	3.83	6.86	3.85	6.92	3.86
	mean	2.87	6.71	3.67	6.76	3.70	6.78	3.72	6.82	3.74	6.83	3.75	6.86	3.77	6.92	3.78
K1m1	a	2.78	5.91	3.25	5.99	3.29	6.04	3.32	6.11	3.35	6.16	3.36	6.23	3.39	6.35	3.41
Diabase	b	2.78	5.82	3.40	5.91	3.43	5.96	3.46	6.04	3.48	6.10	3.49	6.17	3.51	6.31	3.52
	c	2.78	5.90	3.35	5.97	3.38	6.02	3.41	6.09	3.44	6.14	3.45	6.21	3.47	6.33	3.50
	mean	2.78	5.86	3.33	5.95	3.37	6.01	3.39	6.08	3.42	6.13	3.44	6.20	3.46	6.33	3.48
OM-172	a	2.77	6.01	3.49	6.10	3.51	6.14	3.52	6.19	3.54	6.23	3.55	6.29	3.57	6.38	3.59
Diabase	b	2.77	6.03	3.49	6.09	3.55	6.14	3.57	6.21	3.58	6.25	3.59	6.33	3.60	6.46	3.61
	c	2.77	6.00	3.47	6.10	3.53	6.14	3.54	6.19	3.55	6.23	3.56	6.29	3.57	6.38	3.58
	mean	2.77	6.10	3.48	6.10	3.53	6.14	3.54	6.20	3.56	6.24	3.57	6.30	3.58	6.41	3.59
OM-95	a	2.83	6.18	3.41	6.29	3.45	6.36	3.48	6.46	3.53	6.55	3.57	6.66	3.62	6.79	3.66
Diabase	b	2.82	6.18	3.28	6.29	3.36	6.36	3.39	6.46	3.43	6.55	3.44	6.65	3.46	6.79	3.48
	c	2.80	6.06	3.40	6.21	3.46	6.29	3.49	6.39	3.54	6.46	3.58	6.57	3.62	6.75	3.63
	mean	2.82	6.14	3.36	6.26	3.42	6.34	3.45	6.44	3.50	6.52	3.53	6.63	3.57	6.78	3.59
OM-126	a	2.71	5.42	3.02	5.65	3.18	5.75	3.25	5.85	3.32	5.91	3.37	5.96	3.41		
Diabase	b	2.70	5.50	3.00	5.67	3.18	5.74	3.26	5.80	3.33	5.86	3.37	5.93	3.42		
	c	2.70	5.44	3.02	5.64	3.21	5.72	3.29	5.81	3.36	5.86	3.41	5.97	3.45		
	mean	2.70	5.45	3.01	5.65	3.19	5.74	3.26	5.82	3.34	5.88	3.38	5.95	3.43		
K3m1	a	2.61	5.56	3.32	5.73	3.45	5.84	3.49	5.95	3.54	6.02	3.57	6.06	3.59	6.19	3.62
Plagio-	b	2.62	5.57	3.30	5.74	3.43	5.84	3.48	5.92	3.53	5.94	3.57	6.00	3.61	6.08	3.65
granite	c	2.62	5.47	3.29	5.70	3.41	5.81	3.46	5.93	3.52	5.98	3.54	6.03	3.57	6.17	3.59
	mean	2.61	5.53	3.30	5.73	3.43	5.83	3.48	5.93	3.53	5.98	3.56	6.03	3.59	6.14	3.60
H618m1	a	2.64	5.73	3.45	5.94	3.56	6.04	3.61	6.13	3.67	6.19	3.69	6.29	3.71	6.37	3.73
Plagio-	b	2.64	5.83	3.46	5.98	3.53	6.04	3.57	7.12	3.62	6.16	3.64	6.20	3.65	6.24	3.66
granite	c	2.65	6.03	3.43	6.10	3.46	6.14	3.48	6.19	3.50	6.21	3.51	6.24	3.52	6.32	3.53
	mean	2.64	5.86	3.45	6.00	3.52	6.07	3.56	6.15	3.60	6.19	3.61	6.24	3.63	6.31	3.64

TABLE 4. (Continued) Compressional (V_p) and Shear (V_s) Wave Velocities in the Samail Ophiolite Samples to 0.3, 0.5, and 1.0 GPa Confining Pressures at 25°C

Sample No. and Rock Type	Core	Ambient ρ g cm^{-3}	Velocity (km sec^{-1}) Pressure (GPa) .005		.05		.1		.2		.3		.5		1.0	
			Vp	Vs	Vp	Vs	Vp	Vs	Vp	Vs	Vp	Vs	Vp	Vs	Vp	Vs
GE2ml	a	3.01	6.65	3.63	6.71	3.66	6.76	3.69	6.82	3.71	6.86	3.73	6.91	3.75	7.04	3.78
High-	b	2.96	6.56	3.62	6.64	3.66	6.69	3.69	6.75	3.72	6.79	3.74	6.85	3.76	7.00	3.79
Level	c	2.99	6.58	3.68	6.63	3.69	6.66	3.71	6.71	3.73	6.76	3.75	6.81	3.77	6.94	3.79
Gabbro	mean	2.99	6.60	3.64	6.66	3.67	6.70	3.70	6.76	3.72	6.80	3.74	6.86	3.76	7.00	3.79
GE3ml	a	2.96	7.17	3.92	7.25	3.95	7.28	3.97	7.31	3.99	7.33	3.99	7.36	4.00	7.43	4.02
High-	b	3.13	7.14	3.92	7.22	3.95	7.27	3.97	7.32	3.98	7.35	4.00	7.38	4.02	7.47	4.05
Level	c	2.97	7.01	3.89	7.05	3.92	7.08	3.94	7.11	3.96	7.13	3.98	7.16	3.99	7.21	4.02
Gabbro	mean	3.02	7.11	3.91	7.17	3.94	7.21	3.96	7.25	3.98	7.27	3.99	7.30	4.00	7.37	4.03
GE4ml	a	2.91	6.99	3.66	7.03	3.69	7.05	3.72	7.08	3.75	7.10	3.77	7.11	3.79	7.14	3.82
Wehrlite	b	2.91	6.92	3.62	6.97	3.65	7.00	3.68	7.04	3.71	7.06	3.73	7.09	3.76		
+	c	2.92	7.02	3.86	7.08	3.88	7.12	3.90	7.15	3.91	7.16	3.92	7.18	3.94		
Gabbro	mean	2.91	6.97	3.71	7.03	3.74	7.06	3.76	7.10	3.79	7.11	3.81	7.13	3.83		
GE5ml	a	2.97	6.91	3.72	6.99	3.78	7.04	3.81	7.11	3.83	7.15	3.85	7.20	3.87	7.26	3.89
Transi-	b	3.03	7.01	3.74	7.09	3.78	7.13	3.80	7.18	3.82	7.21	3.83	7.26	3.85	7.33	3.88
tional	c	2.96	6.87	3.82	7.00	3.85	7.05	3.88	7.13	3.90	7.17	3.91	7.22	3.93	7.28	3.95
Gabbro	mean	2.98	6.93	3.76	7.03	3.80	7.07	3.83	7.14	3.85	7.18	3.86	7.23	3.88	7.29	3.91
GE6ml	a	2.91	7.32	3.73	7.39	3.77	7.42	3.80	7.44	3.82	7.47	3.84	7.50	3.86	7.57	3.87
Cumulate	b	2.94	7.15	3.63	7.20	3.66	7.24	3.68	7.27	3.70	7.30	3.71	7.34	3.72	7.41	3.73
Gabbro	c	2.90	7.11	3.70	7.16	3.72	7.18	3.73	7.22	3.15	7.25	3.76	7.29	3.78	7.37	3.78
	mean	2.92	7.19	3.69	7.25	3.72	7.28	3.74	7.31	3.76	7.34	3.77	7.37	3.78	7.45	3.80
GE7ml	a	2.91	7.11	3.73	7.18	3.75	7.21	3.76	7.25	3.78	7.28	3.79	7.31	3.80	7.38	3.82
Cumulate	b	2.92	7.05	3.64	7.11	3.67	7.13	3.68	7.15	3.70	7.16	3.71	7.18	3.72	7.23	3.73
Gabbro	c	2.93	7.09	3.80	7.14	3.82	7.17	3.84	7.20	3.86	7.21	3.86	7.22	3.88	7.26	3.88
	mean	2.92	7.08	3.74	7.14	3.74	7.17	3.76	7.20	3.78	7.22	3.79	7.24	3.80	7.29	3.81

TABLE 4. (Continued) Compressional (V_p) and Shear (V_s) Wave Velocities in the Samail Ophiolite Samples to 0.3, 0.5, and 1.0 GPa Confining Pressures at 25°C

Sample No. and Rock Type	Core	Ambient ρ g cm^{-3}	Velocity (km sec^{-1}) Pressure (GPa) .005 Vp	.005 Vs	.05 Vp	.05 Vs	.1 Vp	.1 Vs	.2 Vp	.2 Vs	.3 Vp	.3 Vs	.5 Vp	.5 Vs	1.0 Vp	1.0 Vs
GE8ml	a	2.95	7.17	3.80	7.27	3.83	7.32	3.86	7.38	3.89	7.41	3.90	7.46	3.93	7.55	3.95
Cumulate	b	2.96	7.09	3.89	7.17	3.94	7.20	3.96	7.25	3.99	7.27	4.01	7.32	4.04		
Gabbro	c	2.94	7.01	3.81	7.08	3.85	7.12	3.87	7.17	3.89	7.21	3.91	7.26	3.92	7.37	3.95
	mean	2.95	7.09	3.83	7.17	3.87	7.21	3.90	7.26	3.92	7.30	3.94	7.35	3.96	7.46	3.95
GE9ml	a	2.99	7.30	3.81	7.37	3.82	7.40	3.84	7.44	3.85	7.46	3.87	7.49	3.88	7.57	3.89
Cumulate	b	2.92	6.98	3.70	7.08	3.76	7.12	3.79	7.17	3.82	7.21	3.84	7.25	3.85	7.32	3.87
Gabbro	c	2.94	7.17	3.81	7.24	3.83	7.27	3.85	7.30	3.86	7.33	3.87	7.36	3.88	7.42	3.89
	mean	2.95	7.15	3.77	7.23	3.80	7.26	3.83	7.30	3.84	7.33	3.86	7.37	3.87	7.44	3.88
GE11ml	a	2.95	7.13	3.89	7.23	3.94	7.26	3.97	7.31	4.00	7.34	4.02	7.38	4.02	7.46	4.07
Cumulate	b	2.95	7.19	3.95	7.27	3.99	7.31	4.01	7.38	4.04	7.41	4.06	7.47	4.08	7.53	4.11
Gabbro	c	2.94	7.16	3.74	7.24	3.76	7.28	3.78	7.32	3.81	7.34	3.82	7.38	3.85	7.42	3.87
	mean	2.95	7.16	3.86	7.25	3.90	7.29	3.92	7.34	3.95	7.36	3.97	7.41	3.98	7.47	4.02
GE13ml	a	2.97	7.29	3.87	7.36	3.89	7.40	3.91	7.44	3.92	7.46	3.94	7.49	3.95	7.54	3.96
Cumulate	b	2.98	7.30	3.84	7.35	3.88	7.36	3.90	7.43	3.92	7.45	3.94	7.50	3.95	7.57	3.96
Gabbro	c	2.96	7.24	3.79	7.31	3.82	7.34	3.84	7.39	3.86	7.42	3.88	7.45	3.90	7.51	3.93
	mean	2.97	7.27	3.84	7.34	3.86	7.37	3.88	7.42	3.90	7.44	3.92	7.48	3.93	7.54	3.95
GE14ml	a	2.89	6.89	3.67	6.98	3.71	7.04	3.74	7.11	3.76	7.15	3.78	7.20	3.79	7.28	3.81
Cumulate	b	2.97	7.17	3.87	7.24	3.82	7.27	3.89	7.31	3.91	7.33	3.91	7.35	3.92	7.41	3.93
Gabbro	c	2.91	6.94	3.71	7.05	3.75	7.11	3.77	7.15	3.80	7.22	3.82	7.25	3.83	7.30	3.85
	mean	2.92	7.00	3.75	7.09	3.78	7.14	3.80	7.19	3.82	7.23	3.84	7.27	3.85	7.33	3.86
K2ml	a	2.97	6.90	3.94	6.98	3.96	7.03	3.98	7.08	4.00	7.12	4.02	7.17	4.04	7.26	4.06
High-	b	2.95	6.91	3.86	6.94	3.89	6.98	3.91	7.02	3.94	7.05	3.95	7.09	3.97	7.16	3.99
Level	c	2.96	6.91	3.87	6.95	3.90	6.98	3.92	7.03	3.94	7.06	3.95	7.10	3.97	7.16	3.99
Gabbro	mean	2.96	6.91	3.89	6.96	3.92	7.00	3.94	7.04	3.96	7.08	3.96	7.12	3.99	7.19	4.01

TABLE 4. (Continued) Compressional (V_p) and Shear (V_s) Wave Velocities in the Samail Ophiolite Samples to 0.3, 0.5, and 1.0 GPa Confining Pressures at 25°C

Sample No. and Rock Type	Core	Ambient ρ g cm^{-3}	Velocity (km sec^{-1}) Pressure (GPa) .005		.05		.1		.2		.3		.5		1.0	
			Vp	Vs	Vp	Vs	Vp	Vs	Vp	Vs	Vp	Vs	Vp	Vs	Vp	Vs
K4ml	a	2.98	7.09	3.86	7.17	3.90	7.21	3.92	7.25	3.94	7.27	3.96	7.31	3.97	7.40	3.99
Transi-	b	2.99	7.09	3.86	7.19	3.89	7.24	3.91	7.29	3.93	7.31	3.94	7.32	3.96	7.36	3.98
tional	c	2.89	7.13	3.93	7.23	3.96	7.28	3.97	7.34	3.99	7.37	4.01	7.40	4.02	7.41	4.04
Gabbro	mean	2.99	7.10	3.88	7.20	3.91	7.24	3.93	7.29	3.96	7.32	3.97	7.34	3.99	7.39	4.00
K5pl	a	3.00	7.20	3.77	7.29	3.81	7.32	3.83	7.37	3.86	7.41	3.87	7.44	3.90		
Cumulate	b	2.97	7.32	3.77	7.41	3.81	7.45	3.84	7.48	3.86	7.50	3.87	7.53	3.89		
Gabbro	c	2.99	7.14	3.77	7.26	3.81	7.31	3.84	7.37	3.87	7.41	3.89	7.45	3.93		
	mean	2.99	7.22	3.77	7.32	3.81	7.36	3.83	7.41	3.86	7.44	3.88	7.47	3.91		
K6ml	a	2.97	7.07	3.70	7.15	3.73	7.20	3.76	7.25	3.78	7.27	2.79	7.30	3.80	7.39	3.82
Cumulate	b	2.98	7.16	3.89	7.22	3.93	7.27	3.95	7.32	3.97	7.35	3.99	7.39	4.01	7.46	4.03
Gabbro	c	2.98	7.02	3.83	7.13	3.87	7.18	3.89	7.26	3.92	7.29	3.94	7.33	3.96	7.41	3.98
	mean	2.97	7.08	3.81	7.17	3.84	7.22	3.87	7.27	3.89	7.31	3.91	7.34	3.92	7.42	3.94
K7ml	a	2.98	7.10	3.80	7.32	3.86	7.39	3.89	7.47	3.92	7.51	3.94	7.56	3.95	7.64	3.98
Cumulate	b	2.98	7.14	3.82	7.24	3.87	7.30	3.89	7.36	3.92	7.40	3.93	7.43	3.95	7.50	3.96
Gabbro	c	2.98	7.22	3.86	7.31	3.88	7.36	3.90	7.41	3.92	7.43	3.93	7.45	3.95	7.50	3.97
	mean	2.98	7.15	3.83	7.29	3.87	7.35	3.89	7.41	3.92	7.44	3.93	7.48	3.95	7.55	3.97
K8ml	a	2.96	7.26	3.82	7.32	3.85	7.35	3.88	7.38	3.90	7.41	3.92	7.43	3.93	7.47	3.95
Cumulate	b	3.06	7.45	3.99	7.51	4.02	7.54	4.04	7.56	4.06	7.57	4.07	7.60	4.09	7.66	4.12
Gabbro	c	2.96	7.31	3.91	7.38	3.93	7.43	3.95	7.48	3.97	7.50	3.98	7.52	4.00	7.56	4.02
	mean	2.99	7.34	3.91	7.40	3.93	7.44	3.95	7.47	3.98	7.49	3.99	7.52	4.01	7.57	4.03
K9ml	a	2.86	7.26	3.67	7.34	3.70	7.39	3.73	7.45	3.76	7.48	3.77	7.52	3.79	7.56	3.81
Cumulate	b	2.88	7.15	3.76	7.21	3.79	7.25	3.81	7.29	3.82	7.31	3.84	7.33	3.85	7.40	3.86
Gabbro	c	2.93	7.26	3.66	7.31	3.70	7.34	3.72	7.38	3.75	7.40	3.76	7.42	3.78	7.47	3.80
	mean	2.89	7.22	3.70	7.28	3.73	7.33	3.75	7.37	3.78	7.50	3.79	7.43	3.80	7.47	3.82

TABLE 4. (Continued) Compressional (V_p) and Shear (V_s) Wave Velocities in the Samail Ophiolite Samples to 0.3, 0.5, and 1.0 GPa Confining Pressures at 25°C

Sample No. and Rock Type	Core	Ambient ρ g cm^{-3}	Velocity (km sec^{-1}) Pressure (GPa) .005		.05		.1		.2		.3		.5		1.0	
			Vp	Vs	Vp	Vs	Vp	Vs	Vp	Vs	Vp	Vs	Vp	Vs	Vp	Vs
K10ml Cumulate Gabbro	a	2.96	7.11	3.71	7.16	3.75	7.19	3.77	7.22	3.80	7.25	3.82	7.28	3.84	7.34	3.87
K11ml	a	2.92	7.16	3.74	7.22	3.76	7.26	3.78	7.30	3.80	7.33	3.81	7.37	3.83	7.44	3.85
Cumulate	b	2.89	6.91	3.57	6.98	3.59	7.01	3.62	7.05	3.64	7.07	3.66	7.10	3.68	7.16	3.70
Gabbro	c	2.97	7.21	3.72	7.31	3.78	7.37	3.82	7.43	3.86	7.46	3.89	7.51	3.92	7.57	3.96
	mean	2.93	7.09	3.68	7.17	3.87	7.21	3.89	7.25	3.90	7.29	3.92	7.33	3.93	7.39	3.94
K12ml	a	2.96	7.28	3.81	7.38	3.83	7.42	3.85	7.45	3.87	7.47	3.88	7.49	3.89	7.51	3.91
Cumulate	b	2.89	7.15	3.64	7.21	3.66	7.24	3.67	7.26	3.68	7.28	3.69	7.29	3.70	7.33	3.71
Gabbro	c	2.97	7.16	3.90	7.21	3.91	7.24	3.92	7.26	3.93	7.27	3.94	7.29	3.94	7.33	3.95
	mean	2.94	7.19	3.79	7.27	3.80	7.30	3.81	7.32	3.83	7.34	3.84	7.36	3.84	7.39	3.86
K13ml	a	2.95	6.79	3.61	7.01	3.68	7.09	3.72	7.18	3.77	7.23	3.79	7.31	3.81	7.41	3.84
Cumulate	b	2.96	6.96	3.75	7.04	3.79	7.08	3.82	7.13	3.84	7.16	3.86	7.22	3.88	7.29	3.91
Gabbro	c	2.96	6.93	3.70	7.04	3.74	7.10	3.77	7.17	3.80	7.22	3.81	7.27	3.84	7.35	3.87
	mean	2.96	6.89	3.69	7.03	3.74	7.09	3.77	7.16	3.80	7.20	3.82	7.26	3.84	7.35	3.87
K14ml	a	3.01	7.09	3.11	7.38	3.17	7.49	3.20	7.59	3.23	7.64	3.24	7.69	3.26	7.80	3.27
Cumulate	b	3.06	7.24	3.99	7.40	4.05	7.47	4.09	7.55	4.12	7.59	4.14	7.62	4.16	7.70	4.18
Gabbro	c	3.03	7.17	3.90	7.31	3.99	7.38	4.03	7.48	4.07	7.53	4.09	7.60	4.12	7.65	4.16
	mean	3.03	7.17	3.66	7.36	3.74	7.45	3.77	7.54	3.80	7.59	3.82	7.63	3.84	7.72	3.87
K16ml	a	2.86	7.30	3.71	7.41	3.75	7.46	3.78	7.52	3.80	7.54	3.81	7.56	3.83		
Cumulate	b	3.08	7.72	3.93	7.75	3.96	7.78	3.98	7.81	4.01	7.83	4.03	7.86	4.06	7.91	4.09
Gabbro	c	2.83	7.01	3.68	7.12	3.73	7.17	3.75	7.23	3.78	7.26	3.79	7.28	3.80	7.34	3.81
	mean	2.92	7.34	3.77	7.43	3.81	7.47	3.84	7.52	3.86	7.54	3.88	7.57	3.90	7.63	3.95
K17ml	a	2.95	7.16	3.70	7.20	3.72	7.23	3.73	7.26	3.74	7.28	3.74	7.30	3.75	7.34	3.75
Cumulate	b	3.03	7.16	3.68	7.19	3.70	7.22	3.71	7.24	3.73	7.26	3.73	7.28	3.74	7.30	3.76
Gabbro	c	2.97	7.25	3.98	7.31	3.99	7.34	4.01	7.38	4.02	7.41	4.03	7.43	4.04	7.49	4.06
	mean	2.97	7.19	3.79	7.24	3.80	7.26	3.82	7.30	3.83	7.31	3.84	7.34	3.84	7.38	3.86

TABLE 4. (Continued) Compressional (V_p) and Shear (V_s) Wave Velocities in the Samail Ophiolite Samples to 0.3, 0.5, and 1.0 GPa Confining Pressures at 25°C

Sample No. and Rock Type	Core	Ambient ρ g cm^{-3}	Velocity (km sec^{-1})													
			Pressure (GPa)													
			.005		.05		.1		.2		.3		.5		1.0	
			Vp	Vs	Vp	Vs	Vp	Vs	Vp	Vs	Vp	Vs	Vp	Vs	Vp	Vs
K21ml Harzburgite	c	2.84	6.44	3.29	6.52	3.31	6.55	3.33	6.58	3.35	6.60	3.37	6.61	3.39	6.64	3.41
K22ml	a	2.91	6.08	3.16	6.17	3.19	6.20	3.22	6.23	3.26	6.26	3.29	6.32	3.34	6.47	3.43
Harzburgite	b	2.92	6.46	3.25	6.51	3.30	6.54	3.31	6.58	3.33	6.61	3.34	6.66	3.36	6.76	3.39
+	c	2.90	6.39	3.20	6.43	3.24	6.46	3.26	6.51	3.28	6.54	3.29	6.60	3.33	6.72	3.41
Dunite	mean	2.91	6.31	3.20	6.37	3.24	6.40	3.26	6.44	3.29	6.47	3.31	6.53	3.34	6.65	3.41
O-1	a	2.95	6.30	3.38	6.39	3.42	6.44	3.44	6.49	3.46	6.54	3.48	6.61	3.52	6.76	3.58
Harzburgite	b	2.94	6.21	3.34	6.31	3.37	6.35	3.40	6.40	3.44	6.44	3.46	6.51	3.50	6.69	3.57
	c	2.93	6.06	3.15	6.18	3.18	6.22	3.20	6.27	3.24	6.31	3.27	6.38	3.30	6.53	3.34
	mean	2.94	6.19	3.29	6.29	3.32	6.34	3.35	6.39	3.38	6.43	3.40	6.50	3.44	6.66	3.50
O-2	a	2.91	6.71	3.33	6.75	3.35	6.79	3.36	6.83	3.38	6.87	3.39	6.92	3.41	7.02	3.44
Harzburgite	b	2.88	6.20	3.16	6.25	3.19	6.27	3.20	6.31	3.21	6.34	3.21	6.40	3.22	6.52	3.24
	c	2.89	6.15	3.44	6.21	3.45	6.24	3.46	6.29	3.48	6.32	3.50	6.38	3.52	6.50	3.57
	mean	2.90	6.35	3.31	6.40	3.33	6.43	3.34	6.48	3.36	6.51	3.37	6.57	3.38	6.68	3.42
O-3	a	3.00	6.66	3.50	6.77	3.53	6.83	3.56	6.87	3.57	6.91	3.58	6.97	3.61	7.07	3.66
Harzburgite	b	2.98	6.15	3.39	6.27	3.44	6.33	3.46	6.40	3.48	6.45	3.50	6.51	3.54	6.65	3.56
	c	2.98	6.33	3.44	6.46	3.48	6.51	3.51	6.57	3.53	6.62	3.56	6.66	3.60	6.79	3.66
	mean	2.99	6.38	3.44	6.50	3.48	6.56	3.51	6.61	3.53	6.66	3.55	6.71	3.58	6.84	3.63
O-5	a	2.83	6.02	3.15	6.24	3.22	6.32	3.26	6.40	3.29	6.44	3.32	6.52	3.37	6.66	3.39
Harzburgite	b	2.84	5.58	3.01	5.77	3.09	5.84	3.12	5.91	3.15	5.97	3.16	6.06	3.20	6.23	3.22
	c	2.82	5.80	3.22	6.04	3.28	6.11	3.31	6.14	3.34	6.22	3.35	6.30	3.38	6.43	3.41
	mean	2.83	5.80	3.13	6.02	3.20	6.09	3.23	6.15	3.26	6.21	3.28	6.29	3.32	6.44	3.34
O-6	a	2.90	6.30	3.34	6.37	3.39	6.40	3.40	6.45	3.42	6.48	3.44	6.54	3.47	6.66	3.52
Harzburgite	b	2.89	5.90	3.12	6.05	3.17	6.10	3.20	6.15	3.23	6.18	3.25	6.25	3.29	6.33	3.34
	c	2.86	6.04	3.08	6.17	3.11	6.21	3.13	6.25	3.15	6.28	3.16	6.35	3.18	6.47	3.23
	mean	2.88	6.08	3.18	6.20	3.22	6.24	3.24	6.28	3.27	6.31	3.28	6.38	3.31	6.49	3.36

TABLE 4. (Continued) Compressional (V_p) and Shear (V_s) Wave Velocities in the Samail Ophiolite Samples to 0.3, 0.5, and 1.0 GPa Confining Pressures at 25°C

Sample No. and Rock Type	Core	Ambient ρ g cm^{-3}	Velocity (km sec^{-1}) Pressure (GPa) .005		.05		.1		.2		.3		.5		1.0	
			Vp	Vs	Vp	Vs	Vp	Vs	Vp	Vs	Vp	Vs	Vp	Vs	Vp	Vs
0-7	a	2.94	6.26	3.35	6.35	3.37	6.39	3.39	6.43	3.41	6.46	3.42	6.52	3.44	6.66	3.48
Harzburgite	b	2.95	6.31	3.44	6.40	3.47	6.44	3.49	6.49	3.51	6.53	3.52	6.59	3.55	6.71	3.58
	c	2.94	6.57	3.42	6.65	3.48	6.70	3.50	6.75	3.52	6.79	3.54	6.86	3.56	6.97	3.60
	mean	2.94	6.38	3.40	6.47	3.44	6.51	3.46	6.56	3.48	6.59	3.49	6.66	3.52	6.78	3.55
0-10	a	2.70	5.52	2.85	5.76	2.93	5.87	2.96	5.96	2.98	6.01	3.00	6.08	3.02	6.22	3.06
Harzburgite	b	2.70	5.82	2.98	5.94	3.00	6.00	3.02	6.08	3.04	6.13	3.05	6.21	3.07	6.31	3.09
	c	2.68	5.74	3.08	5.91	3.13	6.00	3.16	6.09	3.08	6.13	3.19	6.19	3.21	6.29	3.24
	mean	2.69	5.69	2.97	5.87	3.02	5.95	3.05	6.04	3.07	6.09	3.08	6.16	3.10	6.27	3.13
0-11	a	2.70	5.61	2.89	5.81	2.99	5.91	3.02	6.00	3.05	6.07	3.07	6.14	3.10	6.27	3.16
Harzburgite	b	2.70	5.57	3.02	5.84	3.12	5.95	3.16	6.05	3.18	6.11	3.20	6.18	3.22	6.31	3.27
	c	2.68	5.98	3.01	6.05	3.06	6.08	3.08	6.12	3.09	6.15	3.10	6.21	3.12	6.35	3.16
	mean	2.69	5.72	2.97	5.90	3.05	5.98	3.09	6.06	3.11	6.11	3.12	6.18	3.15	6.31	3.20
0-12	a	2.74	5.83	3.12	5.98	3.18	6.05	3.20	6.13	3.24	6.18	3.23	6.27	3.26	6.43	3.29
Harzburgite	b	2.73	6.00	3.01	6.07	3.03	6.10	3.05	6.13	3.07	6.16	3.08	6.22	3.10	6.34	3.14
	c	2.75	5.85	3.16	6.00	3.21	6.04	3.23	6.09	3.24	6.12	3.26	6.20	3.28	6.35	3.33
	mean	2.74	5.89	3.10	6.02	3.14	6.06	3.16	6.11	3.18	6.16	3.19	6.23	3.21	6.37	3.26
0-13	a	2.71	5.49	2.93	5.71	3.00	5.79	3.03	5.89	3.06	5.94	3.08	6.00	3.11	6.12	3.16
Harzburgite	b	2.74	5.52	3.00	5.78	3.03	5.89	3.04	5.98	3.07	6.03	3.09	6.10	3.13	6.25	3.20
	c	2.71	5.92	3.06	6.18	3.10	6.25	3.12	6.31	6.15	6.35	3.16	6.41	3.19	6.53	3.26
	mean	2.72	5.65	3.00	5.89	3.04	5.98	3.07	6.06	3.09	6.10	3.11	6.17	3.14	6.30	3.21
0-14	a	2.72	5.78	3.07	5.88	3.11	5.92	3.12	5.97	3.13	6.01	3.14	6.08	3.17	6.22	3.20
Harzburgite	b	2.72	5.83	3.00	5.93	3.03	5.98	3.05	6.03	3.07	6.06	3.08	6.12	3.11	6.25	3.14
	c	2.71	5.78	2.98	5.97	3.04	6.03	3.07	6.08	3.09	6.11	3.10	6.16	3.12	6.29	3.16
	mean	2.72	5.79	3.01	5.93	3.06	5.98	3.08	6.03	3.10	6.06	3.11	6.12	3.13	6.25	3.17

TABLE 4. (Continued) Compressional (V_p) and Shear (V_s) Wave Velocities in the Samail Ophiolite Samples to 0.3, 0.5, and 1.0 GPa Confining Pressures at 25°C

Sample No. and Rock Type	Core	Ambient ρ g cm^{-3}	Velocity (km sec^{-1}) Pressure (GPa) .005		.05		.1		.2		.3		.5		1.0	
			Vp	Vs	Vp	Vs	Vp	Vs	Vp	Vs	Vp	Vs	Vp	Vs	Vp	Vs
O-15 Harzburgite	a	2.68	5.69	2.90	5.82	2.96	5.87	2.98	5.94	3.00	5.98	3.01	6.04	3.03	6.17	3.08
	b	2.65	5.22	2.75	5.73	2.85	5.81	2.89	5.88	2.92	5.93	2.93	5.99	2.95	6.12	2.99
	c	2.67	5.44	2.78	5.72	2.90	5.84	2.94	5.92	2.97	5.98	2.98	6.05	3.00	6.18	3.04
	mean	2.67	5.45	2.81	5.76	2.90	5.84	2.93	5.91	2.96	5.96	2.98	6.03	2.99	6.15	3.04
O-16 Harzburgite	a	2.74	5.86	2.95	6.05	3.00	6.11	3.11	6.15	3.03	6.17	3.05	6.22	3.08	6.30	3.14
	c	2.70	5.84	2.94	5.95	2.97	6.00	2.98	6.06	3.00	6.11	3.01	6.18	3.04	6.31	3.11
	mean	2.72	5.85	2.95	6.00	2.98	6.05	3.04	6.11	3.02	6.14	3.03	6.20	3.06	6.31	3.12
OM-51 Harzburgite	a	3.27	7.99	4.58	8.12	4.63	8.19	4.65	8.27	4.67	8.32	4.69	8.38	4.71	8.48	4.75
	b	3.27	8.05	4.50	8.15	4.55	8.21	4.59	8.27	4.64	8.33	4.68	8.41	4.73	8.46	4.79
	c	3.27	8.03	4.55	8.14	4.60	8.20	4.63	8.27	4.65	8.33	4.69	8.40	4.72	8.47	4.76
	mean	3.27	8.02	4.54	8.14	4.59	8.20	4.62	8.27	4.66	8.33	4.69	8.40	4.72	8.47	4.77
OM-53 Harzburgite	a	3.04	6.80	3.59	6.97	3.67	7.03	3.72	7.09	3.76	7.15	3.78	7.24	3.80	7.39	3.84
	b	3.05	7.08	3.72	7.23	3.82	7.30	3.86	7.37	3.90	7.44	3.93	7.52	3.96	7.66	3.98
	c	3.05	6.39	3.62	6.88	3.68	6.94	3.71	7.01	3.74	7.06	3.77	7.14	3.79	7.26	3.84
	mean	3.05	6.76	3.64	7.03	3.72	7.09	3.76	7.16	3.80	7.22	3.83	7.30	3.85	7.44	3.89
OMB-47 Harzburgite	a	2.73	5.84	2.89	5.89	2.90	5.92	2.92	5.96	2.94	6.00	2.96	6.06	2.98	6.19	3.00
	b	2.74	6.01	3.02	6.08	3.05	6.12	3.07	6.18	3.10	6.22	3.12	6.29	3.16	6.42	3.20
	c	2.72	6.08	3.10	6.14	3.12	6.18	3.14	6.24	3.17	6.29	3.19	6.34	3.21	6.56	3.26
	mean	2.73	5.98	3.00	6.04	3.02	6.07	3.04	6.13	3.12	6.17	3.09	6.23	3.12	6.39	3.15
OMB-38 Harzburgite	a	2.82	5.84	2.98	6.04	3.07	6.13	3.12	6.23	3.18	6.29	3.22	6.37	3.26	6.51	3.29
C-98-1 Harzburgite	a	2.93	6.43	3.37	6.51	3.41	6.56	3.45	6.62	3.51	6.67	3.54	6.73	3.58	6.84	3.63
	b	2.95	6.54	3.35	6.61	3.40	6.65	3.43	6.71	3.48	6.74	3.50	6.80	3.55	6.91	3.62
	c	2.95	6.41	3.43	6.47	3.48	6.52	3.51	6.59	3.55	6.64	3.57	6.70	3.59	6.75	3.62
	mean	2.94	6.46	3.38	6.53	3.43	6.58	3.46	6.64	3.51	6.68	3.54	6.74	3.57	6.83	3.62
OMB-11 Harzburgite	a	2.89	6.52	3.60	6.66	3.68	6.74	3.73	6.82	3.81	6.87	3.86	6.97	3.92	7.31	3.99

APPENDIX B

IN SITU ELASTIC AND PHYSICAL PROPERTIES, STRATIGRAPHIC POSITION, AND LITHOLOGY OF THE SAMAIL OPHIOLITE SAMPLES

TABLE 5

In Situ Elastic and Physical Properties, Stratigraphic Position, and Lithology of the Samail Ophiolite Samples

Sample No. and Rock Type	Core	Vs (km sec^{-1})	ΔVs (%)	Vp (km sec^{-1})	ΔVp (%)	Bulk Density (g cm^{-3})	Δρ (%)	Depth (km)	Confining Pressure (GPa)	Temperature (°C)	Porosity (%)	Poisson's Ratio
OM-342 Pillow Basalt	a	2.62		4.78		2.28		0.10	0.53	3.5	17.11	.285
OM-253 Pillow Basalt	a	2.85		5.13		2.46		0.25	0.57	8.8	11.22	.277
OM-327 Pillow Basalt	a	2.75		5.04		2.51		0.45	0.62	15.8	10.87	.288
O-8	a	2.58		4.73		2.54					10.36	.288
Pillow	b	2.67		4.88		2.57					9.98	.286
Basalt	c	2.67		4.74		2.60					9.51	.268
	mean	2.64	3.41	4.78	3.14	2.57	2.33	0.60	0.67	21.0	9.95	.281
O-9	a	2.83		5.24		2.58					9.92	.294
Pillow	b	3.05		5.55		2.60					8.48	.284
Basalt	c	2.98		5.38		2.62					8.37	.279
	mean	2.95	7.46	5.39	5.75	2.60	1.54	0.70	0.69	24.5	8.92	.286
OM-162 Massive Basalt	a	3.13		5.53		2.68		0.95	0.76	33.3	0.13	.265
OM-126	a	3.52		6.14		2.78					0.23	.265
Diabase	b	3.26		5.74		2.83					0.15	.262
	c	3.29		5.72		2.81					0.17	.253
	mean	3.26	1.20	5.74	0.69	2.83	0.37	1.10	0.80	38.5	0.18	.260
OM-172	a	3.52		6.14		2.78					0.11	.255
Diabase	b	3.57		6.14		2.78					0.15	.245
	c	3.54		6.16		2.78					0.10	.250
	mean	3.54	1.40	6.15	0.16	2.78	0.0	1.35	0.87	47.3	0.12	.250

TABLE 5. (Continued) In Situ Elastic and Physical Properties, Stratigraphic Position, and Lithology of the Samail Ophiolite Samples

Sample No. and Rock Type	Core	Vs (km sec^{-1})	ΔVs (%)	Vp (km sec^{-1})	ΔVp (%)	Bulk Density (g cm^{-3})	Δρ (%)	Depth (km)	Confining Pressure (GPa)	Temperature (°C)	Porosity (%)	Poisson's Ratio
OM-95	a	3.48		6.36		2.72					0.11	.286
Diabase	b	3.39		6.36		2.71					0.09	.302
	c	3.49		6.29		2.71					0.10	.278
	mean	3.45	2.86	6.34	1.25	2.71	1.06	1.65	0.96	57.8	0.10	.289
GE1m2	a	3.83		6.80		2.86					0.10	.267
Diabase	b	3.81		6.95		2.87					0.07	.284
	c	3.83		6.80		2.87					0.10	.267
	mean	3.82	0.52	6.85	2.16	2.87	0.35	2.40	0.13	84.0	0.09	.273
GE2m1	a	3.69		6.77		3.01					0.20	.288
High-	b	3.69		6.70		2.97					0.07	.282
Level	c	3.71		6.67		3.00					0.12	.276
Gabbro	mean	3.69	0.54	6.71	1.48	2.99	1.33	2.60	0.136	91.0	0.13	.282
GE3m1	a	3.97		7.28		2.96					0.05	.288
High-	b	3.96		7.28		3.13					0.07	.290
Level	c	3.94		7.08		2.98						.276
Gabbro	mean	3.96	0.76	7.21	2.75	3.02	5.43	2.90	0.145	101.5		.284
GE3m2	a	3.62		6.81		2.87					0.11	.302
Diabase	b	3.80		6.79		2.87					0.03	.272
	mean	3.71		6.79		2.87		2.90	0.145	101.5	0.07	.287
GE4m1	a	3.68		7.01		2.91					0.01	.309
Wehrlite	b	3.64		7.97		2.92					0.03	.312
+	c	3.85		7.08		2.93						.290
Gabbro	mean	3.73	5.45	7.02	1.55	2.92	0.68	3.50	0.162	122.5		.304
GE5m1	a	3.77		7.02		2.98					0.04	.298
Transi-	b	3.75		7.10		3.03					0.04	.307
tional	c	3.84		7.05		2.96					0.07	.289
Gabbro	mean	3.78	2.34	7.06	0.99	2.99	2.31	3.97	0.175	139.5	0.05	.298

TABLE 5. (Continued) In Situ Elastic and Physical Properties, Stratigraphic Position, and Lithology of the Samail Ophiolite Samples

Sample No. and Rock Type	Core	Vs (km sec^{-1})	ΔVs (%)	Vp (km sec^{-1})	ΔVp (%)	Bulk Density (g cm^{-3})	Δρ (%)	Depth (km)	Confining Pressure (GPa)	Temperature (°C)	Porosity (%)	Poisson's Ratio
GE6ml	a	3.75		7.36		2.92					0.01	.325
Cumulate	b	3.63		7.19		2.94					0.02	.330
Gabbro	c	3.76		7.14		2.90					0.05	.307
	mean	3.72	4.47	7.23	2.99	2.92	1.36	4.60	0.194	161.0	0.03	.319
GE7ml	a	3.71		7.17		2.92					0.01	.318
Cumulate	b	3.76		7.07		2.93					0.03	.304
Gabbro	c	3.79		7.11		2.93					0.05	.302
	mean	3.76	2.11	7.12	1.39	2.93	0.34	4.70	0.197	164.5	0.03	.307
GE8ml	a	3.81		7.30		2.96					0.01	.313
Cumulate	b	3.88		7.17		2.96					0.04	.293
Gabbro	c	3.81		7.09		2.94					0.02	.297
	mean	3.83	1.80	7.18	2.88	2.95	1.34	5.12	0.209	179.2	0.02	.301
GE9ml	a	3.77		7.35		2.99					0.02	.321
Cumulate	b	3.73		7.09		2.92					0.08	.308
Gabbro	c	3.83		7.22		2.95					0.00	.304
	mean	3.78	2.61	7.22	3.54	2.89	1.34	5.50	0.220	192.5	0.03	.311
GE11ml	a	3.98		7.22		2.95					0.05	.283
Cumulate	b	3.95		7.28		2.96					0.02	.292
Gabbro	c	3.72		7.22		2.95					0.11	.320
	mean	3.88	6.53	7.24	0.82	2.95	0.34	6.05	0.237	211.8	0.06	.298
GE13ml	a	3.83		7.35		2.98					0.04	.313
Cumulate	b	3.89		7.34		2.99					0.02	.304
Gabbro	c	3.87		7.30		2.97					0.10	.304
	mean	3.86	1.54	7.33	0.68	2.98	0.67	6.55	0.248	229.3	0.05	.307
GE14ml	a	3.67		7.02		2.90					0.05	.313
Cumulate	b	3.81		7.21		2.97					0.02	.307
Gabbro	c	3.71		7.15		2.91					0.10	.316
	mean	3.73	3.68	7.13	2.62	2.93	2.50	6.73	0.256	235.6	0.06	.312

TABLE 5. (Continued) In Situ Elastic and Physical Properties, Stratigraphic Position, and Lithology of the Samail Ophiolite Samples

Sample No. and Rock Type	Core	Vs (km sec^{-1})	ΔVs (%)	Vp (km sec^{-1})	ΔVp (%)	Bulk Density (g cm^{-3})	Δρ (%)	Depth (km)	Confining Pressure (GPa)	Temperature (°C)	Porosity (%)	Poisson's Ratio
K1ml	a	3.31		6.04		2.78					0.03	.285
Diabase	b	3.45		5.97		2.78					0.64	.249
	c	3.40		6.03		2.78					0.59	.267
	mean	3.39	4.06	6.01	1.16	2.78	0.00	2.13	0.129	74.6	0.42	.267
K2ml	a	3.98		7.04		2.98					0.05	.265
High-	b	3.91		6.98		2.96					0.06	.271
Level	c	3.91		6.99		2.97						.272
Gabbro	mean	3.94	1.76	7.00	0.85	2.97	0.67	2.65	0.139	92.8		.269
H618ml	a	3.60		6.04		2.64						.224
Plagio-	b	3.55		6.04		2.65						.235
granite	c	3.45		6.12		2.65						.267
	mean	3.54	4.17	6.07	1.31	2.65	0.38	2.45	0.133	85.8		.242
K3ml	a	3.47		5.83		2.61					1.39	.225
Plagio-	b	3.46		5.82		2.63					1.65	.226
granite	c	3.44		5.81		2.62					1.74	.230
	mean	3.46	0.86	5.82	0.34	2.62	0.76	2.50	0.133	87.5	1.59	.227
K4ml	a	3.95		7.21		2.99					0.07	.285
Transi-	b	3.90		7.24		3.00					0.02	.295
tional	c	3.97		7.29		2.90					0.06	.289
Gabbro	mean	3.94	1.76	7.25	1.72	2.96	3.33	2.80	0.143	92.8	0.05	.290
K5pl	a	3.79		7.30		3.00					0.02	.315
Cumulate	b	3.79		7.42		2.99					0.05	.323
Gabbro	c	3.81		7.30		2.99					0.12	.313
	mean	3.80	0.52	7.34	1.62	2.99	0.33	3.75	0.170	131.3	0.06	.317
K6ml	a	3.71		7.17		2.97					0.13	.317
Cumulate	b	3.90		7.24		2.98					0.06	.295
Gabbro	c	3.71		7.17		2.98					0.11	.317
	mean	3.78	4.87	7.19	0.97	2.98	0.34	4.20	0.184	147.0	0.10	.310

TABLE 5. (Continued) In Situ Elastic and Physical Properties, Stratigraphic Position, and Lithology of the Samail Ophiolite Samples

Sample No. and Rock Type	Core	Vs (km sec^{-1})	ΔVs (%)	Vp (km sec^{-1})	ΔVp (%)	Bulk Density (g cm^{-3})	Δρ (%)	Depth (km)	Confining Pressure (GPa)	Temperature (°C)	Porosity (%)	Poisson's Ratio
K7ml	a	3.85		7.38		2.99					0.02	.310
Cumulate	b	3.90		7.28		2.99					0.02	.300
Gabbro	c	3.90		7.32		2.98					0.05	.300
	mean	3.91	2.53	7.33	1.36	2.98	0.33	4.67	.198	163.5	0.03	.300
K8ml	a	3.82		7.30		2.97					0.01	.311
Cumulate	b	4.07		7.48		3.06					0.02	.289
Gabbro	c	3.96		7.40		2.97					0.06	.299
	mean	3.95	6.14	7.39	2.42	3.00	2.94	5.04	0.208	176.4	0.03	.300
K9ml	a	3.68		7.36		2.87					0.05	.334
Cumulate	b	3.78		7.20		2.88					0.03	.310
Gabbro	c	3.76		7.29		2.94					0.06	.319
	mean	3.74	2.65	7.29	2.16	2.90	2.38	5.20	0.213	182.0	0.05	.321
K10ml Cumulate Gabbro	a	3.71		7.14		2.96		5.45	0.220	190.8	0.04	.315
K11ml	a	3.71		7.21		2.93					0.03	.320
Cumulate	b	3.62		6.96		2.97					0.03	.314
Gabbro	c	3.72		7.35		3.02					0.24	.322
	mean	3.70	3.72	7.17	5.30	2.97	2.98	5.62	0.225	196.7	0.10	.319
K12ml	a	3.78		7.36		2.97					0.05	.322
Cumulate	b	3.83		7.17		2.90					0.05	.301
Gabbro	c	3.84		7.16		2.97					0.05	.299
	mean	3.81	1.56	7.23	2.72	2.95	2.36	6.03	0.237	211.1	0.05	.307
K13ml	a	3.68		7.09		2.96					0.28	.315
Cumulate	b	3.79		7.04		2.97					0.14	.295
Gabbro	c	3.79		7.08		2.96						.299
	mean	3.76	2.90	7.07	0.71	2.97	0.34	6.15	0.240	215.3	0.21	.303
K14ml	b	3.95		7.46		3.07						.299
Cumulate	c	3.98		7.40		3.04						.297
Gabbro	mean	3.99		7.43		3.05		6.65	0.255	232.8		.298

TABLE 5. (Continued) In Situ Elastic and Physical Properties, Stratigraphic Position, and Lithology of the Samail Ophiolite Samples

Sample No. and Rock Type	Core	Vs (km sec^{-1})	ΔVs (%)	Vp (km sec^{-1})	ΔVp (%)	Bulk Density (g cm^{-3})	Δρ (%)	Depth (km)	Confining Pressure (GPa)	Temperature (°C)	Porosity (%)	Poisson's Ratio
K16ml	a	3.70		7.42		2.87						.334
Cumulate	b	3.91		7.71		3.08						.326
Gabbro	c	3.67		7.13		2.84						.319
	mean	3.76	6.14	7.42	7.52	2.93	7.79	7.55	0.281	264.3		.327
K17ml	a	3.62		7.15		2.96						.327
Cumulate	b	3.61		7.3		3.04						.327
Gabbro	c	3.76		7.28		2.96						.318
	mean	3.66	3.99	7.18	2.06	2.98	2.63	7.78	0.288	272.3		.324
K21ml	a	3.24		6.45		2.85		8.12	0.298	284.2		.331
Harzburgite												
K22ml	a	3.17		6.11		2.92						.317
Harzburgite	b	3.22		6.45		2.93						.335
	c	3.15		6.18		2.91						.325
	mean	3.18	1.55	6.25	5.28	2.92	0.58	8.63	0.314	302.1		.326
O-1	a	3.36		6.39		2.97						.309
Harzburgite	b	3.34		6.28		2.95						.302
	c	3.14		6.18		2.94						.326
	mean	3.28	6.55	6.28	3.29	2.95	1.01	10.17	0.329	356.0		.312
O-2	a	3.24		6.69		2.92						.347
Harzburgite	b	3.06		6.17		2.89						.337
	c	3.35		6.15		2.91						.289
	mean	3.22	8.66	6.34	8.78	2.91	1.03	12.03	0.389	421.1		.324
O-3	a	3.44		6.74		3.01						.324
Harzburgite	b	3.36		6.28		3.00						.299
	c	3.42		6.42		3.00						.302
	mean	3.41	2.33	6.48	6.82	3.00	0.33	12.46	0.403	436.1		.308
O-5	a	3.18		6.23		2.84						.324
Harzburgite	b	3.02		5.81		2.86						.316
	c	3.20		6.01		2.83						.303
	mean	3.13	5.63	6.02	6.74	2.85	1.05	13.14	0.425	460.0		.314

TABLE 5. (Continued) In Situ Elastic and Physical Properties, Stratigraphic Position, and Lithology of the Samail Ophiolite Samples

Sample No. and Rock Type	Core	Vs (km sec^{-1})	ΔVs (%)	Vp (km sec^{-1})	ΔVp (%)	Bulk Density (g cm^{-3})	Δρ (%)	Depth (km)	Confining Pressure (GPa)	Temperature (°C)	Porosity (%)	Poisson's Ratio
O-6	a	3.29		6.31		2.92						.313
Harzburgite	b	3.11		6.02		2.90						.318
	c	3.01		6.11		2.88						.340
	mean	3.14	8.51	6.14	4.60	2.90	1.37	13.20	0.425	462.0		.323
O-7	a	3.26		6.29		2.96						.316
Harzburgite	b	3.37		6.35		2.97						.304
	c	3.38		6.62		2.95						.323
	mean	3.34	3.55	6.42	4.98	2.96	0.67	13.05	0.422	456.8		.314
O-10	a	2.80		5.81		2.72						.349
Harzburgite	b	2.84		5.94		2.73						.352
	c	2.99		5.92		2.71						.329
	mean	2.88	6.35	5.89	2.19	2.71	0.74	17.23	0.571	603.1		.343
O-11	a	2.88		5.87		2.72						.341
Harzburgite	b	3.00		5.86		2.72						.322
	c	2.90		5.94		2.70						.343
	mean	2.93	4.00	5.89	1.35	2.72	0.74	17.27	0.571	604.5		.336
O-12	a	3.04		6.00		2.76						.327
Harzburgite	b	2.88		5.95		2.75						.347
	c	3.06		5.93		2.77						.318
	mean	3.00	5.88	5.96	1.17	2.76	0.73	17.30	0.571	605.5		.331
O-13	a	2.89		5.73		2.74						.329
Harzburgite	b	2.91		5.82		2.76						.333
	c	2.97		6.14		2.74						.347
	mean	2.93	2.69	5.90	5.21	2.75	0.72	17.32	0.572	606.2		.337
O-14	a	2.94		5.81		2.74						.328
Harzburgite	b	2.89		5.85		2.74						.338
	c	2.90		5.89		2.73						.340
	mean	2.91	1.70	5.85	1.36	2.74	0.37	17.36	0.572	606.9		.335

TABLE 5. (Continued) In Situ Elastic and Physical Properties, Stratigraphic Position, and Lithology of the Samail Ophiolite Samples

Sample No. and Rock Type	Core	Vs (km sec^{-1})	ΔVs (%)	Vp (km sec^{-1})	ΔVp (%)	Bulk Density (g cm^{-3})	Δρ (%)	Depth (km)	Confining Pressure (GPa)	Temperature (°C)	Porosity (%)	Poisson's Ratio
O-15	a	2.81		5.77		2.71						.344
Harzburgite	b	2.73		5.72		2.67						.352
	c	2.78		5.78		2.70						.349
	mean	2.78	2.85	5.76	1.04	2.69	1.48	17.36	0.573	607.6		.349
O-16	a	2.86		5.88		2.76						.345
Harzburgite	b	2.82		5.91		2.721						.353
	mean	2.84	1.30	5.90	0.49	2.74	1.47	17.38	0.573	608.3		.349
OMB-47	a	2.84		5.85		2.75						.346
Harzburgite	b	3.02		6.07		2.76						.335
	c	3.07		6.14		2.74						.333
	mean	2.98	7.49	6.02	4.72	2.75	0.73	9.18	0.297	321.3		.338
OMB-38	a	3.08		6.14		2.84			0.401	434.0		.331
Harzburgite												
C-98-1	a	3.41		6.50		2.95						.311
Harzburgite	b	3.37		6.58		2.97						.323
	c	3.43		6.48		2.97						.306
	mean	3.40	1.75	6.52	1.52	2.96	0.68	12.68	0.410	443.8		.314
OMB-11	a	3.70		6.72		2.91			0.610	609.0		.282
Harzburgite												
OM-51	a	4.51		8.13		3.29						.278
Harzburgite	b	4.53		8.16		3.29						.278
	c	4.52		8.15		3.29						.278
	mean	4.52	0.44	8.14	0.36	3.29	0.0	15.46	0.500	541.1		.278
OM-53	a	3.80		7.24		3.09						.310
Harzburgite	b	3.96		7.52		3.09						.308
	c	3.79		7.14		3.09						.304
	mean	3.85	4.29	7.30	5.05	3.09	0.0	15.65	0.500	546.4		.307

APPENDIX C

PETROGRAPHIC MODAL ANALYSES OF THE SAMAIL OPHIOLITE SAMPLES

TABLE 6

Petrographic Modal Analyses of the Samail Ophiolite Samples

Sample Description			Major Minerals (modal %)											
Sample Number	Rock Type	Texture	ol	opx	cpx	plag + saus	hb	ural	Ti-Fe opa	serp	mag + hem	chl	ta	other
OM-342a	Metabasalt	Aphyric												cl 80, ca 15, pr 5
OM-253a	Metabasalt	Intersertal				50					10	15		cl 15, qtz 2
OM-327a	Metabasalt	Intersertal	3			45					10	15		cl 23, qtz 2
O-8	Metabasalt	Intersertal			3	25								pr and altered glass 72
O-9	Metabasalt	Intersertal			1	20								pr and altered glass 79
OM-162a	Metabasalt	Intersertal			3	60					5	2		cl 15, pr 10
OM-126	Metadiabase	Subophitic				70		5			3	4		epi 10, qtz 4
OM-172	Metadiabase	Subophitic			5	50		5			5	10		epi 15, qtz 4
OM-95	Metadiabase	Subophitic			10	60		10			3	10		epi 5, qtz 2
GE1m2	Metadiabase	Subophitic			1	64		33	1		1			qtz 1
GE2m1	Metagabbro	Hypidiomorphic Granular			4	51	10	26	8		1			
GE3m1	Metagabbro	Hypidiomorphic Granular			17	43	6	27	3					
GE3m2	Metadiabase	Relict Ophitic				56		43	3					sph 1
GE4m1	Gabbro	Mesocumulate	4		26	56	7	2	tr	5		tr		
GE5m1	Gabbro	Mesocumulate			31	49	3	3	4		2	6	2	

TABLE 6. (Continued) Petrographic Modal Analyses of the Samail Ophiolite Samples

Sample Description			Major Minerals (modal %)												
Sample Number	Rock Type	Texture	ol	opx	cpx	plag + saus	hb	ural	Ti-Fe opa	serp	mag + hem	chl	ta	other
GE6ml	Gabbro	Adcumulate			37	58	2	2						pr 1
GE7ml	Gabbro	Adcumulate	8		26	60	1	2		3			tr	
GE8ml	Gabbro	Adcumulate	1		41	52		2		1		3		
GE9ml	Gabbro	Adcumulate	5		33	56		1	tr	5	tr	tr		
GE11ml	Gabbro	Adcumulate	11		32	40	1	2		14				trem 11?
GE13ml	Gabbro	Adcumulate	7		38	52		2		1				
GE14ml	Gabbro	Adcumulate	7		34	56		2		1				
K1ml	Metadiabase	Intergranular				60		25	7			4		qtz 4
K2ml	Metagabbro	Hypidiomorphic Granular			15	37	1	47			<1			
K3ml	Plagiogranite	Hypidiomorphic Granular				73			2			2		qtz 22, epi
H618ml	Plagiogranite	Hypidiomorphic Granular				69		5	1					qtz 25, epi
K4ml	Gabbro	Mesocumulate	1		44	47	6	tr	2			1		
K5pl	Gabbro	Adcumulate			43	55	<1	1						
K6ml	Gabbro	Mesocumulate	5		41	49	1	2	1	1		tr		
K7ml	Gabbro	Mesocumulate	11		40	47	1	1					tr	
K8ml	Gabbro	Adcumulate	5		47	46	tr	1	tr	<1	tr			

TABLE 6. (Continued) Petrographic Modal Analyses of the Samail Ophiolite Samples

Sample Description			Major Minerals (modal %)												
Sample Number	Rock Type	Texture	ol	opx	cpx	plag + saus	hb	ural	Ti-Fe opa	serp	mag + hem	chl	ta	other
K9ml	Gabbro	Mesocumulate	6		27	61	tr	1	1	2	2			
K10ml	Gabbro	Adcumulate	1		31	54	3	6		3	2			
K11ml	Gabbro	Adcumulate	14		19	62	tr	1	1	3	tr	tr		
K12ml	Gabbro	Adcumulate	10		31	54	tr	1		3	1			
K13ml	Gabbro	Adcumulate	10		28	51	1	1	tr	6	3	tr		
K14ml	Gabbro	Adcumulate	3		51	43	tr	1	tr	2				
K16ml	Gabbro	Adcumulate	5		25	66		1		1	1		1	
K17ml	Gabbro	Adcumulate	4		32	60		1			1	2	tr	
K21ml	Harzburgite + Dunite	Protogranular	44	3						46	2			sp 5
K22ml	Harzburgite	Protogranular	44	16						34	2			sp 4
O-1	Harzburgite Tectonite	Protogranular	50	15	tr					32				sp 3
O-2	Harzburgite Tectonite	Protogranular	57		tr					13			29	sp 1
O-3	Harzburgite Tectonite	Protogranular	44	25	tr					30				sp 1
O-5	Harzburgite Tectonite	Protogranular	39	11	tr					48				sp 2
O-6	Harzburgite Tectonite	Protogranular	49	15	tr					46				sp <1

TABLE 6. (Continued) Petrographic Modal Analyses of the Samail Ophiolite Samples

Sample Description			Major Minerals (modal %)											
Sample Number	Rock Type	Texture	ol	opx	cpx	plag + saus	hb	ural	Ti-Fe opa	serp	mag + hem	chl	ta	other
O-7	Harzburgite Tectonite	Protogranular	50	9	tr					38			2	sp 1
O-10	Harzburgite Tectonite	Protogranular	8	5	tr					85				sp 2
O-11	Harzburgite Tectonite	Protogranular	10	4						84				sp 2
O-12	Harzburgite Tectonite	Protogranular	12	22						62				sp 4
O-13	Harzburgite Tectonite	Protogranular	11	20						67				sp 2
O-14	Harzburgite Tectonite	Protogranular	15	16						66				sp 3
O-15	Harzburgite Tectonite	Protogranular	4	7	tr					87				sp 2
O-16	Harzburgite Tectonite	Protogranular	15	18						65				sp 2
OM-51	Harzburgite Tectonite	Mosaic	89	10	tr					tr				sp 1
OM-53	Harzburgite Tectonite	Protogranular	72	8					tr	19				sp 1
OMB-47	Harzburgite Tectonite	Protogranular	23							77				

TABLE 6. (Continued) Petrographic Modal Analyses of the Samail Ophiolite Samples

Sample Description			Major Minerals (modal %)											
Sample Number	Rock Type	Texture	ol	opx	cpx	plag + saus	hb	ural	Ti-Fe opa	serp	mag + hem	chl	ta	other
C-98-1	Harzburgite Tectonite	Protogranular	48	3						48				
OMB-45	Harzburgite Tectonite	Protogranular	45	8						46				sp 1
OMB-11	Harzburgite Tectonite	Protogranular	40	10						50				
OMB-38	Harzburgite Tectonite	Protogranular	33	6						60				sp 1

Explanation: ol = olivine; opx = orthopyroxene; cpx = clinopyroxene; plag = plagioclase; saus = saussuritized plagioclase; hb = brown or green hornblende; ural = uralite; opa = Ti-Fe opaques; serp = serpentine; mag = magnetite; hem = hematite; chl = chlorite; ta = talc; qtz = quartz; cl = clay; ca = carbonate; pr = prehnite; epi = epidote; sph = sphene; sp = spinel; trem = tremolite; tr = trace.

ANALYSTS: J.S. Pallister, at the Univ. of California, Santa Barbara and J.A. Hornbeck, at the Univ. of Hawaii, Honolulu

APPENDIX D

CHEMICAL ANALYSES AND $\bar{M}$ VALUES OF REPRESENTATIVE SAMPLES FROM THE SAMAIL OPHIOLITE

TABLE 7

Chemical Analyses and $\bar{M}$ Values of Representative Samples from the Samail Ophiolite

Sample Number	SiO_2	TiO_2	Al_2O_3	Fe_2O_3	FeO	MnO	MgO	CaO	Na_2O	K_2O	H_2O^-	H_2O^+	P_2O_5	NiO	Cr_2O_3	CO_2	Total (%)	$\bar{M}$
Metabasalts																		
OM-327a	53.80	0.86	15.70	3.50	5.90	0.13	5.50	4.90	5.80	0.24	0.62	2.90	0.08	0.0	0.0	0.08	100.01	21.25
Metadiabases																		
GE1m2	49.70	0.94	15.67	3.21	7.22	0.14	6.14	10.53	2.76	0.18	0.27	2.71	0.08	0.0	0.0	0.47	100.07	21.69
GE3m2	51.60	0.95	15.58	3.24	5.66	0.08	6.77	9.95	3.32	0.20	0.20	2.05	0.10	0.0	0.0	0.07	99.77	21.55
K1m1	54.85	1.71	15.91	6.10	4.82	0.21	3.30	5.02	4.37	0.23	0.46	2.18	0.24	0.0	0.0	0.57	99.96	21.39
OM-95	49.20	2.20	14.80	4.90	6.70	0.06	4.30	6.20	4.20	0.0	9.31	3.50	0.25	0.0	0.0	2.20	98.82	21.40
OM-126	58.50	1.40	15.50	4.40	0.90	0.15	0.30	0.20	6.50	0.42	0.57	1.80	0.36	0.0	0.0	0.11	91.11	20.67
OM-172	57.50	1.40	15.50	4.40	0.90	0.15	0.30	0.20	3.20	0.09	0.53	3.10	0.10	0.0	0.0	0.07	98.69	21.33
Plagiogranites																		
K3m1	69.35	0.45	13.88	4.78	1.73	0.13	0.70	1.35	6.33	0.12	0.15	0.79	0.10	0.0	0.0	0.07	99.93	20.75
H618m1	70.65	0.49	14.36	1.27	2.20	0.01	0.87	3.13	4.81	0.01	0.22	1.39	0.10	0.0	0.0	0.29	99.88	20.57
Gabbros																		
GE2m1	48.70	2.32	14.29	5.88	8.46	0.18	5.91	9.10	3.15	0.13	0.22	1.48	0.10	0.0	0.0	0.07	99.99	22.11
GE3m1	48.15	0.67	14.92	2.90	6.22	0.15	9.43	12.25	2.78	0.10	0.20	1.89	0.02	0.0	0.0	0.0	99.68	21.72
GE4m1	48.20	0.35	17.82	1.95	5.44	0.13	11.45	10.20	1.84	0.06	0.19	1.92	0.08	0.0	0.0	0.06	99.69	21.40
GE5m1	47.95	0.93	17.58	3.08	5.98	0.13	7.40	13.17	1.87	0.03	0.13	1.33	0.01	0.0	0.0	0.05	99.64	21.80
GE7m1	48.05	0.02	18.95	1.88	4.01	0.10	9.59	14.15	1.15	0.03	0.20	1.36	0.01	0.0	0.0	0.09	99.77	21.50
GE8m1	49.90	0.32	16.06	1.18	3.44	0.10	8.28	16.25	3.12	0.02	0.14	1.04	0.01	0.0	0.0	0.01	99.86	21.55
GE11m1	49.95	0.22	17.58	1.32	3.32	0.09	9.03	15.55	1.06	0.02	0.16	1.53	0.0	0.0	0.0	0.06	99.89	21.47
GE14m1	50.80	0.25	17.56	1.67	4.24	0.11	8.43	13.08	2.35	0.03	0.17	0.97	0.01	0.0	0.0	0.03	99.70	21.46
K2M1	49.10	0.57	14.69	2.67	5.62	0.12	9.95	12.94	1.74	0.15	0.18	1.69	0.06	0.0	0.0	0.32	99.80	21.65
K4M1	49.50	0.25	15.76	1.27	3.79	0.10	10.90	15.80	0.72	0.01	0.13	1.12	1.01	0.0	0.0	0.52	99.89	21.50
K6m1	50.70	0.35	15.57	1.57	3.68	0.12	9.27	15.83	1.23	0.06	0.19	1.23	0.02	0.0	0.0	0.06	99.89	21.56
K10m1	49.10	0.32	16.17	1.48	4.92	0.12	9.28	15.05	1.43	0.06	0.15	1.53	0.01	0.0	0.0	0.06	99.68	21.63
K12m1	47.15	0.19	17.22	1.51	5.04	0.12	10.95	14.78	0.79	0.02	0.13	1.61	0.0	0.0	0.0	0.30	99.81	21.59
K13m1	47.65	0.22	16.82	2.47	4.12	0.12	10.43	14.57	0.81	0.02	0.22	2.08	0.01	0.0	0.0	0.32	99.86	21.55
K14m1	49.60	0.24	14.98	1.07	3.12	0.09	10.60	17.82	0.74	0.02	0.01	1.15	0.0	0.0	0.0	0.14	99.67	21.57
K17m1	50.05	0.24	17.38	1.69	4.32	0.11	8.65	13.94	2.04	0.03	0.11	1.04	0.01	0.0	0.0	0.12	99.73	21.52
Harzburgite Tectonites																		
K21m1	39.10	0.04	0.73	3.85	4.36	0.12	41.13	0.58	0.05	0.0	0.29	8.72	0.02	0.29	0.34	0.56	100.18	20.63
K22m1	42.60	0.01	0.94	2.28	5.56	0.12	39.12	0.08	0.02	0.0	0.33	6.89	0.0	0.26	0.44	0.33	99.70	20.69
OM-51	45.50	0.00	1.30	2.20	5.90	0.13	42.90	1.40	0.10	0.0	0.01	0.96	0.03	0.0	0.0	0.03	100.46	20.87

$\bar{M}$ is mean atomic weight.

ANALYST: K. Ramlal, at the Univ. of Manitoba

BIBLIOGRAPHY (References Cited)

Abbotts, I.L., 1980. Intrusive processes at ocean ridges: evidence from the sheeted dyke complex of Masirah, Oman. Tectonophysics, 60: 217-233.

Bailey, E.H., 1981. Pocket map: geologic map of Muscat-Ibra area, Sultanate of Oman. J. Geophys. Res., 86.

Bailey, E.H., Blake, M.C. Jr., and Jones, D.L., 1970. On-land Mesozoic oceanic crust in California coast ranges. U.S. Geol. Surv. Prof. Pap., 700-C: C70-C81.

Birch, F., 1961. The velocity of compressional waves in rocks to 10 kilobars, part 2. J. Geophys. Res., 66: 2199-2224.

Birch, F., 1960. The velocity of compressional waves in rocks to 10 kilobars, part 1. J. Geophys. Res., 65: 1083-1102.

Birch, F., 1958. Interpretation of the seismic structure of the crust in the light of experimental studies of wave velocities in rocks. In: Contributions in Geophysics, Pergamon Press, London: 158 pp.

Boudier F. and Coleman, R.G., 1981. Cross section through the peridotite in the Samail ophiolite, southeastern Oman Mountains. J. Geophys. Res., 86: 2573-2592.

Brace, W.F., 1971. Resistivity of saturated crustal rocks to 40 km based on laboratory studies. In: J.G. Hancock (Editor), The Structure and Physical Properties of the Earth's Crust. Am. Geophys. Union, Monogr., 14: 243-256.

Cann, J.R., 1979. Metamorphism in the ocean crust. In: Implications of Deep Drilling Results in the Atlantic Ocean, Second Maurice Ewing Memorial Volume. Am. Geophys. Union: 230-238.

Cann, J.R., 1968. Geological processes at mid-ocean ridge crests. Geophys. J. R. Astron. Soc., 15: 331-341.

Chen, J.H. and Pallister, J.S., 1981. Lead isotopic studies of the Samail ophiolite, Oman. J. Geophys. Res., 86: 2699-2708.

Cheung, H.P.Y., 1978. Crustal structure near Explorer Ridge: ocean bottom seismometer results Parelle to Revere - Dellwood Fracture Zone. MSc Thesis, Univ. B. C., Vancouver, Can. (unpublished)

Christensen, N.I., 1979. Compressional wave velocities in rocks at high temperatures and pressures, critical thermal gradients, and crustal low-velocity zones. J. Geophys. Res., 84: 6849-6857.

Christensen, N.I., 1978. Ophiolites, seismic velocities and oceanic crustal structure. Tectonophysics, 47: 131-157.

Christensen, N.I., 1972a. The abundance of serpentenites in the oceanic crust. J. Geol., 80: 709-719.

Christensen, N.I., 1972b. Seismic anisotropy in the lower oceanic crust. Nature, 237: 450-451.

Christensen, N.I., 1966. Elasticity of ultrabasic rocks. J. Geophys. Res., 71: 5921-5931.

Christensen, N.I. and Salisbury, M.H., 1979. Seismic anisotropy in the oceanic upper mantle: evidence from the Bay of Islands ophiolite complex. J. Geophys. Res., 84: 4601-4610.

Christensen, N.I. and Salisbury, M.H., 1975. Structure and constitution of the lower oceanic crust. Rev. Geophys. Space Phys., 13: 57-86.

Christensen, N.I. and Salisbury, M.H., 1972. Sea floor spreading, progressive alteration of layer 2 basalts, and associated changes in seismic velocities. Earth Planet. Sci. Lett., 15: 367-375.

Christensen, N.I. and Smewing, J.D., 1981. Geology and seismic structure of the northern section of the Oman ophiolite. J. Geophys. Res., 86: 2545-2555.

Clague, D.A. and Straley, P.F., 1977. Petrologic nature of the oceanic moho. Geol., 5: 133-136.

Coleman, R.G., 1981. Tectonic setting for ophiolite obduction in Oman. J. Geophys. Res., 86: 2497-2508.

Coleman, R.G., 1977. Ophiolites: Ancient Oceanic Lithosphere?. P.J. Wyllie (Editor), Springer, New York: 229 pp.

Coleman, R.G., 1971. Plate tectonic emplacement of upper mantle peridotites along continental edges. J. Geophys. Res., 76: 1212-1222.

Coleman, R.G. and Peterman, Z.E., 1975. Oceanic plagiogranite. J. Geophys. Res., 80: 1099-1108.

Cook, R.K., 1957. Variation of elastic constants and static strains with hydrostatic pressure: a method for calculation from ultrasonic measurements. J. Acoust. Soc. Amer., 29: 445-449.

Davies, H.L., 1971. Peridotite-gabbro-basalt complex in eastern Papua: an overthrust plate of oceanic mantle and crust. Australia Bur. Min. Res. Bull., 128: 48 pp.

Dewey, J.F. and Bird, J.M., 1971. Origin and implacement of the ophiolite suite: Appalachian ophiolites in Newfoundland. J. Geophys. Res., 76: 3179-3206.

Ewing, M., Jardetzky, W.S., and Press, F., 1957. Elastic Waves in Layered Media. McGraw-Hill, New York: 380 pp.

Ewing, M., Worzel, J.L., Hersey, J.B., Press, F., and Hamilton, G.R., 1950. Seismic refraction measurements in the Atlantic Ocean basin. Bull. Seism. Soc. Am., 40: 233-242.

Finlayson, D.M., Muirhead, K.J., Webb, J.P., Gibson, G., Furumoto, A.S., Cooke, R.J.S., and Russell, A.J., 1976. Seismic investigation of the Papuan ultramafic belt. Geophys. J. R. Astron. Soc., 44: 45-60.

Fowler, C.M.R., 1978. The Mid-Atlantic Ridge: structure at 45°N. Geophys. J. R. Astron. Soc., 54: 167-183.

Furukawa, K., Gettrust, J.F., and Kempner, W.C., 1981. Crustal structure near the East Pacific Rise: Project Rose (submitted to J. Geophys. Res.).

Gealey, W.K., 1977. Ophiolite obduction and geologic evolution of the Oman Mountains and adjacent areas. Geol. Soc. Am. Bull., 88: 1183-1191

Glennie, K.W., Boeuf, M.G.A., Hughes Clarke, M.W., Moody-Stuart, M., Pilaar, W.F.H., and Reinhardt, B.M., 1974. Geology of the Oman Mountains. Verh. K. Ned. Geol. Mijnbouwk. Genoot. Geol. Ser., 31: 423 pp.

Gregory, R.T. and Taylor, H.P. Jr., 1981. An oxygen isotope profile in a section of Cretaceous oceanic crust, Samail ophiolite, Oman: evidence for ^{18}O buffering of the oceans by deep (> 5 km) seawater-hydrothermal circulation at mid-ocean ridges. J. Geophys. Res., 86: 2737-2755.

Helmberger, D.V. and Morris, G.B., 1970. A travel time and amplitude interpretation of a marine refraction profile: transformed shear waves. Bull. Seismol. Soc. Am., 600: 593-600.

Hess, H.H., 1964. Seismic anisotropy of the uppermost mantle under oceans. Nature, 203: 629-631.

Hess, H.H., 1962. History of ocean basins. In: A.E.J. Engel, H.L. James, and B.F. Leonard (Editors), Petrologic Studies, Buddington Volume. Geol. Soc. Am., Boulder, Colo., 599-620.

Hill, M.N., 1957. Recent geophysical exploration of the ocean floor. Phys. Chem. Earth, 2: 129-163.

Hopson, C.A., 1981. Oman and California Coast Range ophiolites: differences between remnants of fast and slow-spreading oceanic crust. In: The Generation of the Oceanic Lithosphere. Am. Geophys. Union, Chapman Conference.

Hopson, C.A., Coleman, R.G., Gregory, R.T., Pallister, J.S., and Bailey, E.H., 1981. Geologic section through the Samail ophiolite and associated rocks along a Muscat-Ibra transect, southeastern Oman Mountains. J. Geophys. Res., 86: 2527-2544.

Houtz, R. and Ewing, J., 1976. Upper crustal structure as a function of plate age. J. Geophys. Res., 81: 2490-2498.

Hussong, D.M., 1972. Detailed structural interpretations of the Pacific oceanic crust using ASPER and ocean bottom seismometer methods. PhD Dissertation, Univ. of Hawaii, Honolulu: 165 pp.

Hyndman, R.D., 1979. Poisson's ratio in the oceanic crust - a review. In: C.E. Keen (Editor), Crustal Properties across Passive Margins. Tectonophysics, 59: 321-333.

Hyndman, R.D. and Drury, M.J., 1976. The physical properties of oceanic basement rocks from deep drilling on the Mid-Atlantic Ridge. J. Geophys. Res., 81: 4042-4052.

Kempner, W.C., 1981. Ophiolites, synthetic seismograms, and oceanic crustal structure. PhD Dissertation, Univ. of Hawaii, Honolulu: 146 pp.

Kempner, W.C. and Gettrust, J.F., 1981a. Ophiolites, synthetic seismograms, and oceanic crustal structure, Part II: a comparison of synthetic seismograms of the Samail ophiolite, Oman, and the ROSE refraction data from the East Pacific Rise (submitted to J. Geophys. Res.).

Kempner, W.C. and Gettrust, J.F., 1981b. A comparison of OBS seismic refraction data for young and mature oceanic crust with synthetic seismograms of ophiolites of similar ages (abstract). In: The Generation of the Oceanic Lithosphere. Am. Geophys. Union, Chapman Conference.

Kennett, B.L. and Orcutt, J.A., 1976. A comparison of travel time inversions for marine refraction profiles. J. Geophys. Res., 81: 4061-4070.

Kern, H. and Richter, A., 1981. Temperature derivatives of compressional and shear wave velocities in crustal and mantle rocks at 6 kbar confining pressure. J. Geophys., 49: 47-56.

Kirby, R.K., Hahn, T.H., and Rothrock, B.D., 1972. Thermal Expansion. In: D. Gray (Editor), American Institute of Physics Handbook, 3rd ed., McGraw-Hill, New York: pp. 4-138.

Kroenke, L.W., Manghnani, M.H., Rai, C.S., Fryer, P., and Ramananantoandro, R., 1976. Elastic properties of selected ophiolitic rocks from Papua-New Guinea: Nature and composition of oceanic lower crust and upper mantle. In: G.H. Sutton, M.H. Manghnani, R. Moberly, and E.U. McAfee (Editors), The Geophysics of the Pacific Basin and Its Margin. Am. Geophys. Union, Monogr., 19: 407-423.

Kusznir, N.J., 1980. Thermal evolution of the oceanic crust: its dependence on spreading rate and effect on crustal structure. Geophys. J. R. Astron. Soc., 61: 167-181.

Kusznir, N.J. and Bott, M.H.P., 1976. A thermal study of the formation of oceanic crust. Geophys. J. R. Astron. Soc., 47: 83-95.

Lanphere, M.A., 1981. K-Ar ages of metamorphic rocks at the base of the Samail ophiolite, Oman. J. Geophys. Res., 86: 2777-2782.

Lin, W. and Wang, C., 1980. P-wave velocities in rocks at high pressure and temperature and the constitution of the central California crust. Geophys. J. R. Astron. Soc., 61: 379-400.

Lister, C.R.B., 1972. On the thermal balance of a mid-ocean ridge. Geophys. J. R. Astron. Soc., 26: 515-535.

Manghnani, M.H., Hornbeck, J., Pallister, J.S., and Coleman, R.G., 1981. Velocity structure of the Samail ophiolite, Oman: nature of the layer 3 and upper mantle (submitted to J. Geophys. Res.).

Manghnani, M.H. and Coleman, R.G., 1981. Gravity profiles across the Samail ophiolite, Oman. J. Geophys. Res., 86: 2509-2525.

Manghnani, M.H., Ramananantoandro, R., and Clark, S.P. Jr., 1974. Compressional and shear wave velocities in granulite facies rocks and eclogites to 10 kbar. J. Geophys. Res., 79: 5427-5446.

Manghnani, M.H. and Woollard, G.P., 1968. Elastic wave velocities in Hawaiian rocks at pressures to ten kilobars. In: L. Knopoff, C.L. Drake, and P.J. Hart (Editors), The Crust and Upper Mantle of the Pacific Area. Am. Geophys. Union, Monogr., 12: 501-516.

McCulloch, M.T., Gregory, R.T., Wasserburg, G.J., and Taylor, H.P. Jr., 1981. A neodymium, strontium, and oxygen isotopic study of the Cretaceous Samail ophiolite and implications for the petrogenesis and seawater-hydrothermal alteration of oceanic crust. Earth Planet. Sci. Lett., 46: 201-211.

Milsom, J., 1973. Papuan ultramafic belt: gravity anomalies and the emplacement of ophiolites. Geol. Soc. Am. Bull., 84: 2243-2258.

Miyashiro, A., Shido, F., and Ewing, M., 1970. Crystallization and differentiation in abyssal tholeiites and gabbros from mid-ocean ridges. Earth Planet. Sci. Lett., 7: 361-365.

Moores, E.M. and Jackson, E.D., 1974. Ophiolites and oceanic crust. Nature, 250: 136-139.

Nichols, G.M., 1977. The seismic structure of the Pt. Sal ophiolite and its relationship to oceanic crustal structure. MA Thesis, Univ. of California, Santa Barbara: 156 pp.

Nichols, J., Warren, N., Luyendyk, B.P., and Spudich, P., 1980. Seismic velocity structure of the ophiolite at Point Sal, southern California, determined from laboratory measurements. Geophys. J. R. Astron. Soc., 63: 165-185.

Nur, A. and Simmons, G., 1969. The effect of saturation on velocity in low porosity rocks. Earth Planet. Sci. Lett., 7: 183-193.

Pallister, J.S. and Hopson, C.A., 1981. Samail ophiolite plutonic suite: field relations, phase variation, cryptic layering, and a model of a spreading ridge magma chamber. J. Geophys. Res., 86: 2593-2644.

Pallister, J.S. and Knight, R.J., 1981. Rare-earth element geochemistry of the Samail ophiolite near Ibra, Oman. J. Geophys. Res., 86: 2673-2697.

Peselnick, L. and Nicolas, A., 1978. Seismic anisotropy in an ophiolite peridotite: application to the oceanic upper mantle. J. Geophys. Res., 83: 1227-1235.

Peterson, J.J., Fox, P.J., and Schreiber, E., 1974. Newfoundland ophiolites and the geology of the oceanic layer. Nature, 247: 194-196.

Poster, C.K., 1973. Ultrasonic velocities in rocks from the Troodos massif, Cyprus. Nature, 243: 2-3.

Raitt, R.W., Shor, G.G. Jr., Francis, T.J.G., and Morris, G.B., 1969. Anisotropy of the Pacific upper mantle. J. Geophys. Res., 74: 3095-3109.

Raitt, R.W., 1963. The crustal rocks. In: M.N. Hill (Editor), The Sea, vol. 3. Wiley-Interscience, New York, 85-102.

Ramananantoandro, R. and Manghnani, M.H., 1978. Temperature dependence of the compressional wave velocity in an anisotropic dunite: measurements to 500° C at 10 kbar. Tectonophysics, 47: 73-84.

Salisbury, M.H., Donnelly, T.W., and Francheteau, J., 1980. Geophysical logging in Deep Sea Drilling Project Hole 417D. In: Donnelly, T., Francheteau, J., Bryan, W., Robinson, P., Flower, M., Salisbury, M., et al., Initial Reports of the Deep Sea Drilling Project, v. 51, 52, 53, Part 1: U. S. Government Printing Office, Washington, D. C., 705-713.

Salisbury, M.H. and Christensen, N.I., 1978. The seismic velocity structure of a traverse through the Bay of Islands ophiolite complex, Newfoundland, an exposure of oceanic crust and upper mantle. J. Geophys. Res., 83: 805-817.

Schreiber, E. and Fox, P.J., 1977. Density and P-wave velocity of rocks from the Famous region and their implication to the structure of the oceanic crust. Geol. Soc. Am. Bull., 88: 600-608.

Schreiber, E. and Fox, P.J., 1976. Compressional wave velocities and mineralogy of fresh basalts from the Famous area and the Oceanographer Fracture Zone and texture of layer 2A of the oceanic crust. J. Geophys. Res., 81: 4071-4076.

Shor, G.G., Menard, H.W., and Raitt, R.W., 1971. Structure of the Pacific Basin. In: A.E. Maxwell (Editor), The Sea, vol. 4. Wiley-Interscience, New York: 3-27.

Simmons, G., 1964. Velocity of shear waves in rocks to 10 kbar. J. Geophys. Res., 69: 1123-1130.

Skinner, G.J., 1966. Thermal expansion. In: S.P. Clark (Editor), Handbook of Physical Constants, Geol. Soc. Am. Mem., 97: 75-96.

Sleep, N.H., 1975. Formation of oceanic crust: some thermal constraints. J. Geophys. Res., 80: 4037-4042.

Spooner, E.T.C., 1979. Ophiolitic rocks and evidence for hydrothermal convection of sea water within oceanic crust (abstract). In : Implications of Deep Drilling Results in the Atlantic Ocean, Second Maurice Ewing Memorial Volume. Am. Geophys. Union: 429-431.

Spudich, P. and Orcutt, J., 1980a. Petrology and porosity of an oceanic site: results from wave form modeling of seismic refraction data. J. Geophys. Res., 85: 1409-1433.

Spudich, P. and Orcutt, J., 1980b. A new look at the seismic velocity structure of the oceanic crust. Rev. Geophys. Space Phys., 18: 627-645.

Spudich, P., Salisbury, M.H., and Orcutt, J.A., 1978. Ophiolites found in oceanic crust? Geophys. Res. Lett., 5: 341-344.

Stern, C. and Elthon, D., 1979. Vertical variations in the effects of hydrothermal metamorphism in Chilean ophiolites: their implications for ocean floor metamorphism. In: J. Franchetau (Editor), Processes at Mid-Ocean Ridges. Tectonophysics, 55: 179-213.

Sutton, G.H., Maynard, G.L., and Hussong, D.M., 1971. Widespread occurrence of a high velocity basal layer in the Pacific crust found with repetitive sources and sonobuoys. In: J. G. Heacock (Editor), The Structure and Physical Properties of the Earth's Crust. Am. Geophys. Union, Monogr., 14: 193-209.

Talwani, M., Stoffa, P.L., and Buhl, P., 1981. Seismic reflections from the M-discontinuity (abstract). In: The Generation of the Oceanic Lithosphere. Am. Geophys. Union, Chapman Conference.

Thompson, G., Bryan, W.B., Dick, H., Mottl, M., Karson, J., and Delaney, J., 1981. Stratigraphic, lithologic, and geochemical variations in layer 2 and 3 as observed at the intersection of the Mid-Atlantic Ridge and Kane Fracture Zone, 24°N latitude (abstract). In: The Generation of the Oceanic Lithosphere. Am. Geophys. Union, Chapman Conference.

Tilton, G.R., Hopson, C.A., and Wright, J.E., 1981. Uranium-lead isotopic ages of the Samail ophiolite, Oman, with applications to Tethyan ocean ridge tectonics. J. Geophys. Res., 86: 2763-2775.

Verma, R.K., 1960. Elasticity of some high density crystals. J. Geophys. Res., 65: 757-766.

Yong, C. and Wang, C., 1980. Thermally induced accoustic emission in Westerly Granite. Geophys. Res. Lett., 7: 1089-1092.